

Dynamic localization of the chromosomal passenger complex is controlled by the orphan kinesins KIN-A and KIN-B in the kinetoplastid parasite *Trypanosoma brucei*

Reviewed Preprint

Revised by authors after peer review.


About eLife's process

Reviewed preprint version 2
March 21, 2024 (this version)

Reviewed preprint version 1
January 8, 2024

Sent for peer review
October 17, 2023

Posted to preprint server
October 12, 2023

Daniel Ballmer, Bungo Akiyoshi 

Department of Biochemistry, University of Oxford, South Parks Road, Oxford, OX1 3QU, United Kingdom • The Wellcome Centre for Cell Biology, Institute of Cell Biology, School of Biological Sciences, Edinburgh, EH9 3BF, United Kingdom

 https://en.wikipedia.org/wiki/Open_access

 Copyright information

Abstract

The chromosomal passenger complex (CPC) is an important regulator of cell division, which shows dynamic subcellular localization throughout mitosis, including kinetochores and the spindle midzone. In traditional model eukaryotes such as yeasts and humans, the CPC consists of the catalytic subunit Aurora B kinase, its activator INCENP, and the localization module proteins Borealin and Survivin. Intriguingly, Aurora B and INCENP as well as their localization pattern are conserved in kinetoplastids, an evolutionarily divergent group of eukaryotes that possess a unique set of kinetochore proteins and lack homologs of Borealin or Survivin. It is not understood how the kinetoplastid CPC assembles or how it is targeted to its subcellular destinations during the cell cycle. Here, we identify two orphan kinesins, KIN-A and KIN-B, as bona fide CPC proteins in *Trypanosoma brucei*, the causative agent of African sleeping sickness. By employing biochemical, structural, and cell biological approaches, we demonstrate that KIN-A and KIN-B serve as the scaffold for the assembly of the remaining CPC subunits. Kinetochore localization of the CPC depends on the KKT7 – KKT8 complex pathway, with the C-terminal unstructured tail of KIN-A serving as a key interaction partner for the KKT8 complex. Our data therefore show that, unlike other eukaryotes that take advantage of histone modifications for centromere recruitment, trypanosomes rely on kinetochore proteins to recruit the CPC onto kinetochores. Furthermore, the ATPase activity of KIN-A promotes chromosome alignment in prometaphase and CPC translocation to the central spindle upon anaphase onset. Thus, KIN-A constitutes a unique ‘two-in-one’ CPC localization module in complex with KIN-B, which directs the CPC to kinetochores (from S phase until metaphase) via its C-terminal tail, and to the central spindle (in anaphase) via its N-terminal kinesin motor domain. Our findings highlight the evolutionary diversity of CPC proteins and raise the possibility that kinesins may have served as the original transport vehicles for Aurora B kinases in early eukaryotes.

eLife assessment

This **important** study identifies the mitotic localization mechanism for Aurora B and INCENP (parts of the chromosomal passenger complex, CPC) in *Trypanosoma brucei*. The mechanism differs from that in the more commonly studied opisthokonts and is supported by **compelling** RNAi and imaging experiments, targeted mutations, immunoprecipitations with crosslinking/mass spec, and AlphaFold interaction predictions. The findings will be of interest to cell biologists working on cell division, parasitologists, and those interested in the evolution of mitotic mechanisms.

Introduction

During cell division, duplicated genetic material must be distributed equally into two daughter cells. The Aurora B kinase is a key mitotic regulator widely conserved among eukaryotes (Hochegger et al., 2012 [DOI](#)). It undergoes dynamic localization changes throughout mitosis to enable the spatially restricted phosphorylation of substrates involved in chromosome alignment, chromosome bi-orientation, spindle assembly checkpoint (SAC) signalling, and cytokinesis (Carmena et al., 2012 [DOI](#)). In early mitosis, Aurora B is first detected on chromosome arms and during prometaphase becomes enriched at centromeres, where it destabilizes incorrect kinetochore-microtubule attachments (Krenn and Musacchio, 2015 [DOI](#)). Upon anaphase onset, Aurora B translocates to the spindle midzone, and during cytokinesis associates with the equatorial cortex to regulate cell abscission (Adams et al., 2000 [DOI](#); Cooke et al., 1987 [DOI](#); Trivedi and Stukenberg, 2016 [DOI](#)).

The dynamic localization pattern of the Aurora B kinase is in part achieved through its association with a scaffold comprised of inner centromere protein (INCENP), Borealin and Survivin (Adams et al., 2001 [DOI](#), 2000 [DOI](#); Gassmann et al., 2004 [DOI](#); Romano et al., 2003 [DOI](#); Sampath et al., 2004 [DOI](#); Vader et al., 2006 [DOI](#); Wheatley et al., 2001 [DOI](#)). Together, these proteins form a tetrameric complex referred to as the chromosomal passenger complex (CPC). The CPC can be partitioned into two functional modules: The ‘catalytic module’ and the ‘localization module’. The catalytic module is composed of Aurora B in complex with the IN-box at the INCENP C-terminus, which is required for full activation of the Aurora B kinase (Bishop and Schumacher, 2002 [DOI](#)). The localization module comprises Borealin, Survivin and the N-terminus of INCENP, which are connected to one another via a three-helical bundle (Jeyaprakash et al., 2011 [DOI](#), 2007 [DOI](#); Klein et al., 2006 [DOI](#)). The two modules are linked by the central region of INCENP, composed of an intrinsically disordered domain and a single alpha helical (SAH) domain. INCENP harbors microtubule-binding domains within the N-terminus and the central SAH domain, which play key roles for CPC localization and function (Cormier et al., 2013 [DOI](#); Fink et al., 2017 [DOI](#); Kang et al., 2001 [DOI](#); Mackay et al., 1993 [DOI](#); Nakajima et al., 2011 [DOI](#); Noujaim et al., 2014 [DOI](#); Samejima et al., 2015; van der Horst et al., 2015; Wheatley et al., 2001 [DOI](#); Wheelock et al., 2017 [DOI](#)).

In vertebrates, recruitment of the CPC to centromeric chromatin depends on two pathways, involving the Haspin and Bub1 kinases. Haspin phosphorylates histone H3 on Thr3 (H3T3ph), which is recognized by the baculovirus IAP repeat (BIR) domain of Survivin (Kelly et al., 2010 [DOI](#); Wang et al., 2010 [DOI](#); Yamagishi et al., 2010 [DOI](#)). H3T3ph is initially found along the entire length of chromosomes between sister chromatids but becomes enriched at the inner centromere (the space between sister kinetochores) during late prophase. In contrast, the kinetochore-associated Bub1 kinase phosphorylates histone H2A on Thr120 (H2AT120ph) (Kawashima et al., 2010 [DOI](#)). H2AT120ph recruits Shugoshin-like proteins (Sgo1 and Sgo2), which in turn are bound by Borealin (Tsukahara et al., 2010 [DOI](#); Yamagishi et al., 2010 [DOI](#)). Recently, Sgo1 has also been demonstrated to

interact with the BIR domain of Survivin through an N-terminal histone H3-like motif (Abad et al., 2022 [↗](#); Jeyaprakash et al., 2011 [↗](#)). The interactions of Borealin and Survivin with Sgo1 form the basis for a kinetochore-proximal pool of the CPC which is distinct from the inner centromere pool (Broad et al., 2020 [↗](#); Hadders et al., 2020 [↗](#); Liang et al., 2020 [↗](#)).

In most studied eukaryotes, ranging from yeast to humans, kinetochore assembly is scaffolded by a centromere-specific histone H3 variant, CENP-A (Allshire and Karpen, 2008 [↗](#); Black and Cleveland, 2011 [↗](#); Hori and Fukagawa, 2012 [↗](#); Maddox et al., 2012 [↗](#); Westhorpe and Straight, 2013 [↗](#)). An assembly of inner kinetochore protein complexes, referred to as the constitutive centromere-associated network (CCAN), interacts with centromeric CENP-A chromatin throughout the cell cycle and provides a platform for recruitment of the outer kinetochore KNL1/Mis12 complex/Ndc80 complex (KMN) network that has microtubule-binding activity (Cheeseman et al., 2006 [↗](#); Foltz et al., 2006 [↗](#); Izuta et al., 2006 [↗](#); Okada et al., 2006 [↗](#)). Some of these kinetochore proteins are present in nearly all sequenced eukaryotes, suggesting that key principles of chromosome segregation are widely shared among eukaryotes (Drinnenberg and Akiyoshi, 2017 [↗](#); Van Hooff et al., 2017 [↗](#); Meraldi et al., 2006 [↗](#); Tromer et al., 2019). However, a unique set of kinetochore proteins (KKT1–20, KKT22–25, KKIP1–12) are present in the evolutionarily divergent lineage called kinetoplastids (Akiyoshi, 2020 [↗](#); Akiyoshi and Gull, 2014 [↗](#); D’Archivio and Wickstead, 2017 [↗](#); Nerusheva et al., 2019 [↗](#); Nerusheva and Akiyoshi, 2016 [↗](#)). Kinetoplastids are flagellated protists that are highly divergent from commonly studied eukaryotes (Cavalier-Smith, 2010 [↗](#)). *Trypanosoma brucei*, *Trypanosoma cruzi*, and *Leishmania* spp. are causative agents of African trypanosomiasis, Chagas disease, and leishmaniasis, respectively, and as such pose a serious threat to public health and prosperity across the tropics and subtropics (Stuart et al., 2008 [↗](#); WHO, 2017).

Despite the absence of canonical kinetochore components (Berriman et al., 2005 [↗](#); Lowell and Cross, 2004 [↗](#)), Aurora kinases are conserved in kinetoplastids. Early studies suggested that the Aurora B homolog (Aurora B^{AUK1}) in *T. brucei* forms a complex with chromosomal passenger complex proteins 1 and 2 (CPC1 and CPC2) and plays a crucial role in mitosis and cytokinesis (Li et al., 2008 [↗](#); Tu et al., 2006 [↗](#)). CPC1 was later found to be a divergent INCENP homolog (hereafter referred to as INCENP^{CPC1}) based on the presence of a conserved C-terminal IN-box (Hu et al., 2014 [↗](#)). However, INCENP^{CPC1} lacks the central SAH domain and N-terminal residues, which in other eukaryotes interact with Survivin and Borealin. In addition, two orphan kinesins, KIN-A and KIN-B, have been proposed to transiently associate with Aurora B^{AUK1} during mitosis (Li, 2012 [↗](#); Li et al., 2008 [↗](#)). Although homologs of the ‘localization module’ proteins Survivin and Borealin have not been identified in kinetoplastids (Komaki et al., 2022), the trypanosome CPC displays a dynamic localization pattern similar to that of the metazoan CPC (Li et al., 2008 [↗](#)): Aurora B^{AUK1}, INCENP^{CPC1} and CPC2 localize to kinetochores in early mitosis and then translocate to the central spindle upon anaphase onset. From late anaphase onwards, an additional population of CPC proteins is detectable at the tip of the new flagellum attachment zone (FAZ), the point of cytokinesis initiation in *T. brucei*. It is presently not understood how the CPC assembles in these evolutionarily divergent eukaryotes nor how its localization dynamics are regulated during the cell cycle.

Here, by combining biochemical, structural and cell biological approaches in procyclic form *T. brucei*, we show that the trypanosome CPC is a pentameric complex comprising Aurora B^{AUK1}, INCENP^{CPC1}, CPC2, and the two orphan kinesins KIN-A and KIN-B. KIN-A and KIN-B interact via their coiled-coil domains to form a subcomplex within the CPC, which serves as a scaffold for the catalytic module (Aurora B^{AUK1} + INCENP^{CPC1}). The C-terminal unstructured tail of KIN-A directs kinetochore localization of the CPC from S phase to metaphase, while the N-terminal motor domain promotes the central spindle enrichment in anaphase. Furthermore, we identify the KKT7 – KKT8 complex pathway as the main kinetochore recruitment arm of the trypanosome CPC.

Results

KIN-A and KIN-B are bona fide CPC proteins in trypanosomes

To identify additional interactors of the CPC in trypanosomes, we performed immunoprecipitation followed by liquid chromatography tandem mass spectrometry (IP-MS) of endogenously YFP-tagged Aurora B^{AUK1} (**Fig. S1A** [↗](#), Table S1 and Table S2). Besides Aurora B^{AUK1}, INCENP^{CPC1} and CPC2, we observed notable enrichment of two orphan kinesins, KIN-A and KIN-B ([Wickstead and Gull, 2006](#) [↗](#)), as reported previously ([Li et al., 2008](#) [↗](#)). Both KIN-A and KIN-B were also highly enriched in immunoprecipitates of ectopically expressed GFP-INCENP^{CPC1}. Vice versa, IP-MS of GFP-tagged KIN-A and KIN-B identified Aurora B^{AUK1}, INCENP^{CPC1}, and CPC2 as top hits (**Fig. 1A** [↗](#) and Table S2).

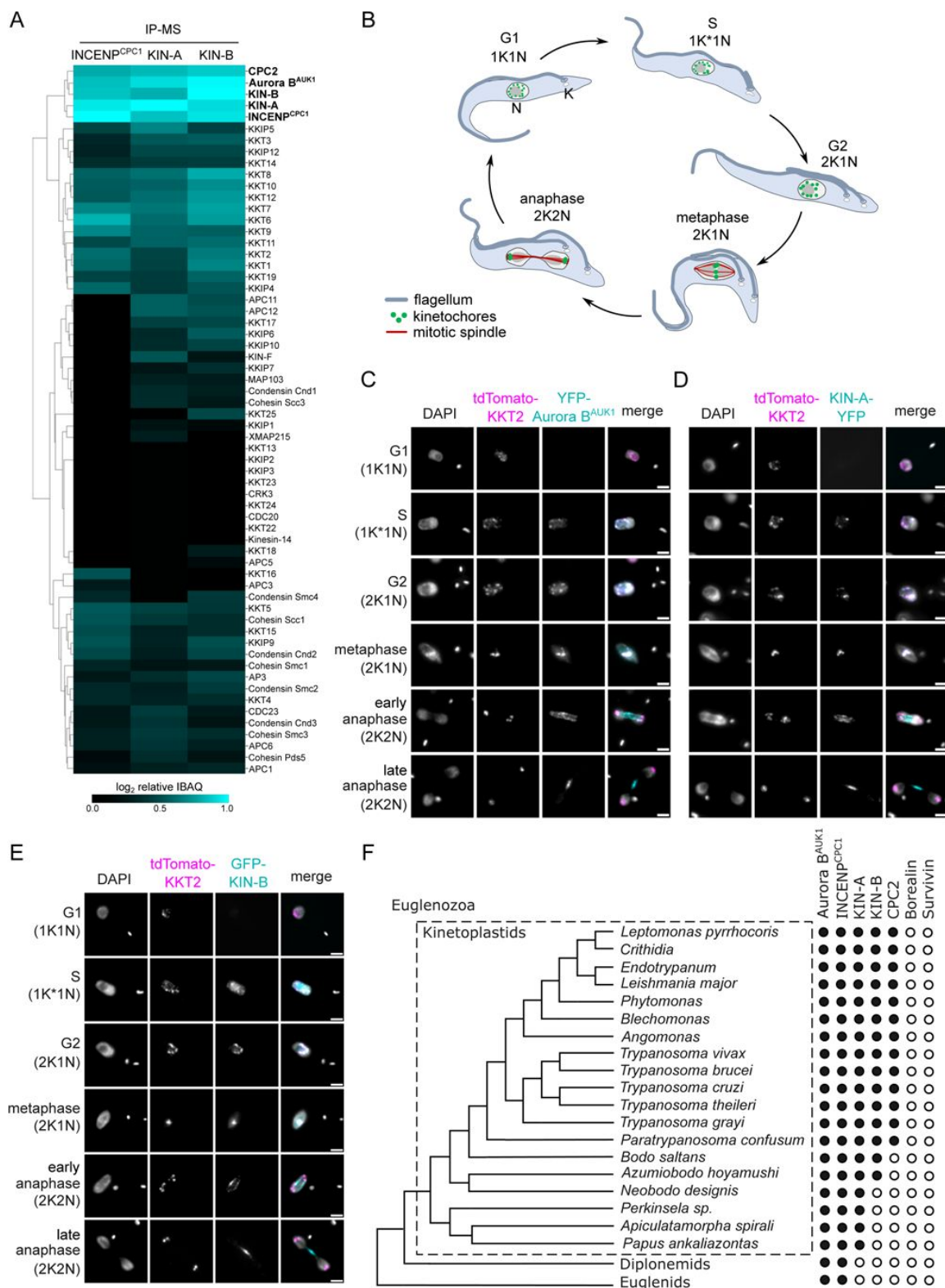


Figure 1.

KIN-A and KIN-B are bona fide CPC proteins in *T. brucei*.

(A) Clustered heatmap showing enrichment (log₂ intensity based absolute quantification (IBAQ)) of mitotic proteins co-purifying with ectopically expressed GFP-INCENP^{CPC1}, GFP-KIN-A and GFP-KIN-B. The heatmap was generated using the Python Seaborn library using WPGMA clustering. Cell lines: BAP2190, BAP2286, BAP2288. Immunoprecipitation was performed using anti-GFP antibodies. See Table S2 for all proteins identified by mass spectrometry. (B) Cartoon depicting the kinetoplast (K) / nucleus (N) configuration throughout the cell cycle in procyclic *T. brucei*, with K* denoting an elongated kinetoplast. The kinetoplast is an organelle found uniquely in kinetoplastids, which contains the mitochondrial DNA and replicates and segregates prior to nuclear division. The KN configuration serves as a cell cycle marker (Siegel et al., 2008; Woodward and Gull, 1990). (C) to (E) Representative fluorescence micrographs showing the dynamic localization of YFP-Aurora B^{AUK1} (C), KIN-A-YFP (D) and GFP-KIN-B (E) over the course of the cell cycle. Kinetochores are marked with tdTomato-KKT2. DNA was stained with DAPI. Cell lines: BAP1515, BAP3066, BAP2288. Scale bars, 2 μm. (F) Phylogenetic tree of kinetoplastids, diplomonids and euglenids along with the presence (black dots) / absence (white dots) patterns of CPC components. The phylogenetic tree of Euglenozoa is based on (Butenko et al., 2020).

We next assessed the localization dynamics of fluorescently tagged KIN-A and KIN-B over the course of the cell cycle (Figs. 1, B-E). *T. brucei* possesses two DNA-containing organelles, the nucleus ('N') and the kinetoplast ('K'). The kinetoplast is an organelle found uniquely in kinetoplastids, which contains the mitochondrial DNA and replicates and segregates prior to nuclear division. The 'KN' configuration serves as a good cell cycle marker (Siegel et al., 2008; Woodward and Gull, 1990). To our surprise, KIN-A-YFP and GFP-KIN-B exhibited a CPC-like localization pattern similar to that of Aurora B^{AUK1}. Both kinesins localized to kinetochores from S phase to metaphase, and then translocated to the central spindle in anaphase (Figs. 1, C-E). Moreover, like Aurora B^{AUK1}, a population of KIN-A and KIN-B localized at the new FAZ tip from late anaphase onwards (Figs. S1, B and C). This was unexpected, because KIN-A and KIN-B were previously reported to localize to the spindle but not to kinetochores or the new FAZ tip (Li et al., 2008). These data suggest that KIN-A and KIN-B are bona fide CPC proteins in trypanosomes, associating with Aurora B^{AUK1}, INCENP^{CPC1}, and CPC2 throughout the cell cycle.

A bioinformatic search for homologs of CPC proteins within Euglenozoa revealed that both KIN-A and KIN-B are present in trypanosomatids and bodonids, with KIN-A homologs detectable even in prokinetoplastids (Fig. 1F) (Materials and Methods). CPC2, on the other hand, was detectable only within trypanosomatids. Aurora B^{AUK1} and INCENP^{CPC1} are present in kinetoplastids as well as in diplomonids and euglenids (sister groups of kinetoplastids). Interestingly, homologs of Borealin, Survivin, KIN-A, or KIN-B were not detectable in diplomonids or euglenids, raising a possibility that these organisms may also possess 'non-canonical' CPC proteins. We conclude that the KIN-A and KIN-B kinesins are highly conserved within kinetoplastids, constituting integral components of the CPC in this evolutionary divergent group of eukaryotes.

KIN-A and KIN-B promote kinetochore localization of the CPC

To investigate which subunits of the CPC are responsible for its kinetochore targeting, we performed a series of RNAi experiments (Figs. 2, A-E). Because CPC2 is poorly conserved among kinetoplastids (Fig. 1F) and depletion of CPC2 using two different hairpin RNAi constructs (Table S1) was inefficient, we did not include CPC2 in these experiments. As previously reported (Li et al., 2008), depletion of Aurora B^{AUK1}, INCENP^{CPC1}, KIN-A or KIN-B resulted in a prominent growth defect (Fig. S2A) with cells arresting in G2/M (2K1N) (Fig. S2B). Knockdown of Aurora B^{AUK1} did not affect the kinetochore localization of YFP-tagged INCENP^{CPC1}, KIN-A or KIN-B (Figs. 2, A and C-E). Knockdown of INCENP^{CPC1} caused delocalization of Aurora B^{AUK1} but not of KIN-

A or KIN-B (Figs. 2, A and B, D and E). In contrast, both Aurora B^{AUK1} and INCENP^{CPC1} were delocalized upon depletion of KIN-A or KIN-B (Figs. 2, A-C). RNAi against KIN-A disrupted KIN-B localization and vice versa (Figs. 2, A, D and E). Moreover, total protein levels of KIN-B were affected by depletion of KIN-A (Fig. S2C), suggesting that the interaction with KIN-A is required to stabilize KIN-B.

We next ectopically expressed GFP-tagged truncations of KIN-A and KIN-B to assess which domains promote their kinetochore targeting. Both KIN-A and KIN-B contain an N-terminal kinesin motor domain followed by several predicted coiled-coil motifs (Li et al., 2008), although KIN-B is predicted to be an inactive motor (Wickstead and Gull, 2006). In addition, KIN-A has a long C-terminal tail. Unlike full-length KIN-B, KIN-B²⁻³¹⁶ (inactive motor domain) failed to enrich at kinetochores and was instead found in the nucleolus (Fig. S2, D and E). KIN-A²⁻³⁰⁹ (motor domain) was also primarily detected in the nucleolus, although we observed additional spindle and weak kinetochore-like signal in some metaphase cells (Fig. 2G). By contrast, both KIN-A³¹⁰⁻⁸⁶² (coiled-coil domain + C-terminal disordered tail) and KIN-B³¹⁷⁻⁶²⁴ (coiled-coil domain) clearly localized to kinetochores from S phase to metaphase (Fig. 2H; Fig. S2F). Intriguingly, unlike endogenously YFP-tagged KIN-A, ectopically expressed GFP fusions of both full-length KIN-A and KIN-A³¹⁰⁻⁸⁶² localized at kinetochores even in anaphase (Figs. 2, F and H). Weak anaphase kinetochore signal was also detectable for KIN-B³¹⁷⁻⁶²⁴ (Fig. S2F). GFP fusions of the central coiled-coil domain or the C-terminal disordered tail of KIN-A did not localize to kinetochores (data not shown). These results show that kinetochore localization of the CPC is mediated by KIN-A and KIN-B and requires both the central coiled-coil domain as well as the C-terminal disordered tail of KIN-A.

Structural model of the trypanosome CPC

To gain structural insights into the trypanosome CPC, we used AlphaFold2 (AF2) (Jumper et al., 2021; Mirdita et al., 2022) to predict the overall structure of the trypanosome CPC by testing combinations of full-length Aurora B^{AUK1}, INCENP^{CPC1}, CPC2, KIN-A, and KIN-B, and truncations thereof (Figs. S3, A-D). AF2 confidently predicted parallel coiled coils between KIN-A and KIN-B, with the main region of interaction contained within the central region of KIN-A (residues ~310–550) and the C-terminal region of KIN-B (residues ~320–580). The C-terminal tail (residues ~550–862) of KIN-A is predicted to be intrinsically disordered (pLDDT scores <20, Figs. S3, A and B). The first ~55 residues of INCENP^{CPC1}, predicted to form two α -helices (residues ~7–20 and ~36–55), interact with the coiled coils of KIN-A:KIN-B in close proximity to the kinesin motors. A flexible central linker in INCENP^{CPC1} bridges the N-terminus of INCENP^{CPC1} and the catalytic module of the CPC (Aurora B^{AUK1} + INCENP^{CPC1} IN-box). Similarly to INCENP^{CPC1}, an N-terminal α -helical region in CPC2 (residues ~19–75) interacts with the KIN-A:KIN-B coiled coils immediately downstream of the INCENP^{CPC1} binding site. Consistent with these predictions, GFP-tagged INCENP^{CPC1} 2-147 or CPC2²⁻¹²⁰ displayed normal localization dynamics indistinguishable from the corresponding full-length constructs (Figs. S3, E-F and H-I). In contrast, deletion of the N-terminal domains of INCENP^{CPC1} or CPC2 impaired kinetochore localization (Figs. S3, G and J). Together, these data suggest that Aurora B^{AUK1} forms a subcomplex with the C-terminus of INCENP^{CPC1}, and that INCENP^{CPC1} and CPC2 interact with the coiled-coil domain of KIN-A:KIN-B via their N-terminal domains.

To validate these findings biochemically, we performed bis(sulfosuccinimidyl) suberate (BS³) cross-linking of native CPC complexes isolated by immunoprecipitation of endogenously tagged YFP-Aurora B^{AUK1} from cells arrested prior to anaphase, followed by mass spectrometry analysis (IP-CLMS) (Fig. 3A and Table S2). Indeed, our IP-CLMS data revealed high-score crosslinks between the predicted coiled-coil domains of KIN-A and KIN-B, suggesting that the two kinesins form a parallel heterodimer. As expected, Aurora B^{AUK1} formed contacts with the C-terminal IN-box of INCENP^{CPC1}, consistent with these two proteins constituting the catalytic module of the CPC. The N-terminal region of INCENP^{CPC1} interacted mainly with KIN-B and to a lesser degree with KIN-A, with most contacts confined to the N-terminal ends of the predicted coiled-coil domains of

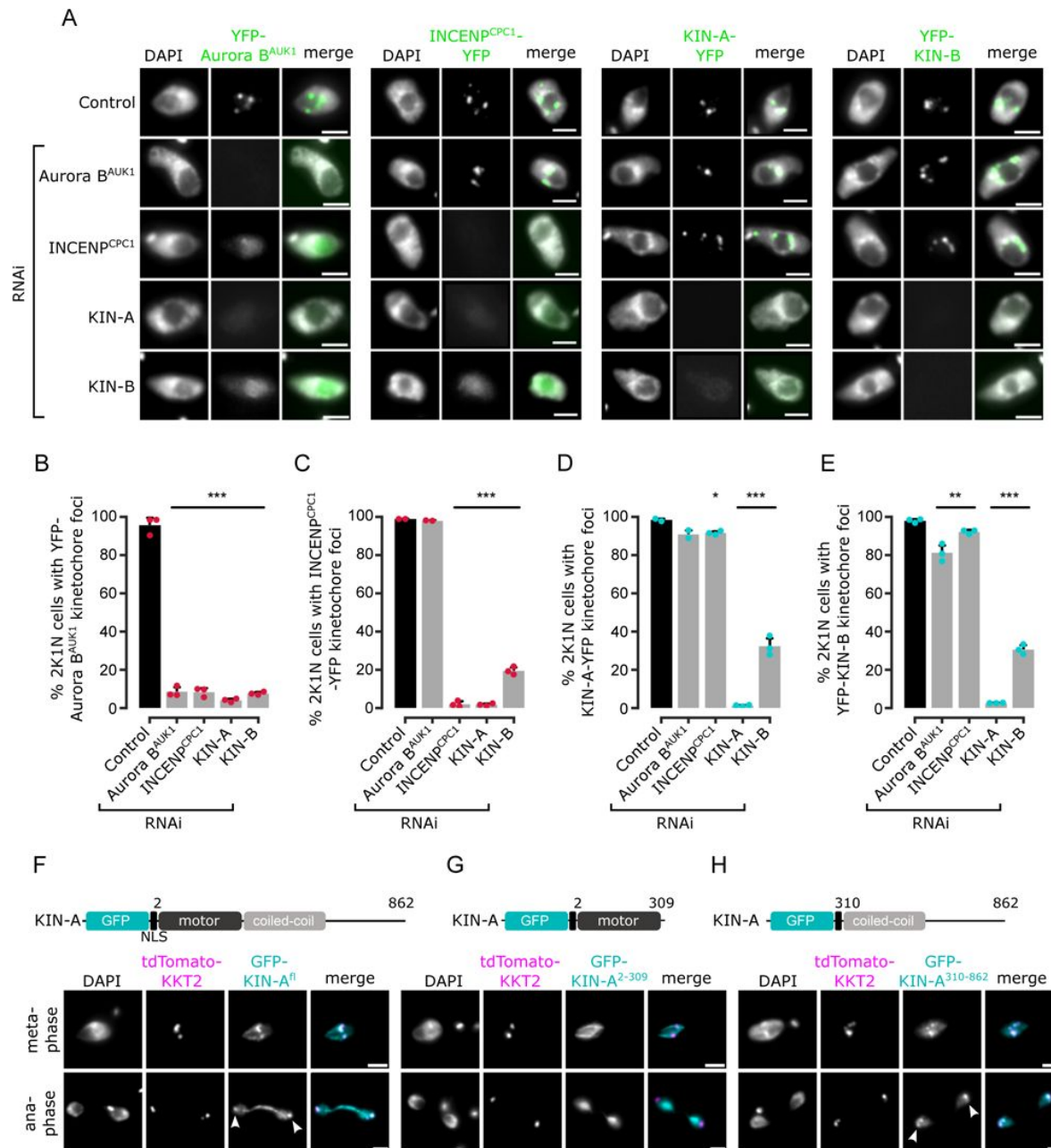


Figure 2.

Kinetochores localization of the CPC depends on KIN-A and KIN-B.

(A) Representative fluorescence micrographs showing the localization of YFP-tagged Aurora B^{AUK1}, INCENP^{CPC1}, KIN-A and KIN-B in 2K1N cells upon RNAi-mediated knockdown of indicated CPC subunits. Note that nuclear close-ups are shown here. CPC proteins were not detected in the cytoplasm. RNAi was induced with 1 µg/mL doxycycline for 24 h (KIN-B RNAi) or 16 h (all others). Cell lines: BAP3092, BAP2552, BAP2557, BAP3093, BAP2906, BAP2900, BAP2904, BAP3094, BAP2899, BAP2893, BAP2897, BAP3095, BAP3096, BAP2560, BAP2564, BAP3097. Scale bars, 2 µm. (B) to (E) Quantification of 2K1N cells that have kinetochore-like dots of YFP-tagged Aurora B^{AUK1} (B), INCENP^{CPC1} (C), KIN-A (D) and KIN-B (E) upon RNAi-mediated depletion of indicated CPC components. All graphs depict the means (bar) ± SD of at least two replicates (shown as dots). A minimum of 100 cells per replicate were quantified. * $P < 0.05$, ** $P \leq 0.01$, *** $P \leq 0.001$ (two-sided, unpaired t-test). (F) to (H) Representative fluorescence micrographs showing the localization of ectopically expressed GFP-KIN-A^{fl} (F), -KIN-A²⁻³⁰⁹ (G) and -KIN-A³¹⁰⁻⁸⁶² (H). Expression of GFP fusion proteins was induced with 10 ng/mL doxycycline for 24 h. Kinetochores are marked with tdTomato-KKT2. Arrowheads indicate KIN-A^{fl} and KIN-A³¹⁰⁻⁸⁶² signals at kinetochores. KIN-A²⁻³⁰⁹ is found at mitotic spindle during metaphase. Cell lines: BAP2286, BAP2297, BAP2287. Scale bars, 2 µm

the kinesins close to their motor domains. The N-terminus of CPC2, on the other hand, formed crosslinks with the coiled-coil domain of KIN-A. We used PyXLinkViewer (Schiffrin et al., 2020) to map our IP-CLMS data onto the assembled AF2 model of the trypanosome CPC (Fig. 3B). Using a Euclidian distance cut-off of 30 Å, ~85% of crosslinks were compatible with the model, providing confidence in the AF2 predictions. The few crosslinks that violated the distance constraints mainly represent intra-protein contacts between the INCENP^{CPC1} N- and C-terminal domains or inter-protein contacts between the INCENP^{CPC1} C-terminal domain and the kinesin motor domain of KIN-A. The central domain of INCENP^{CPC1} is predicted to be unstructured (pLDDT scores <20, Figs. S3, C-D) and may act as a flexible linker, permitting multiple orientations of the catalytic module relative to the KIN-A:KIN-B scaffold. Taken together, these data indicate that KIN-A and KIN-B interact via their coiled-coil domains, which serve as a scaffold for the assembly of the remaining CPC subunits.

The CPC is recruited to kinetochores through the KKT7 – KKT8 complex pathway

Core components of the Haspin-H3T3ph and Bub1-H2AT120ph-Sgo1 pathways that control CPC recruitment to the centromere in other model eukaryotes are not found in kinetoplastids (Berriman, 2005), and so far, no centromere-specific histone modifications and/or histone variants have been uncovered in *T. brucei*. We reasoned that the centromere receptor(s) of the trypanosome CPC may lie within the repertoire of unconventional kinetochore proteins present in kinetoplastids. Our IP-CLMS approach failed to detect crosslinks between CPC subunits and kinetochore components (Table S2), possibly due to the transient nature of these interactions. Nevertheless, several KKT proteins were commonly enriched in the immunoprecipitates of Aurora B^{AUK1}, CPC1, KIN-A and KIN-B, the most abundant ones being KKT6, KKT7, KKT8, KKT9, KKT10, KKT11 and KKT12 (Fig. 1A; Fig. S1A and Table S2). KKT7 is detected at kinetochores from S phase until the end of anaphase and recruits the KKT8 complex (comprising KKT8, KKT9, KKT11 and KKT12) (Akiyoshi and Gull, 2014; Ishii and Akiyoshi, 2020). The KKT8 complex localizes at kinetochores from S phase and dissociates at the metaphase-anaphase transition.

Using previously validated RNAi constructs (Akiyoshi and Gull, 2014; Llauro et al., 2018; Marcianò et al., 2021), we found that knockdown of KKT7 or KKT9 resulted in dispersal of YFP-Aurora B^{AUK1} from kinetochores in ~70% of cells (Figs. 4A, A-D). In contrast, depletion of KKT1, KKT2, KKT3, KKT4, KKT6, KKT10/19, KKT14 and KKT16 had little or no effect on YFP-Aurora B^{AUK1} localization (Figs. S4, A and B). KIN-A-YFP was also lost from kinetochores upon RNAi-mediated depletion of KKT8 complex subunits (Figs. S4, C and D). We next tested whether KKT7 or the KKT8 complex were able to recruit Aurora B^{AUK1} to an ectopic locus using the LacI-LacO system (Landeira and Navarro, 2007). For these experiments, we expressed GFP tagged KKT7²⁻²⁶¹ or KKT8 fused to the Lac repressor (LacI) in trypanosomes containing an ectopic Lac operator (LacO) array stably integrated into rDNA repeats. We previously showed that KKT7 lies upstream of the KKT8 complex (Ishii and Akiyoshi, 2020). Indeed, GFP-KKT7²⁻²⁶¹-LacI recruited tdTomato-KKT8, -KKT9 and -KKT12 (Fig. S4E). Expression of GFP-KKT7²⁻²⁶¹-LacI or GFP-KKT8-LacI resulted in robust recruitment of tdTomato-Aurora B^{AUK1} to LacO foci in S phase (Figs. 4E, E and F). Intriguingly, we also noticed that, unlike endogenous KKT8 (which is not present in anaphase), ectopically expressed GFP-KKT8-LacI remained at kinetochores during anaphase (Fig. 4F). This resulted in a fraction of tdTomato-Aurora B^{AUK1} being trapped at kinetochores during anaphase instead of migrating to the central spindle (Fig. 4F). We observed a comparable situation upon ectopic expression of GFP-KIN-A, which is retained on anaphase kinetochores together with tdTomato-KKT8 (Fig. S4F). In contrast, Aurora B^{AUK1} was not recruited to LacO foci marked by GFP-KKT7²⁻²⁶¹-LacI in anaphase (Fig. 4E).

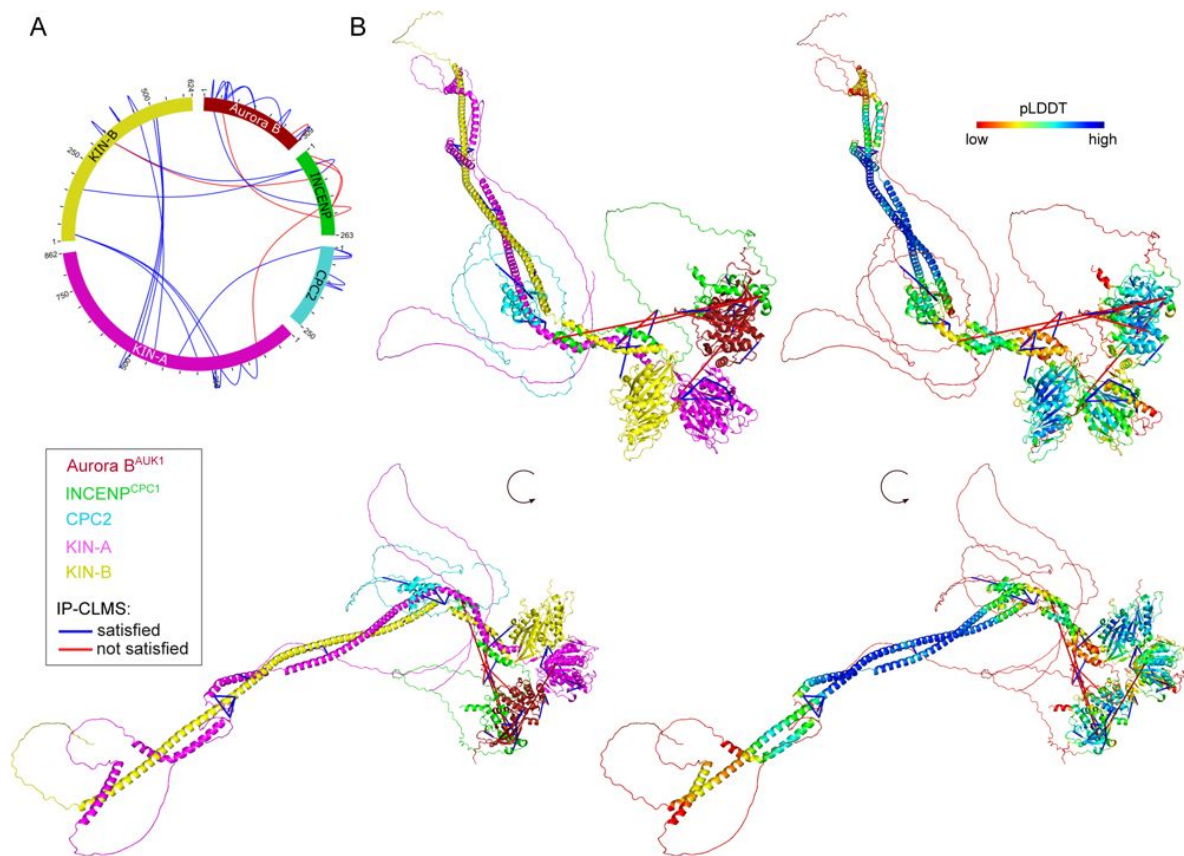


Figure 3.

Structural model of the trypanosome CPC.

(A) Circular view of the BS³ crosslinks observed between the subunits of the trypanosome CPC, obtained from native complexes isolated by immunoprecipitation of YFP-Aurora B^{AUK1} (Cell line: BAP2198). pLink2 (Chen et al., 2019) was used to obtain crosslinks from mass spectrometry data. xiView (Graham et al., 2019) was used for data visualization. Only crosslinks with a score better than E⁻³ are shown. See Table S2 for all crosslinks identified by mass spectrometry. (B) Cartoon representation showing two orientations of the trypanosome CPC, coloured by protein on the left (Aurora B^{AUK1}: crimson, INCENP^{CPC1}: green, CPC2: cyan, KIN-A: magenta, and KIN-B: yellow) or according to their pLDDT values on the right, assembled from AlphaFold2 predictions shown in [Figure S3](#). The pLDDT score is a per-residue estimate of the confidence in the AlphaFold prediction on a scale from 0 – 100. pLDDT > 70 (blue, cyan) indicates a reasonable accuracy of the model, while pLDDT < 50 (red) indicates a low accuracy and often reflects disordered regions of the protein (Jumper et al., 2021). BS³ crosslinks in (B) were mapped onto the model using PyXlinkViewer (blue = distance constraints satisfied, red = distance constraints violated, Ca-Ca Euclidean distance threshold = 30 Å) (Schiffrin et al., 2020).

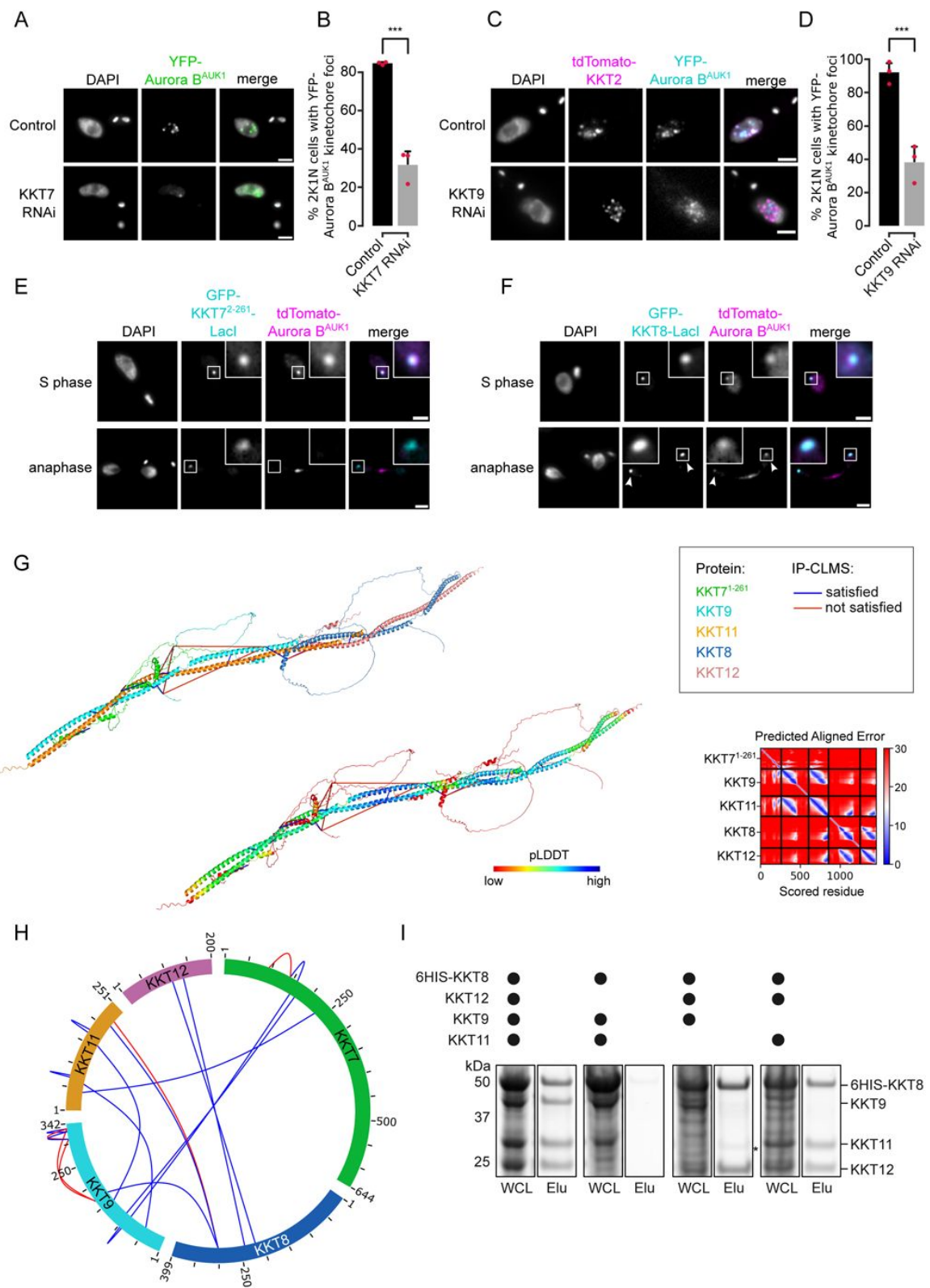


Figure 4.

The CPC is recruited to kinetochores via the KKT7 – KKT8 complex pathway.

(A) Representative fluorescence micrographs showing the localization of YFP-Aurora B^{AUK1} upon RNAi-mediated knockdown of KKT7. RNAi was induced with 1 µg/mL doxycycline for 24 h. Cell line: BAP577. Scale bars, 2 µm. (B) Quantification of 2K1N cells that have kinetochore-like dots of YFP-Aurora B^{AUK1} upon knockdown of KKT7. All graphs depict the means (bar) ± SD of three replicates (shown as dots). A minimum of 50 cells per replicate were quantified. *** $P \leq 0.001$ (two-sided, unpaired t-test). (C) Representative fluorescence micrographs showing the localization of YFP-Aurora B^{AUK1} upon RNAi-mediated knockdown of KKT9. RNAi was induced with 1 µg/mL doxycycline for 24 h. Kinetochores are marked with tdTomato-KKT2. Cell line: BAP2276. Scale bars, 2 µm. (D) Quantification of 2K1N cells that have kinetochore-like dots of YFP-Aurora B^{AUK1} upon knockdown of KKT9. All graphs depict the means (bar) ± SD of three replicates (shown as dots). A minimum of 50 cells per replicate were quantified. *** $P \leq 0.001$ (two-sided, unpaired t-test). (E) and (F) Representative micrographs of cells in S phase and anaphase showing recruitment of tdTomato-Aurora B^{AUK1} to LacO foci marked by ectopically expressed GFP-KKT7²⁻²⁶¹-LacI (E) or -KKT8-LacI (F). The insets show the magnification of the boxed region. Expression of LacI fusion proteins was induced with 10 ng/mL doxycycline for 24 h. Arrowheads in (F) indicate anaphase kinetochore localization of GFP-KKT8-LacI and tdTomato-Aurora B^{AUK1}. Anaphase kinetochore localization of tdTomato-Aurora B^{AUK1} was observed in 75% of anaphase cells expressing GFP-KKT8-LacI (n = 28). Cell lines: BAP1395, BAP2640. Scale bars, 2 µm. Of note, LacI fusions with INCENP^{CPC1}, KIN-A and KIN-B constructs robustly localized to kinetochores like their endogenous counterparts and failed to form distinct LacI foci and could therefore not be used to assess ectopic recruitment of KKT proteins. (G) AlphaFold2 model of the KKT7 – KKT8 complex, coloured by protein (KKT7¹⁻²⁶¹: green, KKT8: blue, KKT12: pink, KKT9: cyan and KKT11: orange) (left) and by pLDDT (center). BS³ crosslinks in (H) were mapped onto the model using PyXlinkViewer (Schiffrin et al., 2020) (blue = distance constraints satisfied, red = distance constraints violated, Cα-Cα Euclidean distance threshold = 30 Å). Right: Predicted Aligned Error (PAE) plot of model shown on the left (rank_2). The colour indicates AlphaFold's expected position error (blue = low, red = high) at the residue on the x axis if the predicted and true structures were aligned on the residue on the y axis (Jumper et al., 2021). (H) Circular view of the BS³ crosslinks observed among KKT7 and KKT8 complex subunits, obtained from native complexes isolated by immunoprecipitation of YFP-tagged KKI1P (Cell line: BAP710a). pLink2 (Chen et al., 2019) was used to obtain crosslinks from mass spectrometry data and xiView (Graham et al., 2019) was used for data visualization. Only crosslinks with a score better than E⁻³ are shown. See Table S2 for all crosslinks identified by mass spectrometry. (I) Indicated combinations of 6HIS-tagged KKT8 (~46 kDa), KKT9 (~39 kDa), KKT11 (~29 kDa) and KKT12 (~23 kDa) were co-expressed in *E. coli*, followed by metal affinity chromatography and SDS-PAGE. The asterisk indicates a common contaminant.

KKT7 recruits the KKT8 complex via the KKT9:KKT11 subcomplex

To gain further insights into the structure and assembly hierarchy within the KKT7 – KKT8 complex pathway, we performed CLMS on native complexes isolated by immunoprecipitation of endogenously YFP-tagged kinetochore proteins and mapped the detected crosslinks onto AF2 structure predictions (Figs. 4, G and H) (Materials & Methods). AF2 confidently predicted coiled coils between KKT8 and KKT12 and between KKT9 and KKT11 (Fig. 4G; Figs. S4, G and H), suggesting that KKT8:KKT12 and KKT9:KKT11 each form distinct subcomplexes. To validate these findings, we co-expressed combinations of 6HIS-KKT8, KKT9, KKT11, and KKT12 in *E. coli* and performed metal affinity chromatography (Fig. 4I). 6HIS-KKT8 efficiently pulled down KKT9, KKT11, and KKT12, as shown previously (Ishii and Akiyoshi, 2020). In the absence of KKT9, 6HIS-KKT8 still pulled down KKT11 and KKT12. Removal of either KKT9 or KKT11 did not impact formation of the KKT8:KKT12 subcomplex. In contrast, 6HIS-KKT8 could not be recovered without KKT12, indicating that KKT12 is required for formation of the full KKT8 complex. These results support the idea that the KKT8 complex consists of KKT8:KKT12 and KKT9:KKT11 subcomplexes. The two subcomplexes appear to be connected to each other through interactions between the C-terminal region of the KKT8:KKT12 coiled coils and the C-terminus of KKT11. Two alpha helices in

KKT7²⁻²⁶¹ (residues ~149–181) are predicted to interact with KKT9:KKT11. Using a distance cut-off of 30 Å, ~70% of crosslinks were compatible with the model (**Figs. 4**, **G** and **H**). Of the crosslinks that failed to meet the distance criteria, ~90% involved unstructured regions within KKT7 or the C-terminal tail of KKT8. Collectively, our results reveal that KKT7 recruits the KKT8 complex through interaction with the KKT9:KKT11 subcomplex.

We next examined the localization dependency of KKT8 complex components in cells. Using RNAi constructs against individual subunits of the KKT8 complex (Akiyoshi and Gull, 2014; Ishii and Akiyoshi, 2020; Marcianò et al., 2021), we assessed localization of endogenously YFP-tagged KKT8, KKT9 and KKT12 (**Figs. S4, I-L**). We found that knockdown of any subunit of the KKT8 complex affected protein levels and kinetochore localization of the other subunits, indicating that presence of all subunits is required to stabilize the full complex. YFP-KKT9 was least affected and was still detectable at kinetochores in ~50% of cells depleted of KKT8, KKT11 or KKT12 (**Fig. S4L**). Thus, KKT9:KKT11 may lie upstream of KKT8:KKT12. Indeed our IP-CLMS data suggest that the KKT9:KKT11 subcomplex directly interacts with the N-terminus of KKT7 (**Fig. 4H**, Table S2). KKT7 also formed robust crosslinks with the KKT10/19 kinases (Table S2), supporting our previous finding that KKT7 and KKT10 form a stable complex (Ishii and Akiyoshi, 2020). Together, these data suggest that the KKT7 – KKT8 complex pathway serves as the main CPC recruitment arm in trypanosomes.

The KIN-A C-terminal tail interacts with the KKT8 complex through a conserved domain

By IP-CLMS we failed to detect reliable crosslinks between the CPC and the KKT7 – KKT8 complex or, in fact, any kinetochore proteins (Table S2). This suggests that the IP-CLMS approach, although well-suited for characterizing stable protein complexes, may not be sensitive enough to detect transient or lower affinity interactions. To overcome this, we used AF2 to probe for potential interactions between the KKT8 complex and CPC (sub)complex. AF2 did not predict interactions between the KKT8 complex and INCENP^{CPC1}, CPC2 or KIN-B (data not shown). Intriguingly, AF2 predicted with high confidence interactions between KKT9:KKT11 and a conserved region (residues ~722–741) within the KIN-A C-terminal tail, which we termed conserved domain 1 (CD1) (**Figs. 5**, **A** and **B**; **Figs. S5, A** and **B**). This interaction involves a triple helix composed of KIN-A CD1, KKT9, and KKT11 in a region close to the KKT7-binding site. pLDDT scores improved significantly for KIN-A CD1 in complex with KKT9:KKT11 (>80) compared to KIN-A CD1 alone (~20) (**Fig. S3, A** and **B**), suggesting that CD1 forms a helical structure upon binding to KKT9:KKT11. Sequence alignment revealed the presence of a second conserved domain (residues ~816–862) within the C-terminal tail of KIN-A, hereafter referred to as CD2 (**Fig. 5B**; **Fig. S5A**). To assess the contributions of CD1 and CD2 for kinetochore recruitment of KIN-A in vivo, we ectopically expressed GFP fusions of the central coiled coils and C-terminal tail of KIN-A (residues ~310–862) lacking either CD1, CD2, or both (**Figs. S5, C-F**). GFP-KIN-A^{310-862 ΔCD2} showed a moderate reduction in kinetochore localization in metaphase and was completely lost from kinetochores in anaphase (**Figs. S5, D** and **G**). By contrast, GFP-KIN-A^{310-862 ΔCD1} was largely dispersed in metaphase but reappeared at kinetochores in anaphase (**Figs. S5, E** and **G**). GFP-KIN-A³¹⁰⁻⁷¹⁶ lacking both CD1 and CD2 failed to enrich at kinetochores both in metaphase and anaphase (**Figs. S5, F** and **G**). These data suggest that CD1 and CD2 synergistically promote kinetochore localization of KIN-A, with CD1 interacting with KKT9:KKT11 and CD2 possibly interacting with another receptor at the kinetochore.

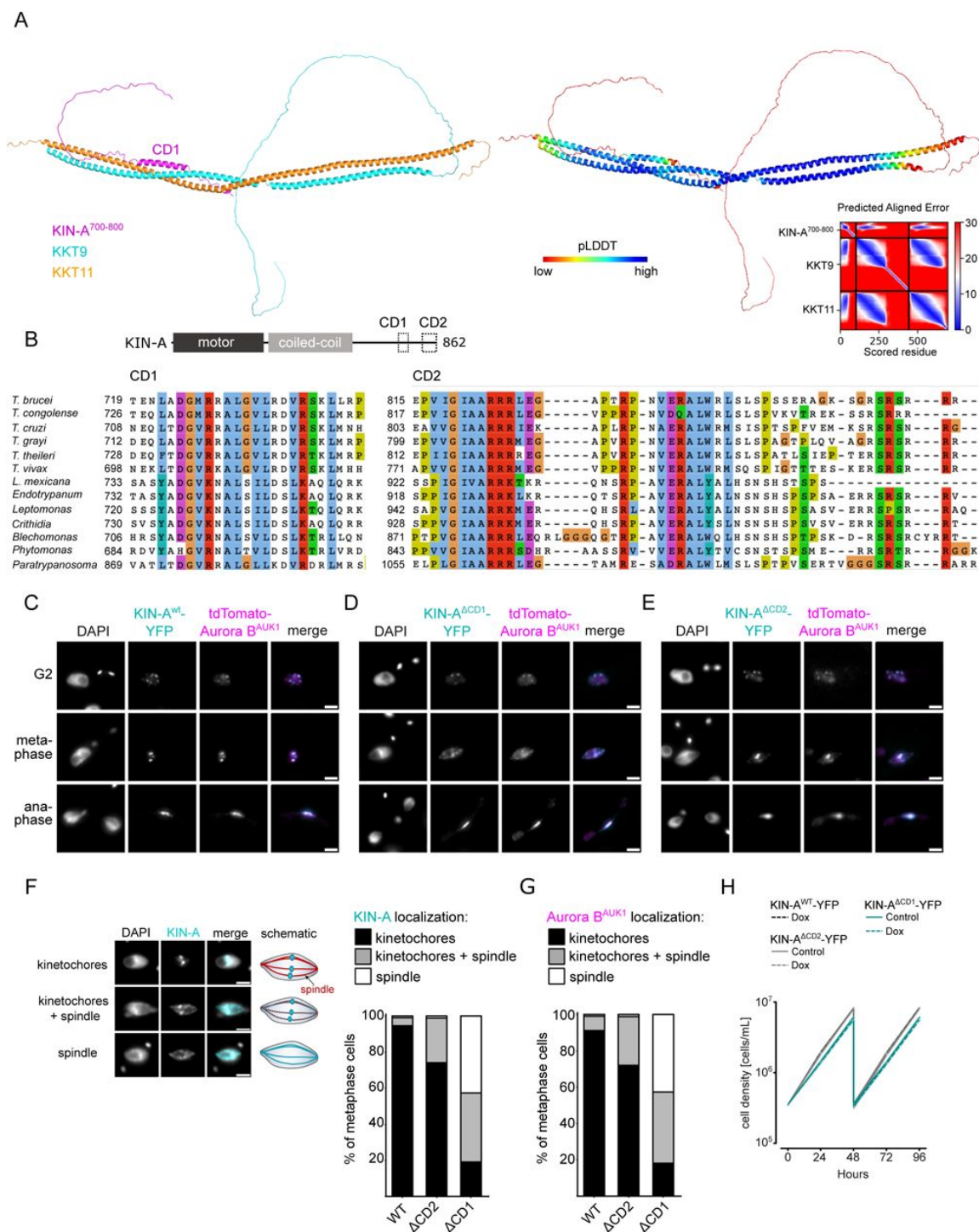


Figure 5.

Two conserved domains within the C-terminal tail of KIN-A promote kinetochore recruitment of the CPC.

(A) Left: AlphaFold2 model of KKT9:KKT11 in complex with KIN-A⁷⁰⁰⁻⁸⁶². Cartoon representations are coloured by protein (KKT9: cyan, KKT11: orange, KIN-A: magenta) (left) or according to their pLDDT values (blue = high confidence, red = low confidence) (center). Right: Predicted Aligned Error (PAE) plot of model (rank_1) predicted by AlphaFold2 (blue = high confidence, red = low confidence in the relative positions of the domains to one another). CD1 of KIN-A was predicted to interact with KKT9:KKT11 in all five AlphaFold2 models (rank_1 to rank_5). (B) Multiple sequence alignment of KIN-A CD1 and CD2 showing conservation. (C) to (E) Representative fluorescence micrographs showing the localization of tdTomato-Aurora B^{AUK1} and YFP-tagged KIN-A^{wt} (C), KIN-A^{ΔCD1} (717–743) (D) and KIN-A^{ΔCD2} (816–862) (E). RNAi was induced with 1 μg/mL doxycycline for 24 h to deplete the untagged KIN-A allele. Cell lines: BAP3067, BAP3128, BAP3127. Scale bars, 2 μm. (F) Stacked bar charts showing the percentage of YFP-tagged KIN-A^{wt}, KIN-A^{ΔCD1} and KIN-A^{ΔCD2} on kinetochores, kinetochores + spindle and spindle only in metaphase cells. Examples and schematic illustrations of the three categories used for scoring are presented on the left. A minimum of 50 cells per condition were quantified. (G) Stacked bar charts showing the percentage of tdTomato-Aurora B^{AUK1} on kinetochores, kinetochores + spindle and spindle only in metaphase cells upon rescue with YFP-tagged KIN-A^{wt}, KIN-A^{ΔCD1} or KIN-A^{ΔCD2}. A minimum of 50 cells per condition were quantified. (H) Growth curves for indicated cell lines and conditions. RNAi was induced with 1 μg/mL doxycycline for to deplete the untagged KIN-A allele in the knockdown conditions and cultures were diluted at day 2. Cell lines: BAP3067, BAP3128, BAP3127.

We next tested the relevance of KIN-A CD1 and CD2 for CPC localization and function by replacing one allele of KIN-A with C-terminally tagged wild-type or mutant constructs lacking either CD1 or CD2 and performed RNAi against the 3'UTR of KIN-A to deplete the untagged allele. We were unable to obtain a rescue cell line lacking both CD1 and CD2 as the double-mutant protein was not properly expressed. Wild-type KIN-A-YFP along with Aurora B^{AUK1} robustly localized to kinetochores from S phase until anaphase onset (Figs. 1, C and D; Fig. 5C). KIN-A^{ΔCD1}-YFP was detectable at kinetochores in G2 but predominantly localized to the mitotic spindle from (pro)metaphase onwards (Figs. 5, D and F), indicating that removal of CD1 severely weakens the affinity of KIN-A for kinetochores and instead shifts the balance towards microtubule binding. Interestingly, expression of KIN-A^{ΔCD1}-YFP similarly affected the localization of Aurora B^{AUK1} (Figs. 5, D and G; Fig. S5H). We also detected partial spindle localization of Aurora B^{AUK1} in a small population (~25%) of metaphase cells expressing KIN-A^{ΔCD2}-YFP (Figs. 5, E-G). Central spindle localization of KIN-A in anaphase was unaffected by deletion of either CD1 or CD2 (Figs. 5, D and E). Remarkably, despite a substantial loss of Aurora B^{AUK1} from kinetochores in metaphase, ΔCD1 cells exhibited normal cell cycle profiles (Fig. S5I) and showed only a modest decrease in proliferation rates (Fig. 5H). This parallels the situation in budding yeast, in which error-free chromosome segregation can be sustained even when inner centromere localization of Aurora B is largely abolished (Campbell and Desai, 2013; García-Rodríguez et al., 2019).

CPC targeting to the central spindle in anaphase depends on KIN-A's ATPase activity

Finally, we asked how translocation of the CPC to the spindle midzone in anaphase is achieved in trypanosomes. In mammalian cells, dephosphorylation of INCENP and the kinesin MKLP2 upon anaphase onset allows formation of a transient CPC-MKLP2 complex (Gruneberg et al., 2004; Hümmel and Mayer, 2009; Kitagawa et al., 2014; Serena et al., 2020). MKLP2 activity then drives plus-directed movement of this complex along microtubules of the anaphase spindle. We therefore speculated that anaphase translocation of the kinetoplastid CPC to the central spindle may involve the kinesin motor domain of KIN-A. KIN-B is unlikely to be a functional kinesin based on the absence of several well-conserved residues and motifs within the motor domain, which are

fully present in KIN-A (Li et al., 2008 [↗](#)). These include the P-loop, switch I and switch II motifs, which form the nucleotide binding cleft, and many conserved residues within the α 4-L12 elements, which interact with tubulin (Fig. S6A [↗](#)) (Endow et al., 2010 [↗](#)). Consistent with this, the motor domain of KIN-B, contrary to KIN-A, failed to localize to the mitotic spindle when expressed ectopically (Fig. S2E [↗](#)) and did not co-sediment with microtubules in our in vitro assay (Fig. S6B [↗](#)).

Ectopically expressed GFP-KIN-A and -KIN-A²⁻³⁰⁹ partially localized to the mitotic spindle but failed to concentrate at the midzone during anaphase (Figs. 2 [↗](#), F and G), suggesting that N-terminal tagging of the KIN-A motor domain may interfere with its function. To address whether the ATPase activity of KIN-A is required for central spindle localization of the CPC, we replaced one allele of KIN-A with a C-terminally YFP-tagged G210A ATP hydrolysis-defective rigor mutant (Fig. 6A [↗](#)) (Rice et al., 1999 [↗](#)) and used an RNAi construct directed against the 3'UTR of KIN-A to deplete the untagged allele. The rigor mutation did not affect recruitment of KIN-A to kinetochores (Figs. S6, C [↗](#) and D). However, KIN-A^{G210A}-YFP marked kinetochores were misaligned in ~50% of cells arrested in metaphase, suggesting that ATPase activity of KIN-A promotes chromosome congression to the metaphase plate (Figs. S6, E-H [↗](#)). In anaphase, the KIN-A rigor mutant failed to concentrate at the central spindle and instead widely decorated the mitotic spindle, with increased signal observed at spindle poles possibly due to poleward flux (Figs. 6 [↗](#), B and C). Expression of the KIN-A^{G210A} rigor mutant prevented Aurora B^{AUK1} from translocating to the central spindle and caused lagging chromosomes (Figs. 6 [↗](#), D-F). The KIN-A rigor mutation also slowed cell proliferation even in the presence of wild-type protein and caused accumulation of cells in anaphase (Figs. 6 [↗](#), G and H). We conclude that central spindle localization of the CPC depends on KIN-A's ATPase activity and is required for proper chromosome segregation.



Figure 6.

KIN-A ATPase activity is required for central spindle localization of the CPC in anaphase.

(A) Multiple sequence alignment showing conservation of Switch II region in KIN-A and KIN-B, with the key glycine residue (G210 in *T. brucei*) targeted for rigor mutation highlighted in red. (B) Representative fluorescence micrographs showing the localization of tdTomato-MAP103 (spindle marker) and YFP-tagged KIN-A^{wt} or KIN-A^{G210A} (rigor mutant). RNAi was induced with 1 µg/mL doxycycline for 24 h to deplete the untagged KIN-A allele. Cell lines: BAP3068, BAP3071. Scale bars, 2 µm. (C) Quantification showing the percentage of anaphase cells that have YFP-tagged KIN-A^{wt} or KIN-A^{G210A} localized at the central spindle. All graphs depict the means (bar) ± SD of three replicates (shown as dots). A minimum of 40 cells per replicate were quantified. *** $P \leq 0.001$ (two-sided, unpaired t-test). (D) and (E) Representative fluorescence micrographs showing the localization of tdTomato-Aurora B^{AUK1} and YFP-tagged KIN-A^{wt} (D) or KIN-A^{G210A} (E). RNAi was induced with 1 µg/mL doxycycline for 24 h to deplete the untagged KIN-A allele. Cell lines: BAP3067, BAP3070. Scale bars, 2 µm. (F) Quantification showing the percentage of anaphase cells that have tdTomato-Aurora B^{AUK1} localized at the central spindle upon rescue with YFP-tagged KIN-A^{wt} or KIN-A^{G210A}. Graphs for the KIN-A^{G210} rescue conditions (grey) depict the means (bar) ± SD of three replicates (shown as dots). A minimum of 30 cells per replicate were quantified. (G) Growth curves for indicated cell lines and conditions. RNAi was induced with 1 µg/mL doxycycline for to deplete the untagged KIN-A allele in the knockdown conditions and cultures were diluted at day 2. Cell lines: BAP3064, BAP3065. (H) Cell cycle profiles for the indicated cell lines and conditions. RNAi was induced with 1 µg/mL doxycycline to deplete the untagged KIN-A allele in the knockdown conditions and cells were fixed after 24 h. All graphs depict the means (bar) ± SD of at least two replicates. A minimum of 300 cells per replicate were quantified. Cell lines: BAP3064, BAP3065. *** $P \leq 0.001$ (two-sided, unpaired t-test).

Discussion

Whereas astonishing diversity in kinetochore composition is seen among eukaryotes (Hooff et al., 2017; Komaki et al., 2022; Tromer et al., 2019), the proteins of the regulatory circuitry underlying chromosome segregation, such as the APC/C, SAC and CPC, are more widely conserved. Homologs of the CPC proteins Aurora B kinase and its associated partner INCENP have been detected in almost all sequenced eukaryotes, including kinetoplastids. The dynamic localization pattern exhibited by the CPC (e.g. transferring from centromeres to the central spindle upon metaphase-anaphase transition) is likewise highly conserved across eukaryotes but appears to be achieved through a variety of mechanisms. For instance, while CPC recruitment to the centromeres in higher eukaryotes is governed by two histone phosphorylation marks (Haspin-mediated H3T3ph and Bub1-mediated H2AT120ph), budding yeasts employ a combination of histone modifications (Bub1-mediated H2AT121ph) and kinetochore proteins as CPC receptors. Borealin^{Bir1} not only recognizes Sgo1 but also interacts with the CBF3 complex through Ndc10 (Cho and Harrison, 2011; Yoon and Carbon, 1999). Furthermore, INCENP^{Sl15}/Aurora B^{Ipl1} interact with the Ctf19 subunit of the COMA complex at kinetochores (Fischböck-Halwachs et al., 2019). The proteins that form the localization module of the CPC in different species appear to mirror the diversity in centromeric CPC receptors. In fact, many phyla lack Borealin or Survivin homologs (Komaki et al., 2022). Komaki et al. recently identified two functionally redundant CPC proteins in *Arabidopsis*, Borealin Related Interactor 1 and 2 (BORI1 and 2), which engage in a triple helix bundle with INCENP and Borealin using a conserved helical domain, but employ an FHA domain instead of a BIR domain to read H3T3ph (Komaki et al., 2022).

In this study, we have identified KIN-A and KIN-B as components of the CPC in trypanosomes, and delineated a novel pathway for centromeric recruitment of the CPC in this evolutionary divergent group of eukaryotes. In agreement with our work, an early study on the CPC in *T. brucei* found that

KIN-A and KIN-B co-purified with Aurora B^{AUK1}, INCENP^{CPC1} and CPC2 based on a pull-down of an Aurora B^{AUK1}-PTP fusion protein followed by mass spectrometry analysis (Li et al., 2008 [DOI](#)). However, HA-tagged KIN-A and KIN-B were not detected at kinetochores (from late interphase until metaphase) nor at the new FAZ tip (from late anaphase), and hence were not interpreted as CPC proteins. Contrary to this report, our data clearly show that KIN-A and KIN-B are constitutive components of the CPC in *T. brucei*. First, YFP-tagged KIN-A and KIN-B co-localize with Aurora B^{AUK1}, INCENP^{CPC1} and CPC2 throughout the cell cycle. Second, KIN-A and KIN-B are readily detected within native CPC complexes isolated by immunoprecipitation of CPC subunits from cells arrested prior to anaphase and form robust crosslinks with the other CPC subunits. Finally, YFP-Aurora B^{AUK1} and INCENP^{CPC1}-YFP are crucially dependent on KIN-A and KIN-B for localizing both to metaphase kinetochores and to the anaphase central spindle. Thus, the KIN-A:KIN-B subcomplex constitutes the localization module of the trypanosome CPC.

Biochemical, cell biological and in silico modelling approaches indicate that the kinesins KIN-A and KIN-B form coiled coils between their central and C-terminal domains, respectively, which then serve as a scaffold onto which INCENP^{CPC1} and CPC2 assemble via their N-terminal α -helical domains. The catalytic module of the trypanosomes CPC, consisting of Aurora B^{AUK1} bound to the C-terminal IN-box of INCENP^{CPC1}, is connected to the KIN-A:KIN-B scaffold through a flexible linker in INCENP^{CPC1}. While our on-beads cross-linking of native CPCs suggests that the catalytic module is positioned in close proximity to the kinesin heads, this may not necessarily be true in vivo. For example, the catalytic module may exist in both 'locked' and 'open' conformations with regard to its association with the kinesin motor domains. We speculate that the interaction of the KIN-A motor domain with microtubules from prometaphase onwards may cause the catalytic module to disengage from its kinesin head-associated state (**Fig. 7** [DOI](#)). In analogy to the SAH domain of INCENP in other model eukaryotes which has been proposed to function as a dog leash (Samejima et al., 2015; Santaguida and Musacchio, 2009 [DOI](#)), the INCENP^{CPC1} flexible linker in trypanosomes (~100 amino acids long) may then permit Aurora B^{AUK1} to roam across a larger but nevertheless spatially constrained target area to phosphorylate its substrates while still being anchored to the kinetochore via KIN-A:KIN-B. Importantly, this mechanism would allow the CPC to act as an intrinsic 'sensor' of KT-MT attachments. Such models dealing with alternative conformations of the CPC in various cellular context will require further testing in the future.

We propose that multiple weak interactions of the KIN-A C-terminal unstructured tail with kinetochore components act in synergy to stabilize the CPC at kinetochores. Critically, these interactions need to be of transient and reversible nature to permit the dynamic release of the CPC upon anaphase onset. Three mechanisms are likely to play a role in this context (**Fig. 7** [DOI](#)). First, removal of the KKT8 complex (the 'CD1 receptor') at the metaphase-anaphase transition effectively eliminates one of the key CPC-kinetochore interfaces. Secondly, the affinity of the KIN-A C-terminal tail for its binding partners at the kinetochore may be further finetuned through reversible post-translational modifications. In support of this, the KIN-A C-terminal tail harbors many putative CRK3 sites (10 sites matching the minimal S/T-P consensus motif for CDKs) and is also heavily phosphorylated by Aurora B^{AUK1} in vitro (Ballmer et al., 2024). Finally, we speculate that the interaction of KIN-A motor domain with microtubules, coupled to the force generating ATP hydrolysis and possibly plus-end directed motion, eventually outcompetes the weakened interactions of the CPC with the kinetochore and facilitates the extraction of the CPC from chromosomes onto spindle microtubules during anaphase. Indeed, deletion of the KIN-A motor domain or impairment of its motor function through N-terminal GFP tagging causes the CPC to be trapped at kinetochores in anaphase. Central spindle localization is additionally dependent on the ATPase activity of the KIN-A motor domain as illustrated by the KIN-A rigor mutant.

It remains to be investigated whether KIN-A functions as a plus-end directed motor. The role of the KIN-B in this context is equally unclear. Because KIN-B does not possess a functional kinesin motor domain, we deem it unlikely that the KIN-A:KIN-B heterodimer moves hand-over-hand along microtubules as do conventional (kinesin-1 family) kinesins. Rather, the KIN-A motor domain may

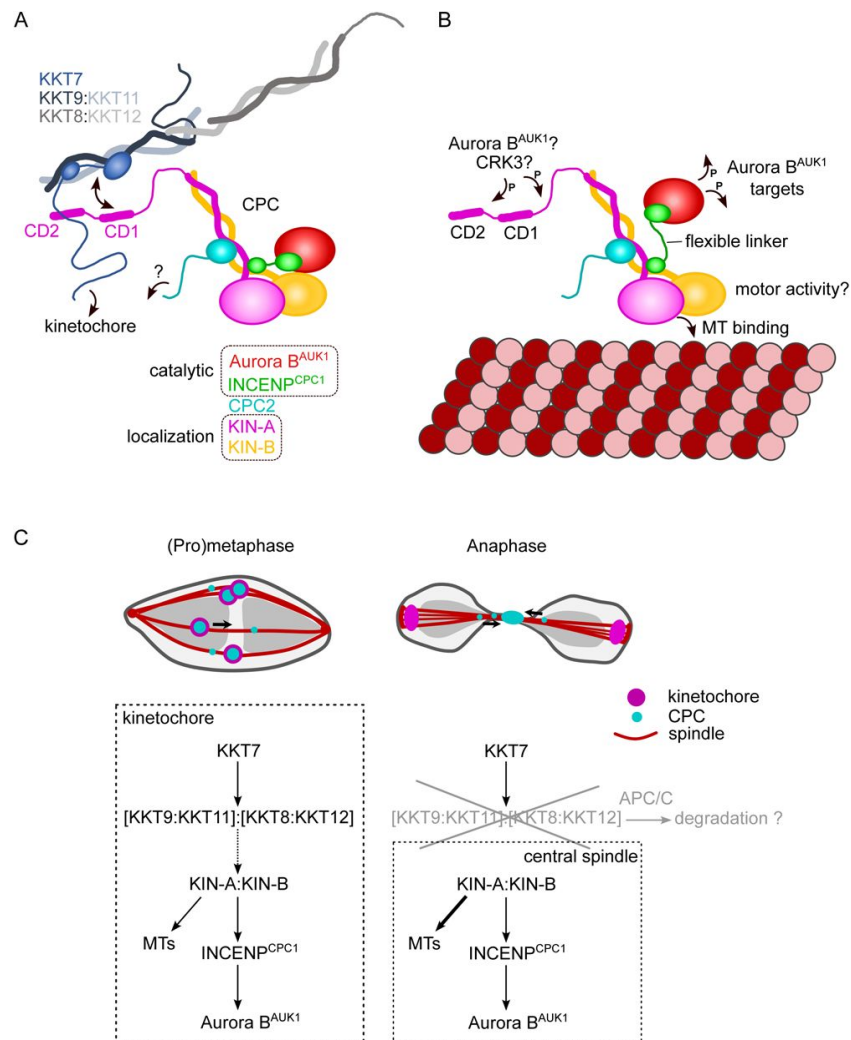


Figure 7.

Model for CPC localization and function in trypanosomes.

(A) KIN-A (magenta) and KIN-B (yellow) interact via their coiled-coil domains and form a scaffold for the assembly of CPC2 (cyan) and the catalytic module of the CPC, composed of Aurora B^{AUK1} (red) and INCENP^{CPC1} (green). During interphase, the catalytic module is positioned close to the kinesin head domains of KIN-A and KIN-B. CPC recruitment to the inner kinetochore is mediated through multiple weak interactions between the C-terminal unstructured tail of KIN-A, containing CD1 and CD2, with the coiled-coil domain of KKT9:KKT11 (dark blue:light blue) and possibly the N-terminus of KKT7 (blue). The KKT8 complex, comprising KKT9:KKT11 and KKT8:KKT12 (dark grey:light grey) subcomplexes, is connected to other kinetochore proteins through KKT7. Additional kinetochore targeting domains of the CPC may reside within the C-terminus of KIN-B and/or CPC2. We propose that the KIN-A:KIN-B subcomplex represents the main localization module of the trypanosome CPC. As illustrated in (B), the affinity of the KIN-A C-terminal tail for its receptor(s) at the kinetochore may be further modulated through phosphorylation by the CDK1 homolog CRK3 and the Aurora B^{AUK1} kinase itself (Ballmer et al., 2024). Interaction of the N-terminal motor domain of KIN-A with spindle microtubules (MTs) from prometaphase onwards causes the catalytic module to disengage from its kinesin head-associated state. The ~100 amino acid long flexible linker within INCENP^{CPC1} would then permit Aurora B^{AUK1} to phosphorylate its substrates within a larger but nevertheless spatially constrained target area while still being anchored to the kinetochore via KIN-A:KIN-B. The motor domain of KIN-A could thus act as built-in sensor for KT-MT attachments. (C) We propose that the trypanosome CPC is recruited to kinetochores via the KKT7-KKT8 complex pathway (dashed arrow) and that motor activity of KIN-A promotes congression of kinetochores to the metaphase plate during early mitosis. The KKT8 complex dissociates from kinetochores at the metaphase-to-anaphase transition and is possibly degraded in an APC/C-dependent manner. Elimination of the KKT8 complex, the primary kinetochore receptor of the CPC, coupled to MT binding and motor activity of the KIN-A motor domain strips the CPC off kinetochores and facilitates its translocation to the central spindle in anaphase.

function as a single-headed unit and drive processive plus-end directed motion using a mechanism similar to the kinesin-3 family kinesin KIF1A (Okada and Hirokawa, 1999 [↗](#)). Formation of transient complexes between the CPC and kinesins or other microtubule plus-end tracking proteins upon anaphase onset appears to be a common theme underlying the central spindle translocation of the CPC. For instance, the CPC interacts with MKLP2 or Bim1^{EB1} in human and yeast cells, respectively (Gruneberg et al., 2004 [↗](#); Zimniak et al., 2012 [↗](#)). Thus, deeper understanding of the CPC regulation in trypanosomes is bound to provide evolutionary insights into fundamental principles of chromosome segregation in eukaryotes and can lead to the discovery of druggable targets to combat kinetoplastid diseases (Saldivia et al., 2020 [↗](#)).

Materials and Methods

Cloning

All primers, plasmids, bacmids, and synthetic DNA used in this study as well as their source or construction details are described in Supplemental Table S1. All constructs were sequence verified.

Trypanosome culture

All trypanosome cell lines used in this study were derived from *T. brucei* SmOxP927 procyclic form cells (TREU 927/4 expressing T7 RNA polymerase and the tetracycline repressor to allow inducible expression; Poon et al., 2012) or from PCF1339 procyclic form cells (TREU 927/4 expressing T7 RNA polymerase, tetracycline repressor and the Cas9 nuclease, Beneke et al., 2017 [↗](#)) and are described in Supplemental Table S1. Cells were grown at 28°C in SDM-79 medium supplemented with 10% (vol/vol) heat-inactivated fetal calf serum, 7.5 µg/ml hemin (Brun and Schönenberger, 1979 [↗](#)), and appropriate selection drugs. Cell growth was monitored using a CASY cell counter (Roche). PCR products or plasmids linearized by NotI were transfected into cells by electroporation (Biorad). Transfected cells were selected by the addition of 30 µg/ml G418 (Sigma), 25 µg/ml hygromycin (Sigma), 5 µg/ml phleomycin (Sigma), or 10 µg/ml blasticidin S (Insight biotechnology). To obtain endogenously tagged clonal strains, transfected cells were selected by the addition of appropriate drugs and cloned by dispensing dilutions into 96-well plates. Endogenous YFP tagging was performed using the pEnT5-Y vector (Kelly et al., 2007 [↗](#)) or a PCR-based method (Dean et al., 2015 [↗](#)). Endogenous tdTomato tagging was performed using pBA148 (Akiyoshi and Gull, 2014 [↗](#)) and its derivatives. All constructs for ectopic expression of GFP fusion proteins include a short nuclear localization signal (NLS) (Marchetti et al., 2000 [↗](#)). For doxycycline inducible expression of head-to-head (pBA3-based) and hairpin (pBA310-based) RNAi constructs, GFP-NLS (pBA310-based) and GFP-NLS-LacI fusion proteins (pBA795-based), the linearized plasmids were integrated into 177-bp repeats on minichromosomes. Expression of GFP-NLS or GFP-NLS-LacI fusions was induced by the addition of 10 ng/mL doxycycline for 24 h. RNAi was induced by the addition of 1 µg/ml doxycycline. LacO–LacI tethering experiments were carried out as described previously using the LacO array inserted at the rDNA locus (Ishii and Akiyoshi, 2020 [↗](#); Landeira and Navarro, 2007 [↗](#)).

Immunoprecipitation followed by mass spectrometry (IP-MS)

For standard IPs, 400-ml cultures of asynchronously growing cells were grown to ~5 – 10 million cells/ml. Cells were pelleted by centrifugation (800 g, 10 min), washed once with PBS, and extracted in PEME (100 mM Pipes-NaOH, pH 6.9, 2 mM EGTA, 1 mM MgSO₄, and 0.1 mM EDTA) with 1% NP-40, protease inhibitors (10 µg/ml leupeptin, 10 µg/ml pepstatin, 10 µg/ml E-64, and 0.2 mM PMSF) and phosphatase inhibitors (1 mM sodium pyrophosphate, 2 mM Na-β-glycerophosphate, 0.1 mM Na₃VO₄, 5 mM NaF, and 100 nM microcystin-LR) for 5 min at RT, followed by centrifugation at 1,800 g for 15 min. Samples were kept on ice from this point on. The pelleted fraction containing kinetochore proteins was resuspended in modified buffer H (BH0.15: 25 mM Hepes, pH 8.0, 2 mM MgCl₂, 0.1 mM EDTA, pH 8.0, 0.5 mM EGTA, pH 8.0, 1% NP-40, 150 mM KCl, and 15% glycerol) with

protease and phosphatase inhibitors. Samples were sonicated to solubilize kinetochore proteins (12 s, three times with 1-min intervals on ice). 12 µg of mouse monoclonal anti-GFP antibodies (11814460001; Roche) pre-conjugated with 60 µl slurry of Protein-G magnetic beads (10004D; Thermo Fisher Scientific) with dimethyl pimelimidate (Unnikrishnan et al., 2012) were incubated with the extracts for 2.5 h with constant rotation, followed by four washes with modified BH0.15 containing protease inhibitors, phosphatase inhibitors and 2 mM DTT. Beads were further washed three times with pre-elution buffer (50 mM Tris-HCl, pH 8.3, 75 mM KCl, and 1 mM EGTA). Bound proteins were eluted from the beads by agitation in 60 µl of elution buffer (0.1% RapiGest [186001860; Waters] and 50 mM Tris-HCl, pH 8.3) for 25 min at RT. Eluates were then incubated at 100°C for 5 min. Proteins were reduced with 5 mM DTT at 37°C for 30 min and alkylated with 10 mM iodoacetamide at 37°C for 30 min. The reaction was quenched by adding 10 mM DTT at 37°C for 30 min, and 100 µl of 20 mM Tris-HCl (pH 8.3) was added. Proteins were digested overnight at 37°C with 0.2 µg trypsin (Promega). Formic acid was then added to 2% and the samples were incubated at 37°C for 30 min to cleave RapiGest, followed by centrifugation for 10 min. The supernatant was desalted over a C18 column and analyzed by electrospray tandem mass spectrometry over a 60-min gradient using Q-Exactive (Thermo Fisher Scientific) at the Advanced Proteomics Facility (University of Oxford). Peptides were identified by searching tandem mass spectrometry spectra against the *T. brucei* protein database with MaxQuant (version 2.0.1) with carbamidomethyl cysteine set as a fixed modification and oxidation (Met), phosphorylation (Ser, Thr, and Tyr), and acetylation (Lys) set as variable modifications. Up to two missed cleavages were allowed. The first peptide tolerance was set to 10 ppm. Results were filtered to remove contaminants and reverse hits. Proteins identified with at least two peptides were considered as significant and shown in Table S2 (protein FDR 1%).

Ex vivo cross-linking of the native CPC and kinetochore complexes (IP-CLMS)

For cross-linking IP-MS experiments, cell cultures were scaled up to 1,600 mL. Cell cultures were treated with 10 µM MG132 for 4 h to enrich for cells in metaphase. Cell lysis and immunoprecipitation steps were carried out as described above. After four washes with modified BH0.15 containing protease inhibitors, phosphatase inhibitors and 2 mM DTT, beads were washed three times with 25 mM HEPES pH7.5, 150 mM NaCl. Proteins were then cross-linked on beads with 0.4 mM BS³ (bis(sulfosuccinimidyl)suberate) (Thermo Fisher Scientific) for 30 min at RT with agitation, followed by three washes in 25 mM HEPES pH7.5, 150 mM NaCl and a further three washes in 0.1 M ammonium bicarbonate. Samples were then incubated in 8 M urea dissolved in 0.1 M ammonium bicarbonate for 10 min at RT with agitation. Proteins were reduced with 10 mM TCEP for 20 min and alkylated with 10 mM iodoacetamide for 40 min at RT. Proteins were then pre-digested with 0.4 µg LysC for 2 h at 37°C. The urea concentration in the sample was brought down to < 1 M by addition of 0.1 M ammonium bicarbonate before adding CaCl₂ (to 2 mM) and 0.7 µg of trypsin for overnight digestion at 37°C. Formic acid was then added to 2% and the samples were frozen. The cross-linked samples were further processed and analyzed at the proteomics core facility at EMBL Heidelberg. Digested peptides were concentrated and desalted using an OASIS HLB µElution Plate (Waters) according to manufacturer instructions. Crosslinked peptides were enriched using size exclusion chromatography (Leitner et al., 2012). In brief, desalted peptides were reconstituted with SEC buffer (30% (v/v) ACN in 0.1% (v/v) TFA) and fractionated using a Superdex Peptide PC 3.2/30 column (GE) on a 1200 Infinity HPLC system (Agilent) at a flow rate of 0.05 ml/min. Fractions eluting between 50-70 µl were evaporated to dryness and reconstituted in 30 µl 4% (v/v) ACN in 1% (v/v) FA. Collected fractions were analyzed by liquid chromatography (LC)-coupled tandem mass spectrometry (MS/MS) using an UltiMate 3000 RSLC nano LC system (Dionex) fitted with a trapping cartridge (µ-Pre-column C18 PepMap 100, 5µm, 300 µm i.d. x 5 mm, 100 Å) and an analytical column (nanoEase M/Z HSS T3 column 75 µm x 250 mm C18, 1.8 µm, 100 Å, Waters). Trapping was carried out with a constant flow of trapping solvent (0.05% trifluoroacetic acid in water) at 30 µl/min onto the trapping column for 6 minutes. Subsequently, peptides were eluted and separated on the analytical column using a

gradient composed of Solvent A (3% DMSO, 0.1% formic acid in water) and solvent B (3% DMSO, 0.1% formic acid in acetonitrile) with a constant flow of 0.3 $\mu\text{l}/\text{min}$. The outlet of the analytical column was coupled directly to an Orbitrap Fusion Lumos (Thermo Scientific, SanJose) mass spectrometer using the nanoFlex source. The peptides were introduced into the Orbitrap Fusion Lumos via a Pico-Tip Emitter 360 μm OD x 20 μm ID; 10 μm tip (CoAnn Technologies) and an applied spray voltage of 2.1 kV, instrument was operated in positive mode. The capillary temperature was set at 275°C. Only charge states of 4-8 were included. The dynamic exclusion was set to 30 sec. and the intensity threshold was $5e^4$. Full mass scans were acquired for a mass range 350-1700 m/z in profile mode in the orbitrap with resolution of 120000. The AGC target was set to Standard and the injection time mode was set to Auto. The instrument was operated in data dependent acquisition (DDA) mode with a cycle time of 3 sec between master scans and MSMS scans were acquired in the Orbitrap with a resolution of 30000, with a fill time of up to 100 ms and a limitation of $2e^5$ ions (AGC target). A normalized collision energy of 32 was applied. MS2 data was acquired in profile mode. RAW MS files were searched by the pLink2 software (Chen et al., 2019), with carbamidomethyl cysteine set as a fixed and oxidation (Met) set as variable modifications. Up to two missed cleavages were allowed. Precursor tolerance was set to 10 ppm. All the identified cross-links are shown in Table S2 (FDR 5%). Cross-links were plotted using xiView (Graham et al., 2019). All raw mass spectrometry files and custom database files used in this study have been deposited with the ProteomeXchange Consortium via the PRIDE partner repository (Deutsch et al., 2020; Perez-Riverol et al., 2019) with the dataset identifier PXD045987.

Fluorescence microscopy

Cells were washed once with PBS, settled onto glass slides, and fixed with 4% paraformaldehyde in PBS for 5 min as described previously (Nerusheva and Akiyoshi, 2016). Cells were then permeabilized with 0.1% NP-40 in PBS for 5 min and embedded in mounting media (1% wt/vol 1,4-diazabicyclo[2.2.2]octane, 90% glycerol, 50 mM sodium phosphate, pH 8.0) containing 100 ng/ml DAPI. Images were captured on a Zeiss Axioimager.Z2 microscope (Zeiss) installed with ZEN using a Hamamatsu ORCA-Flash4.0 camera with 63 \times objective lenses (1.40 NA). Typically, ~20 optical slices spaced 0.2 or 0.24 μm apart were collected. Images were analysed in ImageJ/Fiji (Schneider et al., 2012). Kinetochore localization of endogenously tagged kinetochore proteins or ectopically expressed constructs were examined manually by quantifying the number of cells that clearly had detectable kinetochore-like dots at indicated cell cycle stages. Shown images are central slices.

In silico structure and interaction predictions

Structures and interactions were predicted with AlphaFold2-Multimer-v2 (Evans et al., 2022; Jumper et al., 2021) through ColabFold using MMseqs2 (UniRef+Environmental) and default settings (Mirdita et al., 2022). Structural predictions of KIN-A/KIN-B, KIN-A³¹⁰⁻⁸⁶²/KIN-B³¹⁷⁻⁶²⁴, CPC1/CPC2/KIN-A³⁰⁰⁻⁵⁹⁹/KIN-B³¹⁷⁻⁶²⁴, and KIN-A⁷⁰⁰⁻⁸⁰⁰/KKT9/KKT11 were performed using ColabFold version 1.3.0 (AlphaFold-Multimer version 2), while those of AUK1/CPC1/CPC2/KIN-A¹⁻⁵⁹⁹/KIN-B, KKT7¹⁻²⁶¹/KKT9/KKT11/KKT8/KKT12, KKT9/KKT11/KKT8/KKT12, and KKT7¹⁻²⁶¹/KKT9/KKT11 were performed using ColabFold version 1.5.3 (AlphaFold-Multimer version 2.3.1) using default settings, accessed via <https://colab.research.google.com/github/sokrypton/ColabFold/blob/v1.3.0/AlphaFold2.ipynb> and <https://colab.research.google.com/github/sokrypton/ColabFold/blob/v1.5.3/AlphaFold2.ipynb>. All structure figures were made using PyMOL version 2.5.2 (Schrödinger, LLC). The following command was used to map pLDDT score onto the AF2 predicted structure models: spectrum b, rainbow_rev, maximum=100, minimum=50.

Protein purification from *E. coli*

Recombinant 6HIS-KKT8, KKT9, KKT11, KKT12 (pBA457) and derivatives were expressed in Rosetta 2(DE3)pLys *E. coli* cells (Novagen). 6HIS-KIN-A²⁻³⁰⁹ (pBA2519) and 6HIS-KIN-B²⁻³¹⁶ (pBA2513) were expressed in BL21(DE3) cells. Proteins were purified and eluted from TALON beads as previously

described (Llauró et al., 2018). Briefly, cells were grown in 2xTY media at 37°C to an OD₆₀₀ of ~0.8, at which point protein expression was induced by 0.1 mM IPTG, and then incubated overnight at 20°C. Cells were pelleted at 3,400 g at 4°C and pellets were resuspended in P500 buffer (50 mM sodium phosphate, pH 7.5, 500 mM NaCl, 5 mM imidazole and 10% glycerol) supplemented with protease inhibitors (20 µg/ml leupeptin, 20 µg/ml pepstatin, 20 µg/ml E-64, 0.4 mM PMSF) and 1 mM TCEP, and were sonicated on ice. Lysates were treated with benzonase nuclease (500 U/1 l culture) and spun at 48,000 g at 4°C for 30 min. Supernatant was incubated with TALON beads (Takara Clontech) for 1 h at 4°C, rotating. The beads were washed three times with lysis buffer and proteins were then eluted with elution buffer (P500 buffer containing 250 mM imidazole with 1 mM TCEP). For microtubule co-sedimentation assays, 6HIS-KIN-A²⁻³⁰⁹ and 6HIS-KIN-B²⁻³¹⁶ were buffer exchanged into BRB80 (80 mM Pipes-KOH, pH 6.9, 1 mM EGTA, and 1 mM MgCl₂) with 100 mM KCl using a Zeba columns (Thermo Fisher) and flash-frozen in liquid nitrogen for -80°C storage. Polyacrylamide gels were stained with SimplyBlue SafeStain (Invitrogen).

Microtubule co-sedimentation assay

Microtubule co-sedimentation assays were performed as described previously (Ludzia et al., 2021). Briefly, taxol-stabilised microtubules were prepared by mixing 2.5 ml of 100 µM porcine tubulin (Cytoskeleton) resuspended in BRB80 with 1 mM GTP (Cytoskeleton), 1.25 µl BRB80, 0.5 µl of 40 mM MgCl₂, 0.5 µl of 10 mM GTP, and 0.25 µl DMSO, and incubated for 20 min at 37°C. 120 ml of pre-warmed BRB80 containing 12.5 µM Taxol (paclitaxel; Sigma) was added to the sample to bring the microtubule concentration to ~2 µM. 20 µl of 6HIS-KIN-A²⁻³⁰⁹ or 6HIS-KIN-B²⁻³¹⁶ (at final concentration of 4 µM) in BRB80 with 100 mM KCl were mixed with 20 µl of microtubules (final, 1 µM) and incubated for 45 min at room temperature. As a control, we incubated 6HIS-KIN-A²⁻³⁰⁹ or 6HIS-KIN-B²⁻³¹⁶ with BRB80 (with 12.5 µM Taxol). The samples were spun at 20,000 g at room temperature for 10 min, and the supernatant was collected. To the tubes containing pelleted fractions, we added 40 µl of chilled BRB80 with 5 mM CaCl₂ and incubated on ice for 5 min to depolymerise microtubules. Following the incubation, samples were boiled for 5 min before SDS-PAGE. Gels were stained with SimplyBlue Safe Stain (Invitrogen). Co-sedimentation assays were performed at least twice with similar results.

Immunoblotting

Cells were harvested by centrifugation (800 g, 5 min) and washed with 1 ml PBS. The pellet was resuspended in 1× LDS sample buffer (Thermo Fisher) with 0.1 M DTT. Denaturation of proteins was performed for 5 min at 95°C. SDS-PAGE and immunoblots were performed by standard methods using the following antibodies: rabbit polyclonal anti-GFP (TP401, 1:5000) and mouse monoclonal TAT1 (anti-trypanosomal-alpha-tubulin, 1:5000, a kind gift from Keith Gull) (Woods et al., 1989). Secondary antibodies used were: IRDye 680RD goat anti-mouse (LI-COR, 926-68070) and IRDye 800CW goat anti-rabbit (LI-COR, 926-32211). Bands were visualized on an ODYSSEY Fc Imaging System (LI-COR).

Multiple sequence alignment

Protein sequences and accession numbers for Aurora B^{AUK1}, INCENP^{CPC1}, CPC2, KIN-A and KIN-B used in this study were retrieved from the TriTryp database (Aslett et al., 2010), UniProt (Bateman, 2019), or a published study (Butenko et al., 2020). Searches for homologous proteins were done using BLAST in the TriTryp database (Aslett et al., 2010) or using hmmsearch using manually prepared hmm profiles (HMMER version 3.0; Eddy, 1998). The top hit in each organism was considered as a true ortholog only if the reciprocal BLAST search returned the query protein as a top hit in *T. brucei*. Multiple sequence alignment was performed with MAFFT (L-INS-i method, version 7) (Katoh et al., 2019) and visualised with the Clustalx colouring scheme in Jalview (version 2.10) (Waterhouse et al., 2009).

Acknowledgements

We thank Miguel Navarro (Instituto de Parasitología y Biomedicina López-Neyra, Consejo Superior de Investigaciones Científicas, Spain) for providing pMig75 and pMig96 plasmids and Midori Ishii Kanazawa and William Carter for helping trypanosome strain construction. We thank the Micron Advanced Bioimaging Unit and the Advanced Proteomics Facility at the University of Oxford, and the Proteomics Core Facility at the EMBL in Heidelberg, especially Mandy Rettel and Jennifer Schwarz, for their support. We also thank Patryk Ludzia and Midori Ishii Kanazawa for comments on our manuscript. D. Ballmer was supported by the Berrow Foundation. B. Akiyoshi was supported by a Wellcome Trust Senior Research Fellowship (grant 210622/Z/18/Z).

The authors declare no competing financial interest.

Rights retention: This research was funded in whole or in part by Wellcome Trust (grant 210622/Z/18/Z). For the purpose of Open Access, the author has applied a CC BY public copyright licence to any Author Accepted Manuscript (AAM) version arising from this submission.

Author contributions: D. Ballmer performed essentially all experiments except for some LacI/LacO tethering experiments that were performed by B. Akiyoshi. D. Ballmer wrote the manuscript. B. Akiyoshi edited the manuscript.

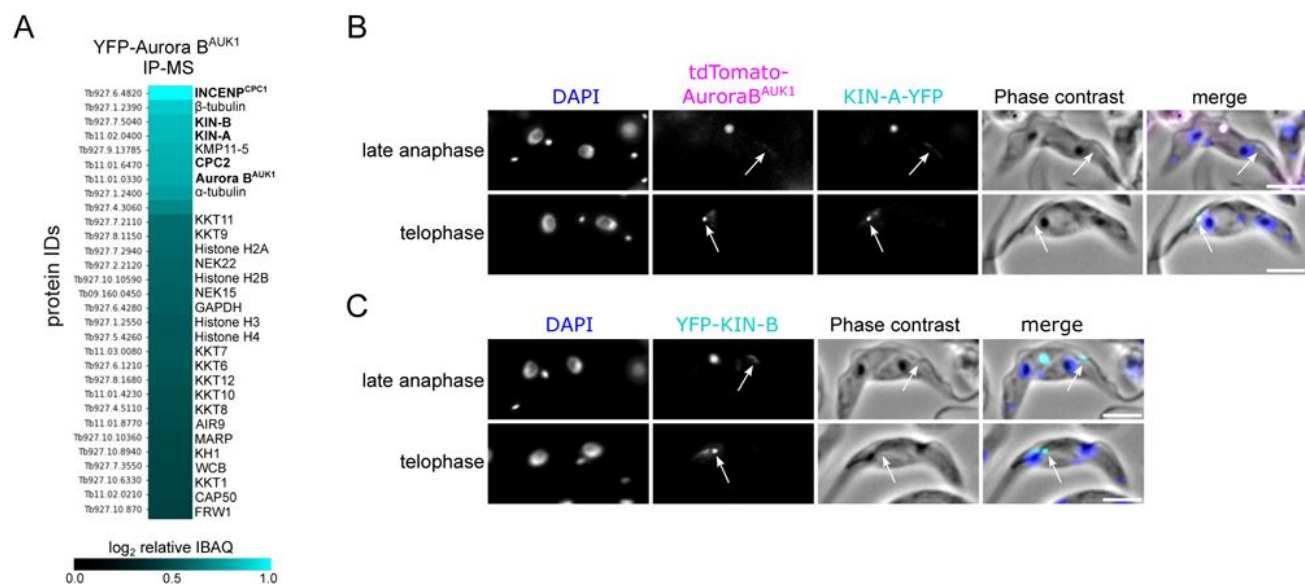
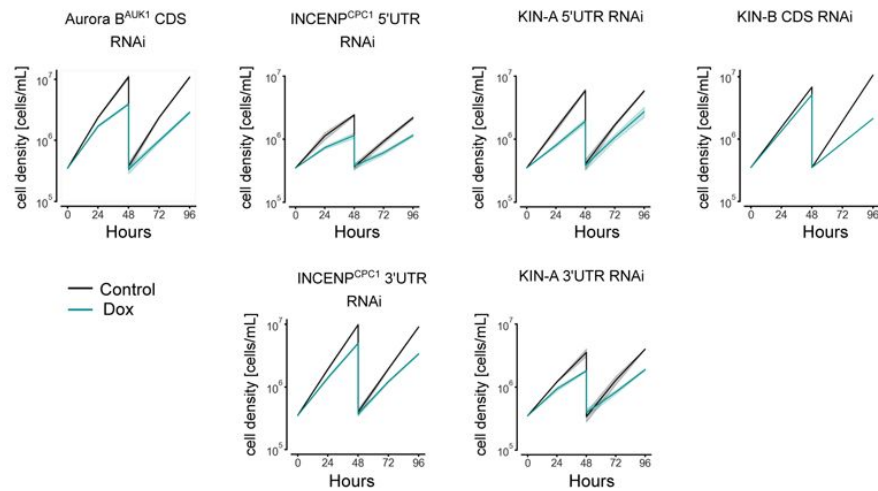


Figure S1.

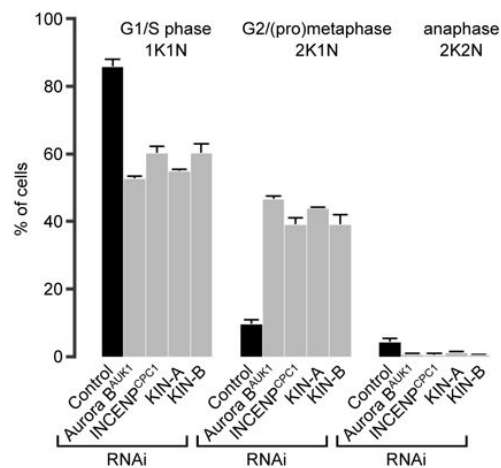
KIN-A and KIN-B are bona fide CPC proteins in *T. brucei*.

(A) Heatmap showing enrichment (log₂ intensity based absolute quantification (IBAQ)) of the top 30 proteins, excluding ribosomal proteins, co-purifying with YFP-Aurora B^{AUK1}. Cell line: BAP73. Immunoprecipitation was performed using anti-GFP antibodies. See Table S2 for all proteins identified by mass spectrometry. (B) and (C) Representative fluorescence micrographs showing the localization of tdTomato-Aurora B^{AUK1} and KIN-A-YFP (B) and YFP-KIN-B (C) in late anaphase and telophase cells. Arrows indicate the population of CPC proteins localized to the new FAZ tip. DNA was stained with DAPI. Cell lines: BAP3067, BAP2528. Scale bars, 2 μm.

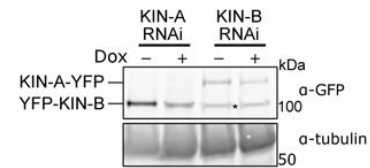
A



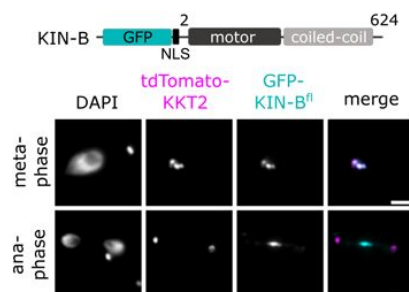
B



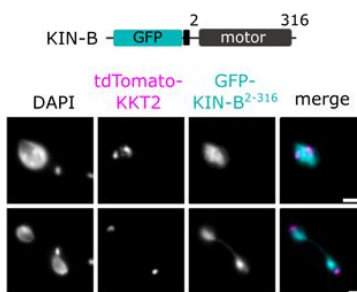
C



D



E



F

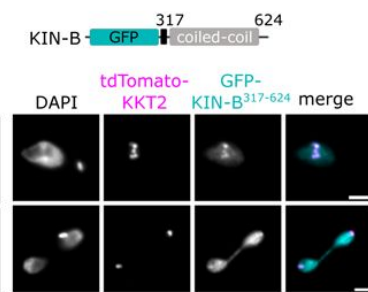


Figure S2.

Depletion of CPC proteins causes growth defects and cell cycle arrest.

(A) Growth curves upon RNAi-mediated knockdown of indicated CPC subunits. Data are presented as the mean \pm SD of at least three replicates. RNAi was induced with 1 μ g/mL doxycycline and cultures were diluted at day 2. CDS stands for coding sequence, UTR for untranslated region. Cell lines: BAP941, BAP2250, BAP2251, BAP2557, BAP2558, BAP3076. (B) Cell cycle profiles upon knockdown of indicated CPC subunits. RNAi was induced with 1 μ g/mL doxycycline and cells were fixed at 16h (for Aurora B^{AUK1}, INCENP^{CPC1} and KIN-A RNAi) or 24 h (CPC2 and KIN-B RNAi). All graphs depict the means (bar) \pm SD of at least two replicates. A minimum of 150 cells per replicate were quantified. Cell lines: BAP3092, BAP2554, BAP2557, BAP3093. (C) Western Blot showing levels of YFP-tagged KIN-A or KIN-B upon RNAi-mediated knockdown of KIN-B and KIN-A, respectively. RNAi was induced with 1 μ g/mL doxycycline for 16 h (KIN-A) or 24 h (KIN-B). Proteins were detected using anti GFP-antibodies. Asterisk indicates unspecific band. Cell lines: BAP3095, BAP2564. (D) to (F) Representative fluorescence micrographs showing the localization of ectopically expressed GFP-KIN-B^{fl} (D), -KIN-B²⁻³¹⁶ (E) and -KIN-B³¹⁷⁻⁶²⁴ (F). Expression of GFP fusion proteins was induced with 10 ng/mL doxycycline for 24 h. Kinetochores are marked with tdTomato-KKT2. Cell lines: BAP2288, BAP2289, BAP2290. Scale bars, 2 μ m.

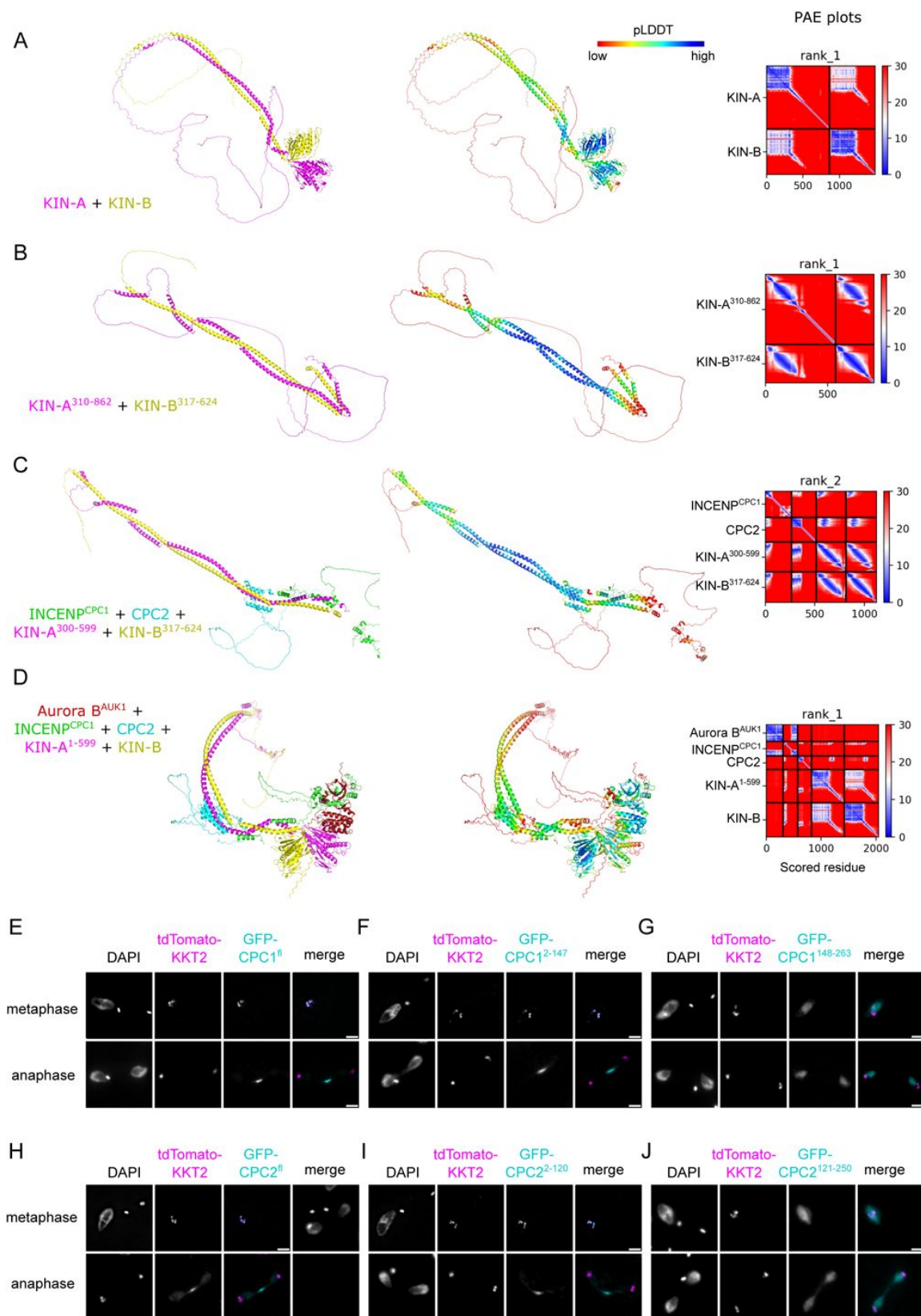


Figure S3.

AlphaFold2 models of CPC subcomplexes and localization of CPC1 and CPC2 truncations.

(A) to (D) Cartoon representations coloured by protein (left) and pLDDT (center), and PAE plots (right) of AlphaFold2 predictions for indicated CPC subcomplexes. (E) to (J) Representative fluorescence micrographs showing the localization of ectopically expressed GFP-INCENP^{CPC1 fl} (E), -INCENP^{CPC1 2-147} (F), -INCENP^{CPC1 2-147} (G), -CPC2^{fl} (H), -CPC2²⁻¹²⁰ (I) and -CPC2¹²¹⁻²⁵⁰ (J) in different cell cycle stages. Expression of GFP fusion proteins was induced with 10 ng/mL doxycycline for 24 h. Kinetochores are marked with tdTomato-KKT2. Cell lines: BAP2190, BAP2191, BAP2193, BAP2194, BAP2195, BAP2196. Scale bars, 2 μ m.

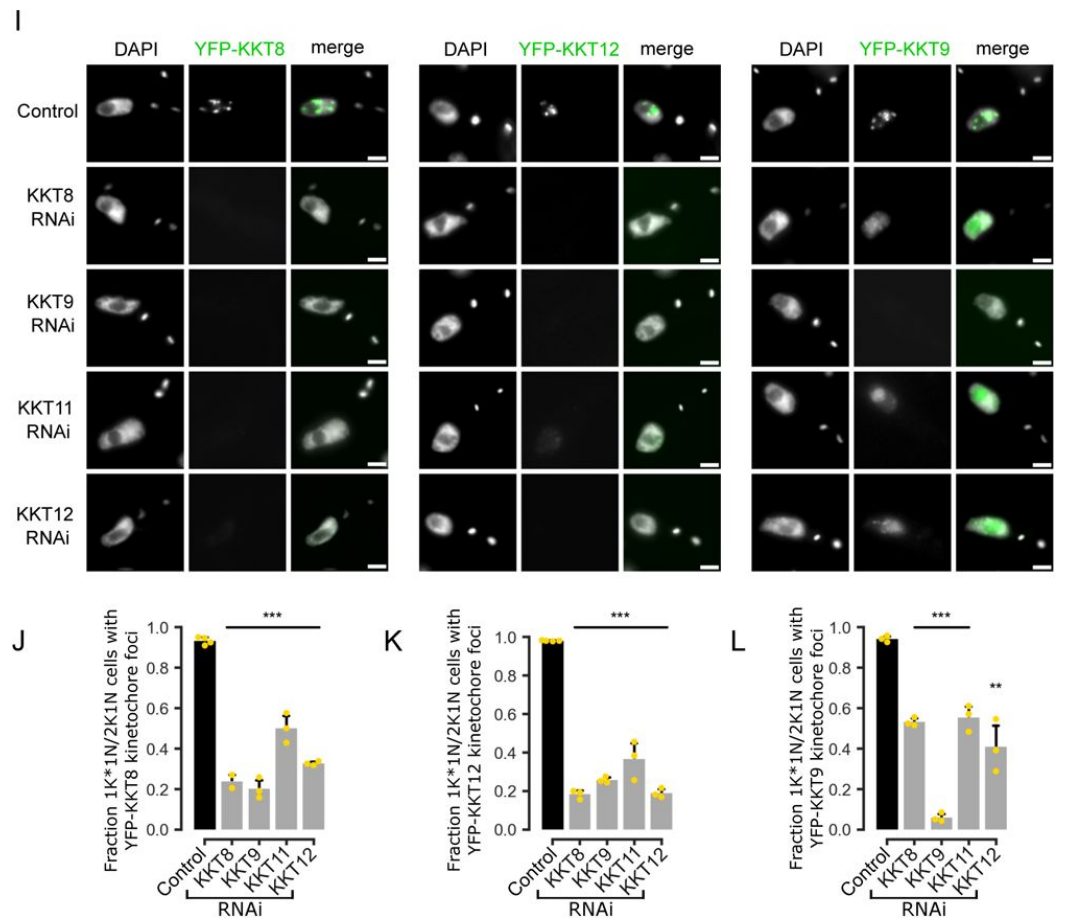


Figure S4.

Kinetochores localization of Aurora B^{AUK1} and KIN-A depends on the KKT7 – KKT8 complex pathway.

(A) Representative fluorescence micrographs showing the localization of YFP-Aurora B^{AUK1} upon RNA-mediated knockdown of indicated KKT proteins. RNAi was induced with 1 µg/mL doxycycline for 24 h. Cell lines: BAP3132, BAP576, BAP2551, BAP2550, BAP3133, BAP1019, BAP2549, BAP2446. Scale bars, 2 µm. (B) Quantification of 2K1N cells that have kinetochore-like dots of YFP-Aurora B^{AUK1} upon knockdown of indicated KKT proteins. A minimum of 40 cells per replicate were examined. (C) Representative fluorescence micrographs showing the localization of KIN-A-YFP upon RNA-mediated knockdown of KKT8 complex subunits. RNAi was induced with 1 µg/mL doxycycline for 24 h. Cell lines: BAP2970, BAP2968, BAP2969, BAP2971. Scale bars, 2 µm. (D) Quantification of 2K1N cells that have kinetochore-like dots of KIN-A-YFP upon knockdown of indicated KKT8 complex subunits. All graphs depict the means (bar) ± SD of at least two replicates (shown as dots). A minimum of 50 cells per replicate were quantified. (E) Representative micrographs showing recruitment of tdTomato-tagged KKT8, KKT9 and KKT12 to LacO foci marked by ectopically expressed GFP-KKT7²⁻²⁶¹-LacI. Expression of GFP fusion proteins was induced with 10 ng/mL doxycycline for 24 h. Cell lines: BAP871, BAP873, BAP874. Scale bars, 2 µm. (F) Representative fluorescence micrograph of an anaphase cell showing localization of tdTomato-KKT8 and ectopically expressed GFP-KIN-A. The insets show the magnification of the boxed region. Expression of GFP-KIN-A was induced with 10 ng/mL doxycycline for 24 h. Cell line: BAP3080. Scale bars, 2 µm. (G) and (H) Cartoon representations coloured by protein (left) and pLDDT (center), and PAE plots (right) of AlphaFold2 predictions for indicated protein complexes. (I) Representative fluorescence micrographs showing localization of YFP-tagged KKT8, KKT12 and KKT9 upon RNAi-mediated knockdown of indicated KKT8 complex subunits. RNAi was induced with 1 µg/mL doxycycline for 24 h. Cell lines: BAP2954, BAP2952, BAP2953, BAP2955, BAP2966, BAP2964, BAP2965, BAP2967, BAP2958, BAP2956, BAP2957, BAP2959. Scale bars, 2 µm. (J) to (L) Quantification of 1K*1N and 2K1N cells that have kinetochore-like dots of YFP-tagged KKT8 (J), KKT12 (K) and KKT9 (L) upon knockdown of indicated KKT8 complex subunits. All graphs depict the means (bar) ± SD of at least three technical replicates (shown as dots) from one experiment. A minimum of 100 cells per replicate were quantified. ** $P \leq 0.01$, *** $P \leq 0.001$ (two-sided, unpaired t-test).

A

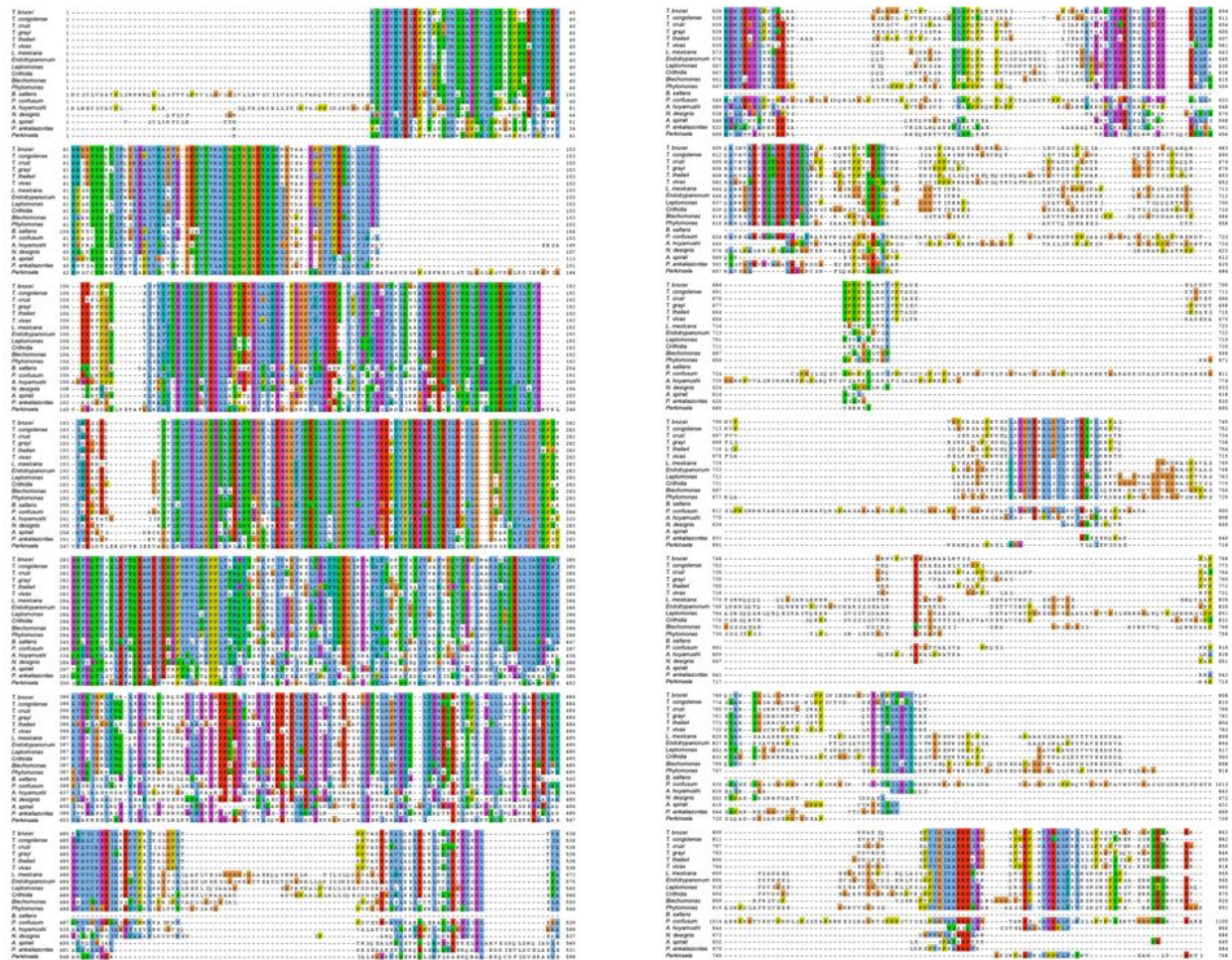


Figure S5.

CD1 and CD2 contribute synergistically to kinetochore localization of KIN-A.

(A) Multiple sequence alignment of KIN-A. (B) PAE (left) and pLDDT plots (right) of AlphaFold2 predictions rank1 to rank5 for KIN-A⁷⁰⁰⁻⁸⁰⁰ in complex with KKT9 and KKT11. (C) to (F) Representative fluorescence micrographs showing the localization of ectopically expressed GFP-KIN-A³¹⁰⁻⁸⁶² (C), -KIN-A³¹⁰⁻⁸⁶² Δ CD2 (D) and -KIN-B³¹⁰⁻⁸⁶² Δ CD1 (E) and -KIN-A³¹⁰⁻⁷¹⁶ (F). Expression of GFP fusion proteins was induced with 10 ng/mL doxycycline for 24 h. Kinetochores are marked with tdTomato-KKT2. Cell lines: BAP2287, BAP2948, BAP2949, BAP2947. Scale bars, 2 μ m. (G) Quantification of metaphase (left) and anaphase (right) cells that have kinetochore-like dots of indicated GFP fusion proteins. All graphs depict the means (bar) \pm SD of three replicates (shown as dots). A minimum of 150 cells per replicate were quantified. *** $P \leq 0.001$ (two-sided, unpaired t-test). (H) Stacked bar charts showing the percentage of KIN-A ^{Δ CD1}-YFP (left) or tdTomato-Aurora B^{AUK1} (right) on kinetochores, kinetochores + spindle and spindle in KIN-A ^{Δ CD1} metaphase cells with and without KIN-A RNAi. A minimum of 70 cells per condition were quantified. Cell line: BAP3128. (I) Cell cycle profiles for the indicated cell lines and conditions. RNAi was induced with 1 μ g/mL doxycycline to deplete the untagged KIN-A allele in the knockdown conditions and cells were fixed after 24 h. All graphs depict the means (bar) \pm SD of three replicates. A minimum of 500 cells per replicate were quantified. Cell lines: BAP3067, BAP3127, BAP3128.

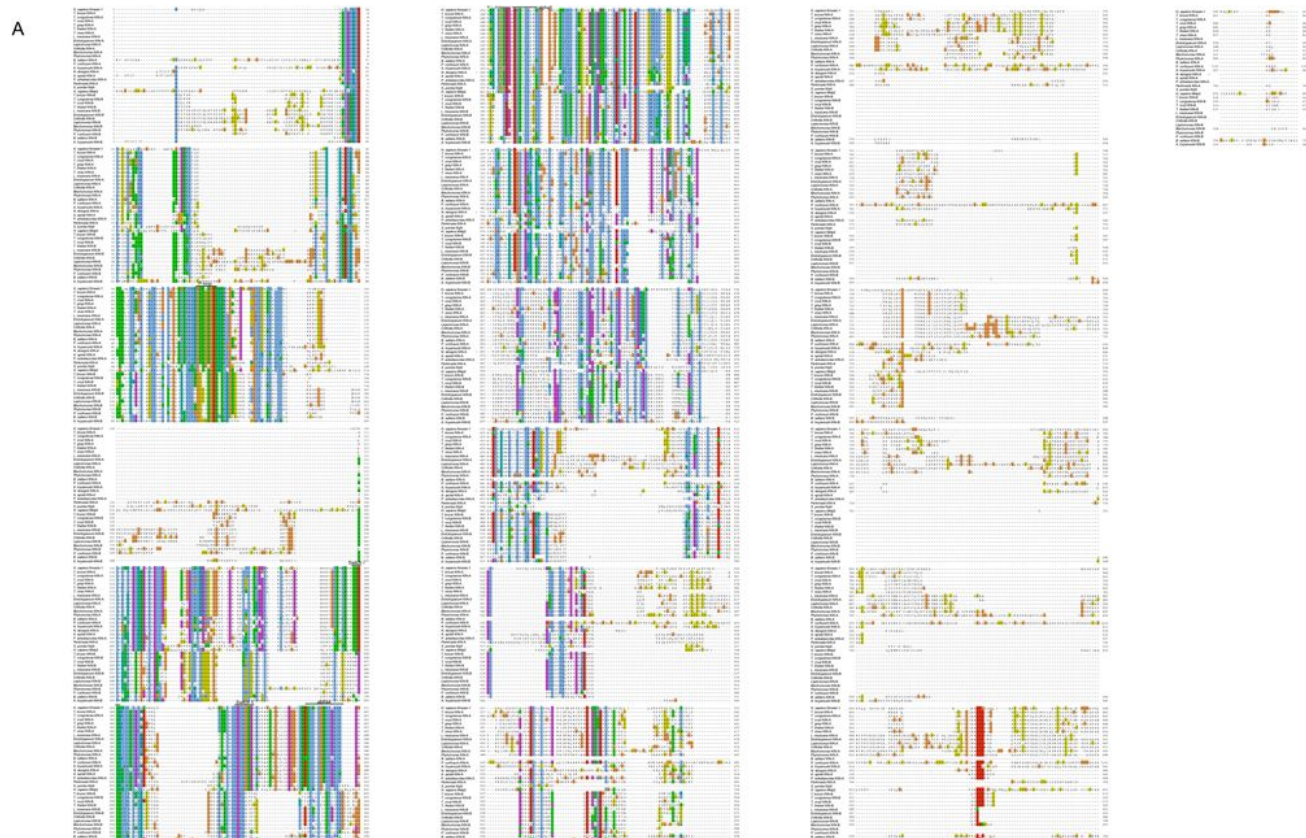


Figure S6.

ATPase activity of KIN-A promotes kinetochore alignment at the metaphase plate.

(A) Multiple sequence alignment of KIN-A and KIN-B from different kinetoplastids, human Kinesin-1, human Mklp2, and yeast Klp9. (B) Microtubule co-sedimentation assay with 6HIS-KIN-A²⁻³⁰⁹ (left) and 6HIS-KIN-B²⁻³¹⁶ (right). S and P correspond to supernatant and pellet fractions, respectively. Note that both constructs to some extent sedimented even in the absence of microtubules. Hence, lack of microtubule binding for KIN-B may be due to the unstable non-functional protein used in this study. (C) and (D) Representative fluorescence micrographs showing localization of YFP-tagged KIN-A (C) and KIN-A^{G210A} (rigor mutant) (D) in G2 and metaphase. Kinetochores are marked with tdTomato-KKT2. Cell lines: BAP3066, BAP3069. Scale bars, 2 μm. (E) and (F) Upper: Representative fluorescence micrographs showing localization of YFP-tagged KIN-A (E) and KIN-A^{G210A} (rigor mutant) (F) in metaphase. The mitotic spindle is marked with tdTomato-MAP103. Bounding boxes indicate area used for generation of intensity profiles in Fiji/Image J. Cell lines: BAP3068, BAP3071. Scale bars, 2 μm. Lower: Example of 1D intensity profiles and corresponding heatmaps from the example cells shown above. (G) and (H) Kinetochore alignment profiles for YFP-tagged KIN-A (G) and KIN-A^{G210A} (H). RNAi was induced with 1 μg/mL doxycycline for 24 h to deplete the untagged KIN-A allele and cells were treated with 10 μM MG132 for 4 h prior to fixing to prevent anaphase entry (Hayashi and Akiyoshi, 2018). WPGMA clustering was performed using the Python Seaborn library. Cell lines: BAP3064, BAP3065.

References

1. Abad MA *et al.* (2022) **Mechanistic basis for Sgo1-mediated centromere localization and function of the CPC** *Journal of Cell Biology* **221** <https://doi.org/10.1083/JCB.202108156/213318>
2. Adams RR, Maiato H, Earnshaw WC, Carmena M (2001) **Essential Roles of Drosophila Inner Centromere Protein (Incenp) and Aurora B in Histone H3 Phosphorylation, Metaphase Chromosome Alignment, Kinetochore Disjunction, and Chromosome Segregation** *Journal of Cell Biology* **153**:865–880 <https://doi.org/10.1083/JCB.153.4.865>
3. Adams RR, Wheatley SP, Gouldsworthy AM, Kandels-Lewis SE, Carmena M, Smythe C, Gerloff DL, Earnshaw WC (2000) **INCENP binds the Aurora-related kinase ATRK2 and is required to target it to chromosomes, the central spindle and cleavage furrow** *Current Biology* **10** [https://doi.org/10.1016/S0960-9822\(00\)00673-4](https://doi.org/10.1016/S0960-9822(00)00673-4)
4. Akiyoshi B (2020) **Analysis of a Mad2 homolog in Trypanosoma brucei provides possible hints on the origin of the spindle checkpoint** *bioRxiv*
5. Akiyoshi B, Gull K (2014) **Discovery of Unconventional Kinetochores in Kinetoplastids** *Cell* **156** <https://doi.org/10.1016/j.cell.2014.01.049>
6. Allshire RC, Karpen GH (2008) **Epigenetic regulation of centromeric chromatin: old dogs, new tricks?** *Nat Rev Genet* **9** <https://doi.org/10.1038/nrg2466>
7. Aslett M *et al.* (2010) **TriTrypDB: a functional genomic resource for the Trypanosomatidae** *Nucleic Acids Res* **38** <https://doi.org/10.1093/NAR/GKP851>
8. Ballmer D, Lou HJ, Ishii M, Turk BE, Akiyoshi B (2024) **An unconventional regulatory circuitry involving Aurora B controls anaphase onset and error-free chromosome segregation in trypanosomes.** *bioRxiv* 2024.01.20.576407 <https://doi.org/10.1101/2024.01.20.576407>
9. Bateman A (2019) **UniProt: a worldwide hub of protein knowledge** *Nucleic Acids Res* **47**:D506–D515 <https://doi.org/10.1093/NAR/GKY1049>
10. Beneke T, Madden R, Makin L, Valli J, Sunter J, Gluenz E (2017) **A CRISPR Cas9 high-throughput genome editing toolkit for kinetoplastids** *R Soc Open Sci* **4**:1–16 <https://doi.org/10.1098/RSOS.170095>
11. Berriman M *et al.* (2005) **The genome of the African trypanosome Trypanosoma brucei** *Science* **309**:416–422 <https://doi.org/10.1126/SCIENCE.1112642>
12. Bishop JD, Schumacher JM (2002) **Phosphorylation of the Carboxyl Terminus of Inner Centromere Protein (INCENP) by the Aurora B Kinase Stimulates Aurora B Kinase Activity** *Journal of Biological Chemistry* **277** <https://doi.org/10.1074/jbc.C200307200>
13. Black BE, Cleveland DW (2011) **Epigenetic Centromere Propagation and the Nature of CENP-A Nucleosomes** *Cell* **144** <https://doi.org/10.1016/j.cell.2011.02.002>
14. Broad AJ, DeLuca KF, DeLuca JG (2020) **Aurora B kinase is recruited to multiple discrete kinetochore and centromere regions in human cells** *J Cell Biol* **219** <https://doi.org/10.1083/JCB.201905144>

15. Brun R, Schönerberger M (1979) **Cultivation and in vitro cloning or procyclic culture forms of *Trypanosoma brucei* in a semi-defined medium** *Acta Trop* **36**:289–292
16. Butenko A, Oppendoes FR, Flegontova O, Horák A, Hampl V, Keeling P, Gawryluk RMR, Tikhonenkov D, Flegontov P, Lukeš J (2020) **Evolution of metabolic capabilities and molecular features of diplomids, kinetoplastids, and euglenids** *BMC Biology* **2020** <https://doi.org/10.1186/S12915-020-0754-1>
17. Campbell CS, Desai A (2013) **Tension sensing by Aurora B kinase is independent of survivin-based centromere localization** *Nature* **2013** <https://doi.org/10.1038/nature12057>
18. Carmena M, Wheelock M, Funabiki H, Earnshaw WC (2012) **The chromosomal passenger complex (CPC): from easy rider to the godfather of mitosis** *Nat Rev Mol Cell Biol* **13** <https://doi.org/10.1038/nrm3474>
19. Cavalier-Smith T (2010) **Kingdoms Protozoa and Chromista and the eozoan root of the eukaryotic tree** *Biol Lett* **6**:342–345 <https://doi.org/10.1098/RSBL.2009.0948>
20. Cheeseman IM, Chappie JS, Wilson-Kubalek EM, Desai A (2006) **The Conserved KMN Network Constitutes the Core Microtubule-Binding Site of the Kinetochore** *Cell* **127** <https://doi.org/10.1016/j.cell.2006.09.039>
21. Chen ZL *et al.* (2019) **A high-speed search engine pLink 2 with systematic evaluation for proteome-scale identification of cross-linked peptides** *Nature Communications* **2019** <https://doi.org/10.1038/s41467-019-11337-z>
22. Cho US, Harrison SC (2011) **Ndc10 is a platform for inner kinetochore assembly in budding yeast** *Nat Struct Mol Biol* **19**:48–56 <https://doi.org/10.1038/NSMB.2178>
23. Cooke CA, Heck MMS, Earnshaw WC (1987) **The inner centromere protein (INCENP) antigens: movement from inner centromere to midbody during mitosis** *J Cell Biol* **105**:2053–2067 <https://doi.org/10.1083/JCB.105.5.2053>
24. Cormier A, Drubin DG, Barnes G (2013) **Phosphorylation regulates kinase and microtubule binding activities of the budding yeast chromosomal passenger complex in vitro** *J Biol Chem* **288**:23203–23211 <https://doi.org/10.1074/JBC.M113.491480>
25. D'Archivio S, Wickstead B (2017) **Trypanosome outer kinetochore proteins suggest conservation of chromosome segregation machinery across eukaryotes** *Journal of Cell Biology* **216** <https://doi.org/10.1083/jcb.201608043>
26. Dean S, Sunter J, Wheeler RJ, Hodgkinson I, Gluenz E, Gull K (2015) **A toolkit enabling efficient, scalable and reproducible gene tagging in trypanosomatids** *Open Biol* **5** <https://doi.org/10.1098/RSOB.140197>
27. Deutsch EW *et al.* (2020) **Deutsch EW, Bandeira N, Sharma V, Perez-Riverol Y, Carver JJ, Kundu DJ, García-Seisdedos D, Jarnuczak AF, Hewapathirana S, Pullman BS, Wertz J, Sun Z, Kawano S, Okuda S, Watanabe Y, Hermjakob H, Maclean B, Maccoss MJ, Zhu Y, Ishihama Y, Vizcaíno JA. 2020. The ProteomeXchange consortium in 2020: enabling 'big data' approaches in proteomics. Nucleic Acids Res 48:D1145. doi:10.1093/NAR/GKZ984 The ProteomeXchange consortium in 2020: enabling 'big data' approaches in proteomics. Nucleic Acids Res **48** <https://doi.org/10.1093/NAR/GKZ984>**

29. Drinnenberg IA, Akiyoshi B (2017) **Evolutionary Lessons from Species with Unique Kinetochores** *Prog Mol Subcell Biol* **56**:111–138 https://doi.org/10.1007/978-3-319-58592-5_5/TABLES/1
30. Eddy SR (1998) **Profile hidden Markov models** *Bioinformatics* **14**:755–763 <https://doi.org/10.1093/BIOINFORMATICS/14.9.755>
31. Endow SA, Kull FJ, Liu H (2010) **Kinesins at a glance** *J Cell Sci* **123** <https://doi.org/10.1242/JCS.064113>
32. Ronneberger O *et al.* (2022) **Protein complex prediction with AlphaFold-Multimer** <https://doi.org/10.1101/2021.10.04.463034>
33. Fink S, Turnbull K, Desai A, Campbell CS (2017) **An engineered minimal chromosomal passenger complex reveals a role for INCENP/Sli15 spindle association in chromosome biorientation** *J Cell Biol* **216**:911–923 <https://doi.org/10.1083/JCB.201609123>
34. Fischböck-Halwachs J *et al.* (2019) **The COMA complex interacts with Cse4 and positions Sli15/Ipl1 at the budding yeast inner kinetochore** *Elife* **8** <https://doi.org/10.7554/ELIFE.42879>
35. Foltz DR, Jansen LET, Black BE, Bailey AO, Yates JR, Cleveland DW (2006) **The human CENP-A centromeric nucleosome-associated complex** *Nat Cell Biol* **8** <https://doi.org/10.1038/ncb1397>
36. García-Rodríguez LJ, Kasciukovic T, Denninger V, Tanaka TU (2019) **Aurora B-INCENP Localization at Centromeres/Inner Kinetochores Is Required for Chromosome Bi-orientation in Budding Yeast** *Current Biology* **29**:1536–1544 <https://doi.org/10.1016/j.CUB.2019.03.051>
37. Gassmann R, Carvalho A, Henzing AJ, Ruchaud S, Hudson DF, Honda R, Nigg EA, Gerloff DL, Earnshaw WC (2004) **Borealin: a novel chromosomal passenger required for stability of the bipolar mitotic spindle** *Journal of Cell Biology* **166** <https://doi.org/10.1083/jcb.200404001>
38. Graham M, Combe C, Kolbowski L, Rappsilber J (2019) **A common platform for the downstream analysis of Crosslinking Mass Spectrometry data.** *bioRxiv* **561829** <https://doi.org/10.1101/561829>
39. Gruneberg U, Neef R, Honda R, Nigg EA, Barr FA (2004) **Relocation of Aurora B from centromeres to the central spindle at the metaphase to anaphase transition requires MKlp2** *J Cell Biol* **166**:167–172 <https://doi.org/10.1083/JCB.200403084>
40. Hadders MA, Hindriksen S, Truong MA, Mhaskar AN, Pepijn Wopken J, Vromans MJM, Lens SMA (2020) **Untangling the contribution of Haspin and Bub1 to Aurora B function during mitosis** *Journal of Cell Biology* **219** <https://doi.org/10.1083/JCB.201907087/133700>
41. Hayashi H, Akiyoshi B (2018) **Degradation of cyclin B is critical for nuclear division in *Trypanosoma brucei*** *Biol Open* <https://doi.org/10.1242/bio.031609>
42. Hochegger H, Hégarat N, Pereira-Leal JB (2012) **Aurora at the pole and equator: overlapping functions of Aurora kinases in the mitotic spindle** *Open Biol* **3** <https://doi.org/10.1098/RSOB.120185>

43. Hooff JJ, Tromer E, Wijk LM, Snel B, Kops GJ (2017) **Evolutionary dynamics of the kinetochore network in eukaryotes as revealed by comparative genomics** *EMBO Rep* **18** <https://doi.org/10.15252/embr.201744102>
44. Hori T, Fukagawa T (2012) **Establishment of the vertebrate kinetochores** *Chromosome Research* **20** <https://doi.org/10.1007/s10577-012-9289-9>
45. Hu H, Yu Z, Liu Y, Wang T, Wei Y, Li Z (2014) **The Aurora B kinase in Trypanosoma brucei undergoes post-translational modifications and is targeted to various subcellular locations through binding to TbCPC1** *Mol Microbiol* **91** <https://doi.org/10.1111/mmi.12458>
46. Hümmer S, Mayer TU (2009) **Cdk1 Negatively Regulates Midzone Localization of the Mitotic Kinesin Mklp2 and the Chromosomal Passenger Complex** *Current Biology* **19**:607–612 <https://doi.org/10.1016/j.CUB.2009.02.046>
47. Integrating Neglected Tropical Diseases into Global Health and Development: Fourth World Health Organization Report on Neglected Tropical Diseases (WHO, 2017) (2017) **Integrating Neglected Tropical Diseases into Global Health and Development: Fourth World Health Organization Report on Neglected Tropical Diseases (WHO, 2017)**. 2017.
48. Ishii M, Akiyoshi B (2020) **Characterization of unconventional kinetochore kinases KKT10/19 in Trypanosoma brucei** *J Cell Sci* <https://doi.org/10.1242/jcs.240978>
49. Izuta H *et al.* (2006) **Comprehensive analysis of the ICEN (Interphase Centromere Complex) components enriched in the CENP-A chromatin of human cells** *Genes to Cells* **11** <https://doi.org/10.1111/j.1365-2443.2006.00969.x>
50. (2017) **Evolutionary dynamics of the kinetochore network in eukaryotes as revealed by comparative genomics** *EMBO Rep* **18**:1559–1571 <https://doi.org/10.15252/EMBR.201744102>
51. Jayaprakash AA, Basquin C, Jayachandran U, Conti E (2011) **Structural Basis for the Recognition of Phosphorylated Histone H3 by the Survivin Subunit of the Chromosomal Passenger Complex** *Structure* **19**:1625–1634 <https://doi.org/10.1016/j.STR.2011.09.002>
52. Jayaprakash AA, Klein UR, Lindner D, Ebert J, Nigg EA, Conti E (2007) **Structure of a Survivin–Borealin–INCENP Core Complex Reveals How Chromosomal Passengers Travel Together** *Cell* **131** <https://doi.org/10.1016/j.cell.2007.07.045>
53. Jumper J, Evans R, Pritzel A, Green T, Figurnov M, Ronneberger O, Tunyasuvunakool K, Bates R, Žídek A, Potapenko A, Bridgland A, Meyer C, Kohl SAA, Ballard AJ, Cowie A, Romera-Paredes B, Nikolov S, Jain R, Adler J, Back T, Petersen S, Reiman D, Clancy E, Zielinski M, Steinegger M, Pacholska M, Berghammer T, Bodenstein S, Silver D, Vinyals O, Senior AW, Kavukcuoglu K, Kohli P, Hassabis D (2021) **Highly accurate protein structure prediction with AlphaFold** *Nature* **2021** <https://doi.org/10.1038/s41586-021-03819-2>
54. Kang JS, Cheeseman IM, Kallstrom G, Velmurugan S, Barnes G, Chan CSM (2001) **Functional cooperation of Dam1** *Ip1* **1** <https://doi.org/10.1083/JCB.200105029>
55. Katoh K, Rozewicki J, Yamada KD (2019) **MAFFT online service: multiple sequence alignment, interactive sequence choice and visualization** *Brief Bioinform* **20**:1160–1166 <https://doi.org/10.1093/BIB/BBX108>

56. Kawashima SA, Yamagishi Y, Honda T, Lshiguro KI, Watanabe Y (2010) **Phosphorylation of H2A by Bub1 prevents chromosomal instability through localizing shugoshin** *Science* **330**:172–177
57. Kelly AE, Ghenoïu C, Xue JZ, Zierhut C, Kimura H, Funabiki H (2010) **Survivin reads phosphorylated histone H3 threonine 3 to activate the mitotic kinase Aurora B** *Science* **330**:235–239 <https://doi.org/10.1126/SCIENCE.1189505>
58. Kelly S *et al.* (2007) **Functional genomics in Trypanosoma brucei: A collection of vectors for the expression of tagged proteins from endogenous and ectopic gene loci** *Mol Biochem Parasitol* **154** <https://doi.org/10.1016/j.molbiopara.2007.03.012>
59. Kitagawa M, Fung SYS, Hameed UFS, Goto H, Inagaki M, Lee SH (2014) **Cdk1 coordinates timely activation of MKlp2 kinesin with relocation of the chromosome passenger complex for cytokinesis** *Cell Rep* **7**:166–179 <https://doi.org/10.1016/j.CELREP.2014.02.034>
60. Klein UR, Nigg EA, Gruneberg U (2006) **Centromere targeting of the chromosomal passenger complex requires a ternary subcomplex of Borealin, Survivin, and the N-terminal domain of INCENP** *Mol Biol Cell* **17**:2547–2558 <https://doi.org/10.1091/MBC.E05-12-1133>
61. Komaki S, Tromer EC, De Jaeger G, De Winne N, Heese M, Schnittger A (2022) **Molecular convergence by differential domain acquisition is a hallmark of chromosomal passenger complex evolution** *Proc Natl Acad Sci U S A* **119** <https://doi.org/10.1073/PNAS.2200108119/-/DCSUPPLEMENTAL>
62. Krenn V, Musacchio A (2015) **The Aurora B Kinase in Chromosome Bi-Orientation and Spindle Checkpoint Signaling** *Front Oncol* **5** <https://doi.org/10.3389/FONC.2015.00225>
63. Landeira D, Navarro M (2007) **Nuclear repositioning of the VSG promoter during developmental silencing in Trypanosoma brucei** *Journal of Cell Biology* **176** <https://doi.org/10.1083/jcb.200607174>
64. Leitner A, Reischl R, Walzthoeni T, Herzog F, Bohn S, Förster F, Aebersold R (2012) **Expanding the chemical cross-linking toolbox by the use of multiple proteases and enrichment by size exclusion chromatography** *Mol Cell Proteomics* **11** <https://doi.org/10.1074/MCP.M111.014126>
65. Li Z (2012) **Regulation of the Cell Division Cycle in Trypanosoma brucei** *Eukaryot Cell* **11** <https://doi.org/10.1128/EC.00145-12>
66. Li Z, Lee JH, Chu F, Burlingame AL, Günzl A, Wang CC (2008) **Identification of a Novel Chromosomal Passenger Complex and Its Unique Localization during Cytokinesis in Trypanosoma brucei** *PLoS One* **3** <https://doi.org/10.1371/journal.pone.0002354>
67. Liang C, Zhang Z, Chen Q, Yan H, Zhang M, Zhou L, Xu J, Lu W, Wang F (2020) **Centromere-localized Aurora B kinase is required for the fidelity of chromosome segregation** *J Cell Biol* **219** <https://doi.org/10.1083/JCB.201907092>
68. Llauró A, Hayashi H, Bailey ME, Wilson A, Ludzia P, Asbury CL, Akiyoshi B (2018) **The kinetoplastid kinetochore protein KKT4 is an unconventional microtubule tip-coupling protein** *Journal of Cell Biology* **217** <https://doi.org/10.1083/jcb.201711181>

69. Lowell JE, Cross GAM (2004) **A variant histone H3 is enriched at telomeres in *Trypanosoma brucei*** *J Cell Sci* **117**:5937–5947 <https://doi.org/10.1242/JCS.01515>
70. Ludzia P, Lowe ED, Marcianò G, Mohammed S, Redfield C, Akiyoshi B (2021) **Structural characterization of KKT4, an unconventional microtubule-binding kinetochore protein** *Structure* **29**:1014–1028 <https://doi.org/10.1016/j.STR.2021.04.004>
71. Mackay AM, Eckley DM, Chue C, Earnshaw WC (1993) **Molecular analysis of the INCENPs (inner centromere proteins): separate domains are required for association with microtubules during interphase and with the central spindle during anaphase** *J Cell Biol* **123**:373–385 <https://doi.org/10.1083/JCB.123.2.373>
72. Maddox PS, Corbett KD, Desai A (2012) **Structure, assembly and reading of centromeric chromatin** *Curr Opin Genet Dev* **22** <https://doi.org/10.1016/j.gde.2011.11.005>
73. Marchetti MA, Tschudi C, Kwon H, Wolin SL, Ullu E (2000) **Import of proteins into the trypanosome nucleus and their distribution at karyokinesis** *J Cell Sci* **113**:899–906 <https://doi.org/10.1242/JCS.113.5.899>
74. Marcianò G, Ishii M, Nerusheva OO, Akiyoshi B (2021) **Kinetoplastid kinetochore proteins KKT2 and KKT3 have unique centromere localization domains** *J Cell Biol* **220** <https://doi.org/10.1083/JCB.202101022>
75. Meraldi P, McAinsh AD, Rheinbay E, Sorger PK (2006) **Phylogenetic and structural analysis of centromeric DNA and kinetochore proteins** *Genome Biol* **7**:1–21 <https://doi.org/10.1186/GB-2006-7-3-R23/FIGURES/11>
76. Mirdita M, Schütze K, Moriwaki Y, Heo L, Ovchinnikov S, Steinegger M (2022) **ColabFold: making protein folding accessible to all** *Nature Methods* **2022** <https://doi.org/10.1038/s41592-022-01488-1>
77. Nakajima Y, Cormier A, Tyers RG, Pigula A, Peng Y, Drubin DG, Barnes G (2011) **Ipl1/Aurora-dependent phosphorylation of Sli15/INCENP regulates CPC-spindle interaction to ensure proper microtubule dynamics** *J Cell Biol* **194**:137–153 <https://doi.org/10.1083/JCB.201009137>
78. Nerusheva OO, Akiyoshi B (2016) **Divergent polo box domains underpin the unique kinetoplastid kinetochore** *Open Biol* **6** <https://doi.org/10.1098/rsob.150206>
79. Nerusheva OO, Ludzia P, Akiyoshi B (2019) **Identification of four unconventional kinetoplastid kinetochore proteins KKT22–25 in *Trypanosoma brucei*** *Open Biol* **9** <https://doi.org/10.1098/rsob.190236>
80. Noujaim M, Bechstedt S, Wiczorek M, Brouhard GJ (2014) **Microtubules accelerate the kinase activity of Aurora-B by a reduction in dimensionality** *PLoS One* **9** <https://doi.org/10.1371/JOURNAL.PONE.0086786>
81. Okada M, Cheeseman IM, Hori T, Okawa K, McLeod IX, Yates JR, Desai A, Fukagawa T (2006) **The CENP-H-I complex is required for the efficient incorporation of newly synthesized CENP-A into centromeres** *Nat Cell Biol* **8** <https://doi.org/10.1038/ncb1396>
82. Okada Y, Hirokawa N (1999) **A processive single-headed motor: Kinesin superfamily protein KIF1A** *Science* **1999** <https://doi.org/10.1126/SCIENCE.283.5405.1152>

83. Perez-Riverol Y *et al.* (2019) **The PRIDE database and related tools and resources in 2019: improving support for quantification data** *Nucleic Acids Res* **47**:D442–D450 <https://doi.org/10.1093/NAR/GKY1106>
84. Rice S *et al.* (1999) **A structural change in the kinesin motor protein that drives motility** *Nature* **1999** <https://doi.org/10.1038/45483>
85. Romano A, Guse A, Krascenicova I, Schnabel H, Schnabel R, Glotzer M (2003) **CSC-1: a subunit of the Aurora B kinase complex that binds to the survivin-like protein BIR-1 and the incenp-like protein ICP-1** *Journal of Cell Biology* **161** <https://doi.org/10.1083/jcb.200207117>
86. Saldivia M *et al.* (2020) **Targeting the trypanosome kinetochore with CLK1 protein kinase inhibitors** *Nat Microbiol* **5**:1207–1216 <https://doi.org/10.1038/s41564-020-0745-6>
87. Samejima K, Platani M, Wolny M, Ogawa H, Vargiu G, Knight PJ, Peckham M, Earnshaw WC (2015) **The Inner Centromere Protein (INCENP) Coil Is a Single α -Helix (SAH) Domain That Binds Directly to Microtubules and Is Important for Chromosome Passenger Complex (CPC) Localization and Function in Mitosis.** *J Biol Chem* **290**:21460–21472 <https://doi.org/10.1074/JBC.M115.645317>
88. Sampath SC, Ohi R, Leismann O, Salic A, Pozniakovski A, Funabiki H (2004) **The Chromosomal Passenger Complex Is Required for Chromatin-Induced Microtubule Stabilization and Spindle Assembly** *Cell* **118** <https://doi.org/10.1016/j.cell.2004.06.026>
89. Santaguida S, Musacchio A (2009) **The life and miracles of kinetochores** *EMBO J* **28**:2511–2531 <https://doi.org/10.1038/EMBOJ.2009.173>
90. Schiffrin B, Radford SE, Brockwell DJ, Calabrese AN (2020) **PyXlinkViewer: A flexible tool for visualization of protein chemical crosslinking data within the PyMOL molecular graphics system** *Protein Sci* **29**:1851–1857 <https://doi.org/10.1002/PRO.3902>
91. Schneider CA, Rasband WS, Eliceiri KW (2012) **NIH Image to ImageJ: 25 years of image analysis** *Nature Methods* **2012** <https://doi.org/10.1038/nmeth.2089>
92. Serena M, Bastos RN, Elliott PR, Barr FA (2020) **Molecular basis of MKLP2-dependent Aurora B transport from chromatin to the anaphase central spindle** *Journal of Cell Biology* **219** <https://doi.org/10.1083/JCB.201910059/151730>
93. Siegel TN, Hekstra DR, Cross GAM (2008) **Analysis of the Trypanosoma brucei cell cycle by quantitative DAPI imaging** *Mol Biochem Parasitol* **160** <https://doi.org/10.1016/j.molbiopara.2008.04.004>
94. Stuart K, Brun R, Croft S, Fairlamb A, Gürtler RE, McKerrow J, Reed S, Tarleton R (2008) **Kinetoplastids: related protozoan pathogens, different diseases** *Journal of Clinical Investigation* **118** <https://doi.org/10.1172/JCI33945>
95. Trivedi P, Stukenberg PT (2016) **A centromere-signaling network underlies the coordination among mitotic events** *Trends Biochem Sci* **41** <https://doi.org/10.1016/J.TIBS.2015.11.002>
96. Tromer EC, van Hooff JJE, Kops GJPL, Snel B (2019) **Mosaic origin of the eukaryotic kinetochore** *Proc Natl Acad Sci U S A* **116**:12873–12882 https://doi.org/10.1073/PNAS.1821945116/SUPPL_FILE/PNAS.1821945116.SD05.XLSX

97. Tsukahara T, Tanno Y, Watanabe Y (2010) **Phosphorylation of the CPC by Cdk1 promotes chromosome bi-orientation** *Nature* **2010** <https://doi.org/10.1038/nature09390>
98. Tu X, Kumar P, Li Z, Wang CC (2006) **An Aurora Kinase Homologue Is Involved in Regulating Both Mitosis and Cytokinesis in Trypanosoma brucei** *Journal of Biological Chemistry* **281** <https://doi.org/10.1074/jbc.M511504200>
99. Unnikrishnan A, Akiyoshi B, Biggins S, Tsukiyama T (2012) **An Efficient Purification System for Native Minichromosome from Saccharomyces cerevisiae** https://doi.org/10.1007/978-1-61779-477-3_8
100. Vader G, Kauw JJW, Medema RH, Lens SMA (2006) **Survivin mediates targeting of the chromosomal passenger complex to the centromere and midbody** *EMBO Rep* **7** <https://doi.org/10.1038/sj.embor.7400562>
101. van der Horst A, Vromans MJM, Bouwman K, van der Waal MS, Hadders MA, Lens SMA (2015) **Inter-domain Cooperation in INCENP Promotes Aurora B Relocation from Centromeres to Microtubules** *Cell Rep* **12**:380–387 <https://doi.org/10.1016/j.CELREP.2015.06.038>
102. Van Der Lee R, Buljan M, Lang B, Weatheritt RJ, Daughdrill GW, Dunker AK, Fuxreiter M, Gough J, Gsponer J, Jones DT, Kim PM, Kriwacki RW, Oldfield CJ, Pappu R V., Tompa P, Uversky VN, Wright PE, Babu MM (2014) **Classification of intrinsically disordered regions and proteins** *Chem Rev* **114**:6589–6631 https://doi.org/10.1021/CR400525M/ASSET/IMAGES/LARGE/CR-2013-00525M_0006.JPEG
103. Wang F, Dai J, Daum JR, Niedzialkowska E, Banerjee B, Stukenberg PT, Gorbsky GJ, Higgins JMG (2010) **Histone H3 Thr-3 phosphorylation by Haspin positions Aurora B at centromeres in mitosis** *Science* **330**:231–235 <https://doi.org/10.1126/SCIENCE.1189435>
104. Waterhouse AM, Procter JB, Martin DMA, Clamp M, Barton GJ (2009) **Jalview Version 2--a multiple sequence alignment editor and analysis workbench** *Bioinformatics* **25**:1189–1191 <https://doi.org/10.1093/BIOINFORMATICS/BTP033>
105. Westhorpe FG, Straight AF (2013) **Functions of the centromere and kinetochore in chromosome segregation** *Curr Opin Cell Biol* **25** <https://doi.org/10.1016/j.ceb.2013.02.001>
106. Wheatley SP, Carvalho A, Vagnarelli P, Earnshaw WC (2001) **INCENP is required for proper targeting of Survivin to the centromeres and the anaphase spindle during mitosis** *Current Biology* **11** [https://doi.org/10.1016/S0960-9822\(01\)00238-X](https://doi.org/10.1016/S0960-9822(01)00238-X)
107. Wheelock MS, Wynne DJ, Tseng BS, Funabiki H (2017) **Dual recognition of chromatin and microtubules by INCENP is important for mitotic progression** *J Cell Biol* **216**:925–941 <https://doi.org/10.1083/JCB.201609061>
108. Wickstead B, Gull K (2006) **A “Holistic” Kinesin Phylogeny Reveals New Kinesin Families and Predicts Protein Functions** *Mol Biol Cell* **17**:1734–1743 <https://doi.org/10.1091/mbc.E05-11-1090>
109. Woods A, Sherwin T, Sasse R, MacRae TH, Baines AJ, Gull K (1989) **Definition of individual components within the cytoskeleton of Trypanosoma brucei by a library of monoclonal antibodies** *J Cell Sci* **93**:491–500 <https://doi.org/10.1242/JCS.93.3.491>

110. Woodward R, Gull K (1990) **Timing of nuclear and kinetoplast DNA replication and early morphological events in the cell cycle of *Trypanosoma brucei*** *J Cell Sci* **95** <https://doi.org/10.1242/jcs.95.1.49>
111. Yamagishi Y, Honda T, Tanno Y, Watanabe Y (2010) **Two histone marks establish the inner centromere and chromosome bi-orientation** *Science* **330**:239–243 <https://doi.org/10.1126/SCIENCE.1194498>
112. Yoon HJ, Carbon J (1999) **Participation of Bir1p, a member of the inhibitor of apoptosis family, in yeast chromosome segregation events** *Proc Natl Acad Sci U S A* **96**:13208–13213 <https://doi.org/10.1073/PNAS.96.23.13208>
113. Zimniak T, Fitz V, Zhou H, Lampert F, Opravil S, Mechtler K, Stolt-Bergner P, Westermann S (2012) **Spatiotemporal regulation of Ipl1/Aurora activity by direct Cdk1 phosphorylation** *Curr Biol* **22**:787–793 <https://doi.org/10.1016/J.CUB.2012.03.007>

Article and author information

Daniel Ballmer

Department of Biochemistry, University of Oxford, South Parks Road, Oxford, OX1 3QU, United Kingdom

ORCID iD: [0000-0002-1966-0960](https://orcid.org/0000-0002-1966-0960)

Bungo Akiyoshi

Department of Biochemistry, University of Oxford, South Parks Road, Oxford, OX1 3QU, United Kingdom, The Wellcome Centre for Cell Biology, Institute of Cell Biology, School of Biological Sciences, Edinburgh, EH9 3BF, United Kingdom

For correspondence: bungo.akiyoshi@ed.ac.uk

ORCID iD: [0000-0001-6010-394X](https://orcid.org/0000-0001-6010-394X)

Copyright

© 2024, Daniel Ballmer & Bungo Akiyoshi

This article is distributed under the terms of the [Creative Commons Attribution License](https://creativecommons.org/licenses/by/4.0/), which permits unrestricted use and redistribution provided that the original author and source are credited.

Editors

Reviewing Editor

Silke Hauf

Virginia Tech, Blacksburg, United States of America

Senior Editor

Yamini Dalal

National Cancer Institute, Bethesda, United States of America

Reviewer #1 (Public Review):

Summary:

The CPC plays multiple essential roles in mitosis such as kinetochore-microtubule attachment regulation, kinetochore assembly, spindle assembly checkpoint activation, anaphase spindle stabilization, cytokinesis, and nuclear envelope formation, as it dynamically changes its mitotic localization: it is enriched at inner centromeres from prophase to metaphase but it is relocalized at the spindle midzone in anaphase. The business end of the CPC is Aurora B and its allosteric activation module IN-box, which is located at the C-terminus of INCENP. In most well-studied eukaryotic species, Aurora B activity is locally controlled by the localization module of the CPC, Survivin, Borealin and the N-terminal portion of INCENP. Survivin and Borealin, which bind the N-terminus of INCENP, recognize histone residues that are specifically phosphorylated in mitosis, while anaphase spindle midzone localization is supported by the direct microtubule-binding capacity of the SAH (single alpha helix) domain of INCENP and other microtubule-binding proteins that specifically interact with INCENP during anaphase, which are under the regulation of CDK activity. One of these examples includes the kinesin-like protein MKLP2 in vertebrates. *Trypanosoma* is an evolutionarily interesting species to study mitosis since its kinetochore and centromere proteins do not show any similarity to other major branches of eukaryotes, while orthologs of Aurora B and INCENP have been identified. Combining molecular genetics, imaging, biochemistry, cross-linking IP-MS (IP-CLMS), and structural modeling, this manuscript reveals that two orphan kinesin-like proteins KIN-A and KIN-B act as localization modules of the CPC in *Trypanosoma brucei*. The IP-CLMS, AlphaFold2 structural predictions, and domain deletion analysis support the idea that (1) KIN-A and KIN-B form a heterodimer via their coiled-coil domains, (2) Two alpha helices of INCENP interact with the coiled-coil of the KIN-A-KIN-B heterodimer, (3) conserved KIN-A C-terminal CD1 and CD2 interact with the heterodimeric KKT9-KKT11 complex, which is a submodule of the KKT7-KKT8 kinetochore complex composed of KKT7, KKT8, KKT9, KKT11, and KKT12 unique to *Trypanosoma*, (4) KIN-A and KIN-B coiled-coil domains and the KKT7-KKT8 complex are required for CPC localization at the centromere, (5) CD1 and CD2 domains of KIN-A support its centromere localization. The authors further introduced a KIN-A rigor mutant and knocked-down wild-type KIN-A to show that the ATPase activity of KIN-A seems dispensable for centromere targeting but critical for spindle midzone enrichment of the CPC. The imaging data of the KIN-A rigor mutant suggest that dynamic KIN-A-microtubule interaction is required for metaphase alignment of the kinetochores and proliferation. Overall, the study reveals novel pathways of CPC localization regulation via KIN-A and KIN-B by multiple complementary approaches.

Strengths:

The major conclusion is collectively supported by multiple approaches, combining CRISPR-mediated gene deletion and complementation/site specific genome engineering, epistasis analysis of cellular localization, AlphaFold2 structure prediction of protein complexes, IP-CLMS and biochemical reconstitution (the complex of KKT8, KKT9, KKT11 and KKT12)

Weaknesses:

Minor weakness. The authors imply that KIN-A, but not KIN-B, interacts with microtubules based on microtubule pelleting assay (Fig. S6), but the substantial insoluble fractions of 6HIS-KIN-A and 6HIS-KIN-B make it difficult to conclusively interpret the data. It is possible that these two proteins are not stable unless they form a heterodimer.

<https://doi.org/10.7554/eLife.93522.2.sa2>

Reviewer #2 (Public Review):

How the chromosomal passenger complex (CPC) and its subunit Aurora B kinase regulate kinetochore-microtubule attachment, and how the CPC relocates from kinetochores to the

spindle midzone as a cell transitions from metaphase to anaphase are questions of great interest. In this study, Ballmer and Akiyoshi take a deep dive into the CPC in *T. brucei*, a kinetoplastid parasite with a kinetochore composition that varies greatly from other organisms.

Using a combination of approaches, most importantly in silico protein predictions using alphafold multimer and light microscopy in dividing *T. brucei*, the authors convincingly present and analyse the composition of the *T. brucei* CPC. This includes the identification of KIN-A and KIN-B, proteins of the kinesin family. This is a clear advancement over earlier work, for example by Li and colleagues in 2008. The involvement of KIN-A and KIN-B is of particular interest, as it provides a clue for the (re)localization of the CPC during the cell cycle. The evolutionary perspective makes the paper potentially interesting for a wide audience of cell biologists, a point that the authors bring across properly in the title, the abstract, and their discussion.

The evolutionary twist of the paper would be strengthened 'experimentally' by predictions of the structure of the CPC beyond *T. brucei*. Depending on how far the authors can extend their in-silico analysis, it would be of interest to discuss a) available/predicted CPC structures in well-studied organisms and b) structural predictions in other euglenozoa. What are the general structural properties of the CPC (e.g. flexible linkers, overall dimensions, structural differences when subunits are missing etc.)? How common is the involvement of kinesin-like proteins?

<https://doi.org/10.7554/eLife.93522.2.sa1>

Reviewer #3 (Public Review):

Summary:

The protein kinase, Aurora B, is a critical regulator of mitosis and cytokinesis in eukaryotes, exhibiting a dynamic localisation. As part of the Chromosomal Passenger Complex (CPC), along with the Aurora B activator, INCENP, and the CPC localisation module comprised of Borealin and Survivin, Aurora B travels from the kinetochores at metaphase to the spindle midzone at anaphase, which ensures its substrates are phosphorylated in a time- and space-dependent manner. In the kinetoplastid parasite, *T. brucei*, the Aurora B orthologue (AUK1), along with an INCENP orthologue known as CPC1, and a kinetoplastid-specific protein CPC2, also displays a dynamic localisation, moving from the kinetochores at metaphase, to the spindle midzone at anaphase, to the anterior end of the newly synthesised flagellum attachment zone (FAZ) at cytokinesis. However, the trypanosome CPC lacks orthologues of Borealin and Survivin, and *T. brucei* kinetochores also have a unique composition, being comprised of dozens of kinetoplastid-specific proteins (KKTs). Of particular importance for this study are KKT7 and the KKT8 complex (comprising KKT8, KKT9, KKT11, and KKT12). Here, Ballmer and Akiyoshi seek to understand how the CPC assembles and is targeted to its different locations during the cell cycle in *T. brucei*.

Strengths & Weaknesses:

Using immunoprecipitation and mass-spectrometry approaches, Ballmer and Akiyoshi show that AUK1, CPC1, and CPC2 associate with two orphan kinesins, KIN-A and KIN-B, and with the use of endogenously expressed fluorescent fusion proteins, demonstrate for the first time that KIN-A and KIN-B display a dynamic localisation pattern similar to other components of the CPC, providing compelling evidence for KIN-A and KIN-B being bona fide CPC proteins.

They then demonstrate, by using RNAi to deplete individual components, that the CPC proteins have hierarchical interdependencies for their localisation to the kinetochores at

metaphase. These experiments appear to have been well performed.

Ballmer and Akiyoshi then go on to determine the kinetochore localisation domains of KIN-A and KIN-B. Using ectopically expressed GFP-tagged truncations, they show that coiled coil domains within KIN-A and KIN-B, as well as a disordered C-terminal tail present only in KIN-A, but not the N-terminal motor domains of KIN-A or KIN-B, are required for kinetochore localisation. These data are strengthened by immunoprecipitating CPC complexes and crosslinking them prior to mass spectrometry analysis (IP-CLMS), a state-of-the-art approach, to determine the contacts between the CPC components. Structural predictions of the CPC structure are also made using AlphaFold2, suggesting that coiled coils form between KIN-A and KIN-B, and that KIN-A/B interact with the N termini of CPC1 and CPC2. Experimental results showing that CPC1 and CPC2 are unable to localise to kinetochores if they lack their N-terminal domains are consistent with these predictions. Altogether these data provide compelling evidence of the protein domains required for CPC kinetochore localisation and CPC protein interactions and indicate that both KIN-A and KIN-B have a role to play.

Next, using a mixture of RNAi depletion and LacI-LacO recruitment experiments, the authors show that kinetochore proteins KKT7 and KKT9 are required for AUK1 to localise to kinetochores (other KKT8 complex components were not tested here) and that all components of the KKT8 complex are required for KIN-A kinetochore localisation. Further, both KKT7 and KKT8 were able to recruit AUK1 to an ectopic locus in S phase, and KKT7 recruited KKT8 complex proteins, indicating it is upstream of KKT8, in line with previous work showing kinetochore localization of KKT7 is unaffected by disruption of the KKT8 complex. This leads to the conclusion that the KKT8 complex is likely the main kinetochore receptor of the CPC.

Further IP-CLMS experiments, in combination with recombinant protein pull down assays and structural predictions, suggested that within the KKT8 complex, there are two subcomplexes of KKT8:KKT12 and KKT9:KKT11, and that KKT7 interacts with KKT9:KKT11 to recruit the remainder of the KKT8 complex. The authors also assess the interdependencies between KKT8 complex components for localisation and expression, showing that all four subunits are required for the assembly of a stable KKT8 complex and present AlphaFold2 structural modelling data to support the two subcomplex model. In general, these data are of high quality and convincing, although it is a shame that data showing the effects of KKT8, KKT9 and KKT12 depletion on KKT11 localisation and abundance could not be presented alongside the reciprocal experiments in Fig S4I-L.

The authors also convincingly show that AlphaFold2 predictions of interactions between KKT9:KKT11 and a conserved domain (CD1) in the C-terminal tail of KIN-A are correct, with CD1 and a second conserved domain, CD2, identified through sequence analysis, acting synergistically to promote KIN-A kinetochore localisation at metaphase, but not being required for KIN-A to move to the central spindle at anaphase. They then hypothesise that the kinesin motor domain of KIN-A (but not KIN-B which is predicted to be inactive based on non-conservation of residues key for activity) determines its central spindle localisation at anaphase through binding to microtubules. In support of this hypothesis, the authors show that KIN-A, but not KIN-B can bind microtubules *in vitro* and *in vivo*. However, ectopically expressed GFP-NLS fusions of full length KIN-A or KIN-A motor domain did not localise to the central spindle at anaphase. The authors suggest this is due to the GFP fusion disrupting the ATPase activity of the motor domain, although they provide no evidence that this is the case. Instead, they replace endogenous KIN-A with a predicted ATPase-defective mutant (G210A), showing that while this still localises to kinetochores, the kinetochores were frequently misaligned at metaphase, and that it no longer concentrates at the central spindle (with concomitant mis-localisation of AUK1), causing cells to accumulate at anaphase. From these data, the authors conclude that KIN-A ATPase activity is required for chromosome congression to the metaphase plate and its central spindle localisation at anaphase. While

these data are highly suggestive that KIN-A possesses ATPase activity, and that this activity is essential for its function, definitive biochemical evidence of KIN-A's ATPase activity is still lacking.

Impact:

Overall, this work uses a wide range of cutting edge molecular and structural predictive tools to provide a significant amount of new and detailed molecular data that shed light on the composition of the unusual trypanosome CPC and how it is assembled and targeted to different cellular locations during cell division. Given the fundamental nature of this research, it will be of interest to many parasitology researchers as well as cell biologists more generally, especially those working on aspects of mitosis and cell division, and those interested in the evolution of the CPC.

<https://doi.org/10.7554/eLife.93522.2.sa0>

Author Response

The following is the authors' response to the original reviews.

eLife assessment

This important study identifies the mitotic localization mechanism for Aurora B and INCENP (parts of the chromosomal passenger complex, CPC) in Trypanosoma brucei. The mechanism is different from that in the more commonly studied opisthokonts and there is solid support from RNAi and imaging experiments, targeted mutations, immunoprecipitations with crosslinking/mass spec, and AlphaFold interaction predictions. The results could be strengthened by biochemically testing proposed direct interactions and demonstrating that the targeting protein KIN-A is a motor. The findings will be of interest to parasitology researchers as well as cell biologists working on mitosis and cell division, and those interested in the evolution of the CPC.

We thank the editor and the reviewers for their thorough and positive assessment of our work and the constructive feedback to further improve our manuscript. Please find below our responses to the reviewers' comments. Please note that the conserved glycine residue in the Switch II helix in KIN-A was mistakenly labelled as G209 in the original manuscript. We now corrected it to G210 in the revised manuscript.

Public Reviews:

Reviewer #1 (Public Review):

Summary:

The CPC plays multiple essential roles in mitosis such as kinetochore-microtubule attachment regulation, kinetochore assembly, spindle assembly checkpoint activation, anaphase spindle stabilization, cytokinesis, and nuclear envelope formation, as it dynamically changes its mitotic localization: it is enriched at inner centromeres from prophase to metaphase but it is relocalized at the spindle midzone in anaphase. The business end of the CPC is Aurora B and its allosteric activation module IN-box, which is located at the C-terminal part of INCENP. In most well-studied eukaryotic species, Aurora B activity is locally controlled by the localization module of the CPC, Survivin, Borealin, and the N-terminal portion of INCENP. Survivin and Borealin, which bind the N terminus of INCENP, recognize histone residues that are specifically phosphorylated in mitosis, while anaphase spindle midzone localization is supported by the direct microtubule-

binding capacity of the SAH (single alpha helix) domain of INCENP and other microtubule-binding proteins that specifically interact with INCENP during anaphase, which are under the regulation of CDK activity. One of these examples includes the kinesin-like protein MKLP2 in vertebrates.

Trypanosoma is an evolutionarily interesting species to study mitosis since its kinetochore and centromere proteins do not show any similarity to other major branches of eukaryotes, while orthologs of Aurora B and INCENP have been identified. Combining molecular genetics, imaging, biochemistry, cross-linking IP-MS (IP-CLMS), and structural modeling, this manuscript reveals that two orphan kinesin-like proteins KIN-A and KIN-B act as localization modules of the CPC in Trypanosoma brucei. The IP-CLMS, AlphaFold2 structural predictions, and domain deletion analysis support the idea that (1) KIN-A and KIN-B form a heterodimer via their coiled-coil domain, (2) Two alpha helices of INCENP interact with the coiled-coil of the KIN-A-KIN-B heterodimer, (3) the conserved KIN-A C-terminal CD1 interacts with the heterodimeric KKT9-KKT11 complex, which is a submodule of the KKT7-KKT8 kinetochore complex unique to Trypanosoma, (4) KIN-A and KIN-B coiled-coil domains and the KKT7-KKT8 complex are required for CPC localization at the centromere, (5) CD1 and CD2 domains of KIN-A support its centromere localization. The authors further show that the ATPase activity of KIN-A is critical for spindle midzone enrichment of the CPC. The imaging data of the KIN-A rigor mutant suggest that dynamic KIN-A-microtubule interaction is required for metaphase alignment of the kinetochores and proliferation. Overall, the study reveals novel pathways of CPC localization regulation via KIN-A and KIN-B by multiple complementary approaches.

Strengths:

The major conclusion is collectively supported by multiple approaches, combining site-specific genome engineering, epistasis analysis of cellular localization, AlphaFold2 structure prediction of protein complexes, IP-CLMS, and biochemical reconstitution (the complex of KKT8, KKT9, KKT11, and KKT12).

We thank the reviewer for her/his positive assessment of our manuscript.

Weaknesses:

- The predictions of direct interactions (e.g. INCENP with KIN-A/KIN-B, or KIN-A with KKT9-KKT11) have not yet been confirmed experimentally, e.g. by domain mutagenesis and interaction studies.*

Thank you for this point. It is true that we do not have evidence for direct interactions between KIN-A with KKT9-KKT11. However, the interaction between INCENP with KIN-A/KIN-B is strongly supported by our cross-linking IP-MS of native complexes. Furthermore, we show that deletion of the INCENPCPC1 N-terminus predicted to interact with KIN-A:KIN-B abolishes kinetochore localization.

- The criteria used to judge a failure of localization are not clearly explained (e.g., Figure 5F, G).*

As suggested by the reviewer in recommendation #14, we have now included example images for each category ('kinetochores', 'kinetochores + spindle', 'spindle') along with a schematic illustration in Fig. 5F.

- It remains to be shown that KIN-A has motor activity.*

We thank the reviewer for this important comment. Indeed, motor activity remains to be demonstrated using an in vitro system, which is beyond the scope of this study. What we show here is that the motor domain of KIN-A effectively co-sediments with microtubules and that spindle localization of KIN-A is abolished upon deletion of the motor domain. Moreover, mutation of a conserved Glycine residue in the Switch II region (G210) to Alanine ('rigor mutation', (Rice et al., 1999)), renders KIN-A incapable of translocating to the central spindle, suggesting that its ATPase activity is required for this process. To clarify this point in the manuscript, we have replaced all instances, where we refer to 'motor activity' of KIN-A with 'ATPase activity' when referring to experiments performed using the KIN-A rigor mutant. In addition, we have included a Multiple Sequence Alignment (MSA) of KIN-A and KIN-B from different kinetoplastids with human Kinesin-1, human Mklp2 and yeast Klp9 in Figure 6A and S6A, showing the conservation of key motifs required for ATP coordination and tubulin interaction. In the corresponding paragraph in the main text, we describe these data as follows:

'We therefore speculated that anaphase translocation of the kinetoplastid CPC to the central spindle may involve the kinesin motor domain of KIN-A. KIN-B is unlikely to be a functional kinesin based on the absence of several well-conserved residues and motifs within the motor domain, which are fully present in KIN-A (Li et al., 2008). These include the P-loop, switch I and switch II motifs, which form the nucleotide binding cleft, and many conserved residues within the α 4-L12 elements, which interact with tubulin (Fig. S6A) (Endow et al., 2010). Consistent with this, the motor domain of KIN-B, contrary to KIN-A, failed to localize to the mitotic spindle when expressed ectopically (Fig. S2E) and did not co-sediment with microtubules in our in vitro assay (Fig. S6B).'

- *The authors imply that KIN-A, but not KIN-B, interacts with microtubules based on microtubule pelleting assay (Fig. S6), but the substantial insoluble fractions of 6HIS-KIN-A and 6HIS-KIN-B make it difficult to conclusively interpret the data. It is possible that these two proteins are not stable unless they form a heterodimer.*

This is indeed a possibility. We are currently aiming at purifying full-length recombinant KIN-A and KIN-B (along with the other CPC components), which will allow us to perform in vitro interaction studies and to investigate biochemical properties of this complex (including the role of the motor domains of KIN-A and KIN-B) within the framework of an in-depth follow-up study. To address the point above, we have added the following text in the legend corresponding to Fig. S6:

'Microtubule co-sedimentation assay with 6HIS-KIN-A2-309 (left) and 6HIS-KIN-B2-316 (right). S and P correspond to supernatant and pellet fractions, respectively. Note that both constructs to some extent sedimented even in the absence of microtubules. Hence, lack of microtubule binding for KIN-B may be due to the unstable non-functional protein used in this study.'

- *For broader context, some prior findings should be introduced, e.g. on the importance of the microtubule-binding capacity of the INCENP SAH domain and its regulation by mitotic phosphorylation (PMID 8408220, 26175154, 26166576, 28314740, 28314741, 21727193), since KIN-A and KIN-B may substitute for the function of the SAH domain.*

We have modified the introduction to include the following text and references mentioned by the reviewer: 'The localization module comprises Borealin, Survivin and the N-terminus of INCENP, which are connected to one another via a three-helical bundle (Jeyapragash et al., 2007, 2011; Klein et al., 2006). The two modules are linked by the central region of INCENP, composed of an intrinsically disordered domain and a single alpha helical (SAH) domain.'

INCENP harbours microtubule-binding domains within the N-terminus and the central SAH domain, which play key roles for CPC localization and function (Samejima et al., 2015; Kang et al., 2001; Noujaim et al., 2014; Cormier et al., 2013; Wheatley et al., 2001; Nakajima et al., 2011; Fink et al., 2017; Wheelock et al., 2017; van der Horst et al., 2015; Mackay et al., 1993).'

Reviewer #2 (Public Review):

*How the chromosomal passenger complex (CPC) and its subunit Aurora B kinase regulate kinetochore-microtubule attachment, and how the CPC relocates from kinetochores to the spindle midzone as a cell transitions from metaphase to anaphase are questions of great interest. In this study, Ballmer and Akiyoshi take a deep dive into the CPC in *T. brucei*, a kinetoplastid parasite with a kinetochore composition that varies greatly from other organisms.*

*Using a combination of approaches, most importantly in silico protein predictions using alphafold multimer and light microscopy in dividing *T. brucei*, the authors convincingly present and analyse the composition of the *T. brucei* CPC. This includes the identification of KIN-A and KIN-B, proteins of the kinesin family, as targeting subunits of the CPC. This is a clear advancement over earlier work, for example by Li and colleagues in 2008. The involvement of KIN-A and KIN-B is of particular interest, as it provides a clue for the (re)localization of the CPC during the cell cycle. The evolutionary perspective makes the paper potentially interesting for a wide audience of cell biologists, a point that the authors bring across properly in the title, the abstract, and their discussion.*

*The evolutionary twist of the paper would be strengthened 'experimentally' by predictions of the structure of the CPC beyond *T. brucei*. Depending on how far the authors can extend their in-silico analysis, it would be of interest to discuss a) available/predicted CPC structures in well-studied organisms and b) structural predictions in other euglenozoa. What are the general structural properties of the CPC (e.g. flexible linkers, overall dimensions, structural differences when subunits are missing etc.)? How common is the involvement of kinesin-like proteins? In line with this, it would be good to display the figure currently shown as S1D (or similar) as a main panel.*

We thank the reviewer for her/his encouraging assessment of our manuscript and the appreciation on the extent of the evolutionary relevance of our work. As suggested, we have moved the phylogenetic tree previously shown in Fig. S1D to the main Fig. 1F. Our AF2 analysis of CPC proteins and (sub)complexes from other kinetoplastids failed to predict reliable interactions among CPC proteins except for that between Aurora B and the IN box. It therefore remains unclear whether CPC structures are conserved among kinetoplastids. Because components of CPC remain unknown in other euglenozoa (other than Aurora B and INCENP), we cannot perform structural predictions of CPC in diplomonads or euglenids.

It remains unclear how common the involvement of kinesin-like proteins with the CPC is in other eukaryotes, partly because we could not identify an obvious homolog of KIN-A/KIN-B outside of kinetoplastids. Addressing this question would require experimental approaches in various eukaryotes (e.g. immunoprecipitation and mass spectrometry of Aurora B) as we carried out in this manuscript using *Trypanosoma brucei*.

Reviewer #3 (Public Review):

Summary:

The protein kinase, Aurora B, is a critical regulator of mitosis and cytokinesis in eukaryotes, exhibiting a dynamic localisation. As part of the Chromosomal Passenger Complex (CPC), along with the Aurora B activator, INCENP, and the CPC localisation module comprised of Borealin and Survivin, Aurora B travels from the kinetochores at

*metaphase to the spindle midzone at anaphase, which ensures its substrates are phosphorylated in a time- and space-dependent manner. In the kinetoplastid parasite, *T. brucei*, the Aurora B orthologue (AUK1), along with an INCENP orthologue known as CPC1, and a kinetoplastid-specific protein CPC2, also displays a dynamic localisation, moving from the kinetochores at metaphase to the spindle midzone at anaphase, to the anterior end of the newly synthesised flagellum attachment zone (FAZ) at cytokinesis. However, the trypanosome CPC lacks orthologues of Borealin and Survivin, and *T. brucei* kinetochores also have a unique composition, being comprised of dozens of kinetoplastid-specific proteins (KKTs). Of particular importance for this study are KKT7 and the KKT8 complex (comprising KKT8, KKT9, KKT11, and KKT12). Here, Ballmer and Akiyoshi seek to understand how the CPC assembles and is targeted to its different locations during the cell cycle in *T. brucei*.*

Strengths & Weaknesses:

Using immunoprecipitation and mass-spectrometry approaches, Ballmer and Akiyoshi show that AUK1, CPC1, and CPC2 associate with two orphan kinesins, KIN-A and KIN-B, and with the use of endogenously expressed fluorescent fusion proteins, demonstrate for the first time that KIN-A and KIN-B display a dynamic localisation pattern similar to other components of the CPC. Most of these data provide convincing evidence for KIN-A and KIN-B being bona fide CPC proteins, although the evidence that KIN-A and KIN-B translocate to the anterior end of the new FAZ at cytokinesis is weak - the KIN-A/B signals are very faint and difficult to see, and cell outlines/brightfield images are not presented to allow the reader to determine the cellular location of these faint signals (Fig S1B).

We thank the reviewer for their thorough assessment of our manuscript and the insightful feedback to further improve our study. To address the point above, we have acquired new microscopy data for Fig. S1B and S1C, which now includes phase contrast images, and have chosen representative cells in late anaphase and telophase. We hope that the signal of Aurora BAUK1, KIN-A and KIN-B at the anterior end of the new FAZ can be now distinguished more clearly.

They then demonstrate, by using RNAi to deplete individual components, that the CPC proteins have hierarchical interdependencies for their localisation to the kinetochores at metaphase. These experiments appear to have been well performed, although only images of cell nuclei were shown (Fig 2A), meaning that the reader cannot properly assess whether CPC components have localised elsewhere in the cell, or if their abundance changes in response to depletion of another CPC protein.

We chose to show close-ups of the nucleus to highlight the different localization patterns of CPC proteins under the different RNAi conditions. In none of these conditions did we observe mis-localization of CPC subunits to the cytoplasm. To clarify this point, we added the following sentence in the legend for Figure 2A:

‘A) Representative fluorescence micrographs showing the localization of YFP-tagged Aurora BAUK1, INCENPCPC1, KIN-A and KIN-B in 2K1N cells upon RNAi-mediated knockdown of indicated CPC subunits. Note that nuclear close-ups are shown here. CPC proteins were not detected in the cytoplasm. RNAi was induced with 1 µg/mL doxycycline for 24 h (KIN-B RNAi) or 16 h (all others). Cell lines: BAP3092, BAP2552, BAP2557, BAP3093, BAP2906, BAP2900, BAP2904, BAP3094, BAP2899, BAP2893, BAP2897, BAP3095, BAP3096, BAP2560, BAP2564, BAP3097. Scale bars, 2 µm.’

Ballmer and Akiyoshi then go on to determine the kinetochore localisation domains of KIN-A and KIN-B. Using ectopically expressed GFP-tagged truncations, they show that coiled-coil domains within KIN-A and KIN-B, as well as a disordered C-terminal tail

present only in KIN-A, but not the N-terminal motor domains of KIN-A or KIN-B, are required for kinetochore localisation. These data are strengthened by immunoprecipitating CPC complexes and crosslinking them prior to mass spectrometry analysis (IP-CLMS), a state-of-the-art approach, to determine the contacts between the CPC components. Structural predictions of the CPC structure are also made using AlphaFold2, suggesting that coiled coils form between KIN-A and KIN-B, and that KIN-A/B interact with the N termini of CPC1 and CPC2. Experimental results show that CPC1 and CPC2 are unable to localise to kinetochores if they lack their N-terminal domains consistent with these predictions. Altogether these data provide convincing evidence of the protein domains required for CPC kinetochore localisation and CPC protein interactions. However, the authors also conclude that KIN-B plays a minor role in localising the CPC to kinetochores compared to KIN-A. This conclusion is not particularly compelling as it stems from the observation that ectopically expressed GFP-NLS-KIN-A (full length or coiled-coil domain + tail) is also present at kinetochores during anaphase unlike endogenously expressed YFP-KIN-A. Not only is this localisation probably an artifact of the ectopic expression, but the KIN-B coiled-coil domain localises to kinetochores from S to metaphase and Fig S2G appears to show a portion of the expressed KIN-B coiled-coil domain colocalising with KKT2 at anaphase. It is unclear why KIN-B has been discounted here.

As the reviewer points out, a small fraction of GFP-NLS-KIN-B317-624 is indeed detectable at kinetochores in anaphase, although most of the protein shows diffuse nuclear staining. There are various explanations for this phenomenon: It is conceivable that the KIN-B motor domain may contribute to microtubule binding and translocation of the CPC from kinetochores onto the spindle in anaphase. In our experiments, ectopically expressed KIN-B317-624 likely outcompetes a fraction of endogenous KIN-B for binding to KIN-A, which could interfere with this translocation process, leaving a population of CPC ‘stranded’ at kinetochores in anaphase. Another possibility, hinted at by the reviewer, is that the C-terminus of KIN-B interacts with receptors at the kinetochore/centromere. Although we do not discount this possibility, we nevertheless decided to focus on KIN-A in this study, because the anaphase kinetochore retention phenotype for both full-length GFP-NLS-KIN-A and -KIN-A309-862 is much stronger than for KIN-B317-624. Two additional reasons were that (i) KIN-A is highly conserved within kinetoplastids, whereas KIN-B orthologs are missing in some kinetoplastids, and (ii) no convincing interactions between KIN-B and kinetochore proteins were predicted by AF2.

To address the reviewer’s point, we decided to include KIN-B in the title of this manuscript, which now reads: ‘Dynamic localization of the chromosomal passenger complex is controlled by the orphan kinesins KIN-A and KIN-B in the kinetoplastid parasite *Trypanosoma brucei*’.

Moreover, we modified the corresponding paragraph in the results section as follows:

‘Intriguingly, unlike endogenously YFP-tagged KIN-A, ectopically expressed GFP fusions of both full-length KIN-A and KIN-A310-862 clearly localized at kinetochores even in anaphase (Figs. 2, F and H). Weak anaphase kinetochore signal was also detectable for KIN-B317-624 (Fig. S2F). GFP fusions of the central coiled-coil domain or the C-terminal disordered tail of KIN-A did not localize to kinetochores (data not shown). These results show that kinetochore localization of the CPC is mediated by KIN-A and KIN-B and requires both the central coiled-coil domain as well as the C-terminal disordered tail of KIN-A.’

Next, using a mixture of RNAi depletion and LacI-LacO recruitment experiments, the authors show that kinetochore proteins KKT7 and KKT9 are required for AUK1 to localise to kinetochores (other KKT8 complex components were not tested here) and that all components of the KKT8 complex are required for KIN-A kinetochore localisation. Further, both KKT7 and KKT8 were able to recruit AUK1 to an ectopic locus in the S phase, and KKT7 recruited KKT8 complex proteins, which the authors suggest indicates it is

upstream of KKT8. However, while these experiments have been performed well, the reciprocal experiment to show that KKT8 complex proteins cannot recruit KKT7, which could have confirmed this hierarchy, does not appear to have been performed. Further, since the LacI fusion proteins used in these experiments were ectopically expressed, they were retained (artificially) at kinetochores into anaphase; KKT8 and KIN-A were both able to recruit AUK1 to LacO foci in anaphase, while KKT7 was not. The authors conclude that this suggests the KKT8 complex is the main kinetochore receptor of the CPC - while very plausible, this conclusion is based on a likely artifact of ectopic expression, and for that reason, should be interpreted with a degree of caution.

We previously showed that RNAi-mediated depletion of KKT7 disrupts kinetochore localization of KKT8 complex members, whereas kinetochore localization of KKT7 is unaffected by disruption of the KKT8 complex (Ishii and Akiyoshi, 2020). Moreover, in contrast to the KKT8 complex, KKT7 remains at kinetochores in anaphase (Akiyoshi and Gull, 2014). These data show that KKT7 is upstream of the KKT8 complex. In this context, the LacI-LacO tethering approach can be very useful to probe whether two proteins (or domains of proteins) could interact in vivo either directly or indirectly. However, a recruitment hierarchy cannot be inferred from such experiments because the data just shows whether X can recruit Y to an ectopic locus (but not whether X is upstream of Y or vice versa). Regarding the retention of Aurora BAUK1 at kinetochores in anaphase upon ectopic expression of GFP-KKT8-LacI, we agree with the reviewer that these data need to be carefully interpreted. Nevertheless, the notion that the KKT7-KKT8 complex recruits the CPC to kinetochores is also strongly supported by IP-MS, RNAi experiments, and AF2 predictions. For clarification and to address the reviewer's point, we re-formulated the corresponding paragraph in the main text:

'We previously showed that KKT7 lies upstream of the KKT8 complex (Ishii and Akiyoshi, 2020). Indeed, GFP-KKT72-261-LacI recruited tdTomato-KKT8, -KKT9 and -KKT12 (Fig. S4E). Expression of both GFP-KKT72-261-LacI and GFP-KKT8-LacI resulted in robust recruitment of tdTomato-Aurora BAUK1 to LacO foci in S phase (Figs. 4, E and F). Intriguingly, we also noticed that, unlike endogenous KKT8 (which is not present in anaphase), ectopically expressed GFP-KKT8-LacI remained at kinetochores during anaphase (Fig. 4F). This resulted in a fraction of tdTomato-Aurora BAUK1 being trapped at kinetochores during anaphase instead of migrating to the central spindle (Fig. 4F). We observed a comparable situation upon ectopic expression of GFP-KIN-A, which is retained on anaphase kinetochores together with tdTomato-KKT8 (Fig. S4F). In contrast, Aurora BAUK1 was not recruited to LacO foci marked by GFP-KKT72-261-LacI in anaphase (Fig. 4E).'

Further IP-CLMS experiments, in combination with recombinant protein pull-down assays and structural predictions, suggested that within the KKT8 complex, there are two subcomplexes of KKT8:KKT12 and KKT9:KKT11, and that KKT7 interacts with KKT9:KKT11 to recruit the remainder of the KKT8 complex. The authors also assess the interdependencies between KKT8 complex components for localisation and expression, showing that all four subunits are required for the assembly of a stable KKT8 complex and present AlphaFold2 structural modelling data to support the two subcomplex models. In general, these data are of high quality and convincing with a few exceptions. The recombinant pulldown assay (Fig. 4H) is not particularly convincing as the 3rd eluate gel appears to show a band at the size of KKT11 (despite the labelling indicating no KKT11 was present in the input) but no pulldown of KKT9, which was present in the input according to the figure legend (although this may be mislabeled since not consistent with the text). The text also states that 6HIS-KKT8 was insoluble in the absence of KKT12, but this is not possible to assess from the data presented.

We thank the reviewer for pointing out an error in the text: ‘Removal of both KKT9 and KKT11 did not impact formation of the KKT8:KKT12 subcomplex’ should read ‘Removal of either KKT9 or KKT11 did not impact formation of the KKT8:KKT12 subcomplex’. Regarding the very faint band perceived to be KKT11 in the 3rd eluate: This band runs slightly lower than KKT11 and likely represents a bacterial contaminant (which we have seen also in other preps in the past). We have made a note of this in the corresponding legend (new Fig. 4I). Moreover, we provide the estimated molecular weights for each subunit, as suggested by the reviewer in recommendation #14 (see below):

‘(I) Indicated combinations of 6HIS-tagged KKT8 (~46 kDa), KKT9 (~39 kDa), KKT11 (~29 kDa) and KKT12 (~23 kDa) were co-expressed in *E. coli*, followed by metal affinity chromatography and SDS-PAGE. The asterisk indicates a common contaminant.’

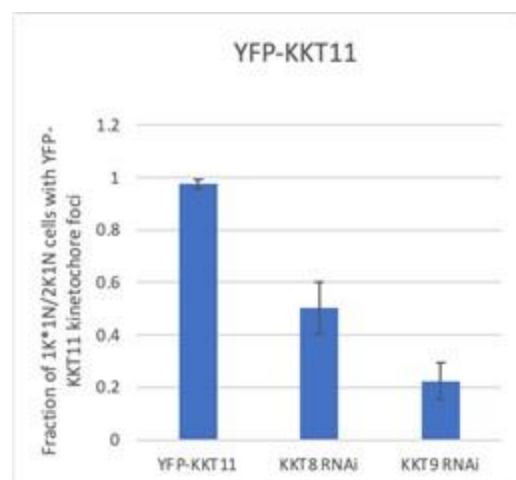
The corresponding paragraph in the results section now reads:

To validate these findings, we co-expressed combinations of 6HIS-KKT8, KKT9, KKT11 and KKT12 in *E. coli* and performed metal affinity chromatography (Fig. 4I). 6HIS-KKT8 efficiently pulled down KKT9, KKT11 and KKT12, as shown previously (Ishii and Akiyoshi, 2020). In the absence of KKT9, 6HIS-KKT8 still pulled down KKT11 and KKT12. Removal of either KKT9 or KKT11 did not impact formation of the KKT8:KKT12 subcomplex. In contrast, 6HIS-KKT8 could not be recovered without KKT12, indicating that KKT12 is required for formation of the full KKT8 complex. These results support the idea that the KKT8 complex consists of KKT8:KKT12 and KKT9:KKT11 subcomplexes.’

It is also surprising that data showing the effects of KKT8, KKT9, and KKT12 depletion on KKT11 localisation and abundance are not presented alongside the reciprocal experiments in Fig S4G-J.

YFP-KKT11 is delocalized upon depletion of KKT8 and KKT9 (see below). Unfortunately, we were unsuccessful in our attempts at deriving the corresponding KKT12 RNAi cell line, rendering this set of data incomplete. Because these data are not of critical importance for this study, we decided not to invest more time in attempting further transfections.

Author response image 1.



The authors also convincingly show that AlphaFold2 predictions of interactions between KKT9:KKT11 and a conserved domain (CD1) in the C-terminal tail of KIN-A are likely correct, with CD1 and a second conserved domain, CD2, identified through sequence

analysis, acting synergistically to promote KIN-A kinetochore localisation at metaphase, but not being required for KIN-A to move to the central spindle at anaphase. They then hypothesise that the kinesin motor domain of KIN-A (but not KIN-B which is predicted to be inactive based on non-conservation of residues key for activity) determines its central spindle localisation at anaphase through binding to microtubules. In support of this hypothesis, the authors show that KIN-A, but not KIN-B can bind microtubules in vitro and in vivo. However, ectopically expressed GFP-NLS fusions of full-length KIN-A or KIN-A motor domain did not localise to the central spindle at anaphase. The authors suggest this is due to the GFP fusion disrupting the ATPase activity of the motor domain, but they provide no evidence that this is the case. Instead, they replace endogenous KIN-A with a predicted ATPase-defective mutant (G209A), showing that while this still localises to kinetochores, the kinetochores were frequently misaligned at metaphase, and that it no longer concentrates at the central spindle (with concomitant mis-localisation of AUK1), causing cells to accumulate at anaphase. From these data, the authors conclude that KIN-A ATPase activity is required for chromosome congression to the metaphase plate and its central spindle localisation at anaphase. While potentially very interesting, these data are incomplete in the absence of any experimental data to show that KIN-A possesses ATPase activity or that this activity is abrogated by the G209A mutation, and the conclusions of this section are rather speculative.

Thank you for this important comment, which relates to a similar point raised by Reviewer 1 (see above). Indeed, ATPase and motor activity of KIN-A remain to be demonstrated biochemically using recombinant proteins, which is beyond the scope of this study. We generated MSAs of KIN-A and KIN-B from different kinetoplastids with human Kinesin-1, human Mklp2 and yeast Klp9, which are now presented in Figure 6A and S6A. These clearly show that key motifs required for ATP or tubulin binding in other kinesins are highly conserved in KIN-A (but not KIN-B). This includes the conserved glycine residue in the Switch II helix (G234 in human Kinesin-1, G210 in *T. brucei* KIN-A), which forms a hydrogen bond with the γ -phosphate of ATP, and upon mutation has been shown to impair ATPase activity and trap the motor head in a strong microtubule ('rigor') state (Rice et al., 1999; Sablin et al., 1996). The prominent rigor phenotype of KIN-AG210A is consistent with KIN-A having ATPase activity. In addition to the data in Fig. 6A and S6A, we made following changes to the main text:

'We therefore speculated that anaphase translocation of the kinetoplastid CPC to the central spindle may involve the kinesin motor domain of KIN-A. KIN-B is unlikely to be a functional kinesin based on the absence of several well-conserved residues and motifs within the motor domain, which are fully present in KIN-A (Li et al., 2008). These include the P-loop, switch I and switch II motifs, which form the nucleotide binding cleft, and many conserved residues within the α 4-L12 elements, which interact with tubulin (Fig. S6A) (Endow et al., 2010). Consistent with this, the motor domain of KIN-B, contrary to KIN-A, failed to localize to the mitotic spindle when expressed ectopically (Fig. S2E) and did not co-sediment with microtubules in our in vitro assay (Fig. S6B).

Ectopically expressed GFP-KIN-A and -KIN-A2-309 partially localized to the mitotic spindle but failed to concentrate at the midzone during anaphase (Figs. 2, F and G), suggesting that N-terminal tagging of the KIN-A motor domain may interfere with its function. To address whether the ATPase activity of KIN-A is required for central spindle localization of the CPC, we replaced one allele of KIN-A with a C-terminally YFP-tagged G210A ATP hydrolysis-defective rigor mutant (Fig. 6A) (Rice et al., 1999) and used an RNAi construct directed against the 3'UTR of KIN-A to deplete the untagged allele. The rigor mutation did not affect recruitment of KIN-A to kinetochores (Figs. S6, C and D). However, KIN-AG210A-YFP marked kinetochores were misaligned in ~50% of cells arrested in metaphase, suggesting that ATPase activity of KIN-A promotes chromosome congression to the metaphase plate (Figs. S6, E-H).'

Impact:

Overall, this work uses a wide range of cutting-edge molecular and structural predictive tools to provide a significant amount of new and detailed molecular data that shed light on the composition of the unusual trypanosome CPC and how it is assembled and targeted to different cellular locations during cell division. Given the fundamental nature of this research, it will be of interest to many parasitology researchers as well as cell biologists more generally, especially those working on aspects of mitosis and cell division, and those interested in the evolution of the CPC.

We thank the reviewer for his/her feedback and thoughtful and thorough assessment of our study.

Recommendations for the authors:

Reviewer #1 (Recommendations For The Authors):

(1) Why did the authors omit KIN-B from the title?

We decided to add KIN-B in the title. Please see our response to Reviewer #3 (public review).

(2) Abstract, line 28, "Furthermore, the kinesin motor activity of KIN-A promotes chromosome alignment in prometaphase and CPC translocation to the central spindle upon anaphase onset." This must be revised - see public review.

We changed this section of the abstract as follows:

‘Furthermore, the ATPase activity of KIN-A promotes chromosome alignment in prometaphase and CPC translocation to the central spindle upon anaphase onset. Thus, KIN-A constitutes a unique ‘two-in-one’ CPC localization module in complex with KIN-B, which directs the CPC to kinetochores (from S phase until metaphase) via its C-terminal tail, and to the central spindle (in anaphase) via its N-terminal kinesin motor domain.’

(3) Line 87-90. The findings by Li et al., 2008 (KIN-A and KIN-B interacting with Aurora B and epistasis analysis) should be introduced more comprehensively in the Introduction section.

We added the following sentence in the introduction:

‘In addition, two orphan kinesins, KIN-A and KIN-B, have been proposed to transiently associate with Aurora BAUK1 during mitosis (Li et al., 2008; Li, 2012).’

(4) Figure 1B. The way the Trypanosoma cell cycle is defined should be briefly explained in the main text, rather than just referring to the figure.

The ‘KN’ annotation of the trypanosome cell cycle is explained in the Figure 1 legend. We now also added a brief description in the main text:

‘We next assessed the localization dynamics of fluorescently tagged KIN-A and KIN-B over the course of the cell cycle (Figs. 1, B-E). *T. brucei* possesses two DNA-containing organelles, the nucleus (‘N’) and the kinetoplast (‘K’). The kinetoplast is an organelle found uniquely in kinetoplastids, which contains the mitochondrial DNA and replicates and segregates prior to nuclear division. The ‘KN’ configuration serves as a good cell cycle marker (Woodward and Gull, 1990; Siegel et al., 2008).’

(5) Line 118. Throughout the paper, it is not clear why GFP-NLS fusion was used instead of GFP fusion. Please justify the fusion of NLS.

NLS refers to a short 'nuclear localization signal' (TGRGHKRSREQ) (Marchetti et al., 2000), which ensures that the ectopically expressed construct is imported into the nucleus. When we previously expressed truncations of KKT2 and KKT3 kinetochore proteins, many fragments did not go into the nucleus presumably due to the lack of an NLS, which prevented us from determining which domains are responsible for their kinetochore localization. We have since then consistently used this short NLS sequence in our inducible GFP fusions in the past without any complications. We added a sentence in the Materials & Methods section under Trypanosome culture: 'All constructs for ectopic expression of GFP fusion proteins include a short nuclear localization signal (NLS) (Marchetti et al., 2000).' To avoid unnecessary confusion, we removed 'NLS' from the main text and figures.

(6) Line 121, "Unexpectedly". It is not clear why this was unexpected.

To clarify this point, we modified this paragraph in the results section:

'To our surprise, KIN-A-YFP and GFP-KIN-B exhibited a CPC-like localization pattern identical to that of Aurora BAUK1: Both kinesins localized to kinetochores from S phase to metaphase, and then translocated to the central spindle in anaphase (Figs. 1, C-E). Moreover, like Aurora BAUK1, a population of KIN-A and KIN-B localized at the new FAZ tip from late anaphase onwards (Figs. S1, B and C). This was unexpected, because KIN-A and KIN-B were previously reported to localize to the spindle but not to kinetochores or the new FAZ tip (Li et al., 2008). These data suggest that KIN-A and KIN-B are bona fide CPC proteins in trypanosomes, associating with AuroraAUK1, INCENPCPC1 and CPC2 throughout the cell cycle.'

(7) Line 127-129. Defining homologs and orthologs is tricky - there are many homologs and paralogs of kinesin-like proteins. The method to define the presence or absence of KIN-A/KIN-B homologs should be described in the Materials and Methods section.

Due to the difficulty in defining true orthologs for kinesin-like proteins, we took a conservative approach: reciprocal best BLAST hits. We first searched KIN-A homologs using BLAST in the TriTryp database or using hmmsearch using manually prepared hmm profiles. When the top hit in a given organism found *T. brucei* KIN-A in a reciprocal BLAST search in *T. brucei* proteome, we considered the hit as a true ortholog. We modified the Materials and Methods section as below.

'Searches for homologous proteins were done using BLAST in the TriTryp database (Aslett et al., 2010) or using hmmsearch using manually prepared hmm profiles (HMMER version 3.0; Eddy, 1998). The top hit was considered as a true ortholog only if the reciprocal BLAST search returned the query protein in *T. brucei*.'

(8) Line 156. For non-experts of Trypanosoma cell biology, it is not clear how the nucleolar localization is defined.

The nucleolus in *T. brucei* is discernible as a DAPI-dim region in the nucleus.

(9) Fig.2G and Fig.S2F. These data imply that the coiled-coil and C-terminal tail domains of KIN-A/KIN-B are important for anaphase spindle midzone enrichment. However, it is odd that this was not mentioned. This reviewer recommends that the authors quantify the midzone localization data of these constructs and discuss the role of the coiled-coil domains.

One possibility is that KIN-A and KIN-B need to form a complex (via their coiled-coil domains) to localize to the spindle midzone. Another likely possibility, which is discussed in the manuscript, is that N-terminal tagging of KIN-A impairs motor activity. This is supported by the fact that the central spindle localization is also disrupted in full-length GFP-KIN-A. We decided not to provide a quantification for these data due to low sample sizes for some of the constructs (e.g. expression not observed in all cells).

(10) Line 288-289, "pLDDT scores improved significantly for KIN-A CD1 in complex with KKT9:KKT11 (>80) compared to KIN-A CD1 alone (~20) (Figs. S3, A and B)." I can see that pLDDT score is about 20 at KIN-A CD1 from Figs S3A, but the basis of pLDDT > 80 upon inclusion go KKT9:KKT11 is missing.

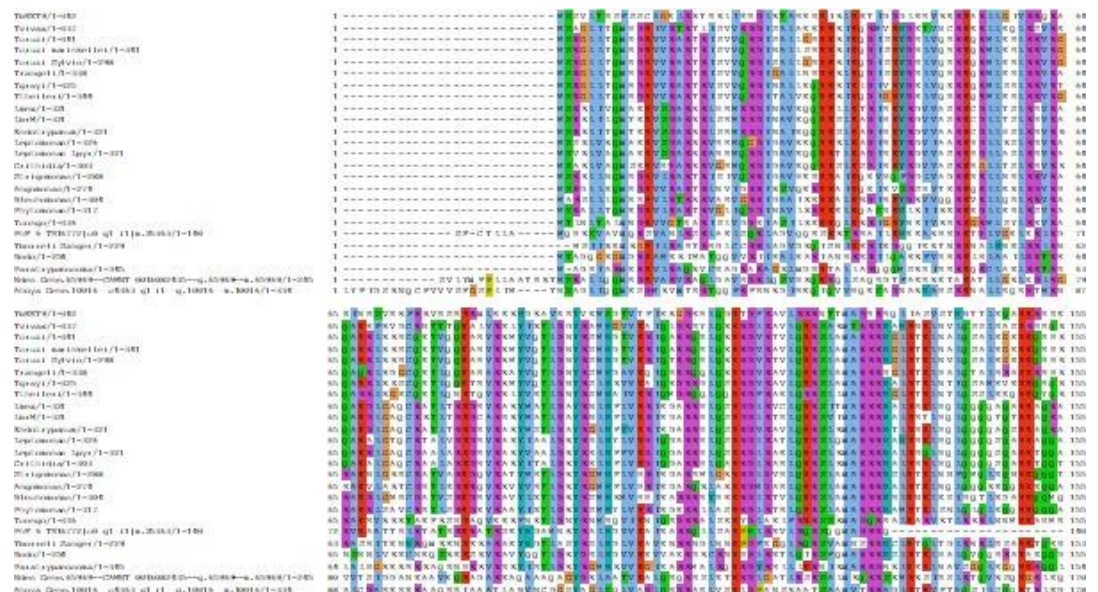
We added the pLDDT and PAE plots for the AF2 prediction of KIN-A700-800 in complex with KKT9:KKT11 in Fig. S5B.

(11) Fig. 5A. Since there is no supporting biochemical data for KIN-A-KKT9-KKT11 interaction, it is important to assess the stability of AlphaFold-based structural predictions of the KIN-A-KKT9-KKT11 interaction. Are there significant differences among the top 5 prediction results, and do these interactions remain stable after the "simulated annealing" process used in the AlphaFold predictions? Are predicted CD1-interacting regions/amino residues in KKT9 and KKT11 evolutionarily conserved?

See above. The interaction was predicted in all 5 predictions as shown in Fig. S5B. Conservation of the CD1-interacting regions in KKT9 and KKT11 are shown below:

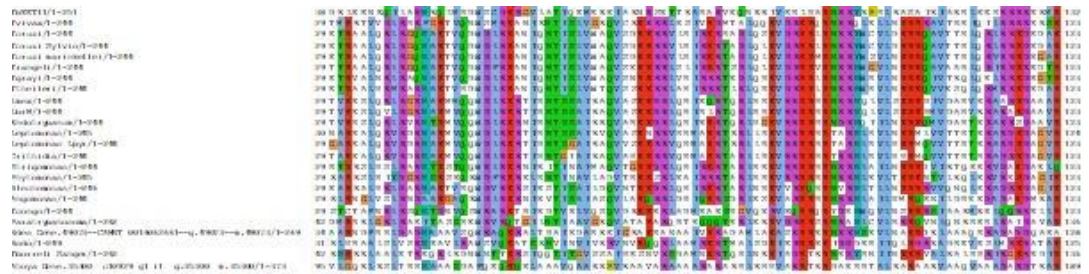
Author response image 2.

KKT9 (residues ~53 – 80 predicted to interact with KIN-A in T. brucei)



Author response image 3.

KKT11 (residues 61-85 predicted to interact with KIN-A in T. brucei)



(12) Line 300, Fig. S5D and E, "failed to localize at kinetochores". From this resolution of the microscopy images, it is not clear if these proteins fail to localize at kinetochores as the KKT and KIN-A310-716 signals overlap. Perhaps, "failed to enrich at kinetochores" is a more appropriate statement.

We changed this sentence according to the reviewer's suggestion.

(13) Line 309 and Fig 5D and F, "predominantly localized to the mitotic spindle". From this image shown in Fig 5D, it is not clear if KIN-AΔCD1-YFP and Aurora B are predominantly localized to the spindle or if they are still localized to centromeres that are misaligned on the spindle. Without microtubule staining, it is also not clear how microtubules are distributed in these cells. Please clarify how the presence or absence of kinetochore/spindle localization was defined.

As shown in Fig. S5E and S5F, deletion of CD1 clearly impairs kinetochore localization of KIN-A (kinetochores marked by tdTomato-KKT2). Moreover, misalignment of kinetochores, as observed upon expression of the KIN-AG210A rigor mutant, would result in an increase in 2K1N cells and proliferation defects, which is not the case for the KIN-ΔCD1 mutant (Fig. 5H, Fig. S5I). KIN-ΔCD1-YFP appears to localize diffusely along the entire length of the mitotic spindle, whereas we still observe kinetochore-like foci in the rigor mutant. Unfortunately, we do not have suitable antibodies that would allow us to distinguish spindle microtubules from the vast subpellicular microtubule array present in *T. brucei* and hence need to rely on tagging spindle-associated proteins such as MAP103.

(14) Fig. 5F, G, S5F. Along the same lines, it would be helpful to show example images for each category - "kinetochores", "kinetochores + spindle", and "spindle".

As suggested by the reviewer, we have now included example images for each category ('kinetochores', 'kinetochores + spindle', 'spindle') along with a schematic illustration in Fig. 5F.

(15) Line 332 and Fig. S6A. The experiment may be repeated in the presence of ATP or nonhydrolyzable ATP analogs.

We thank the reviewer for the suggestion. We envisage such experiments for an in-depth follow-up study.

(16) Line 342, "motor activity of KIN-A". Until KIN-A is shown to have motor activity, the result based on the rigor mutant does not show that the motor activity of KIN-A promotes chromosome congression. The result suggests that the ATPase activity of KIN-A is important.

We changed that sentence as suggested by the reviewer.

(17) Line 419 -. The authors base their discussion on the speculation that KIN-A is a plus-end directed motor. Please justify this speculation.

Indeed, the notion that KIN-A is a plus-end directed motor remains a hypothesis, which is based on sequence alignments with other plus-end directed motors and the observation that the KIN-A motor domain is involved in translocation of the CPC to the central spindle in anaphase. We have modified the corresponding section in the discussion as follows:

‘It remains to be investigated whether KIN-A truly functions as a plus-end directed motor. The role of the KIN-B in this context is equally unclear. Since KIN-B does not possess a functional kinesin motor domain, we deem it unlikely that the KIN-A:KIN-B heterodimer moves hand-over-hand along microtubules as do conventional (kinesin-1 family) kinesins. Rather, the KIN-A motor domain may function as a single-headed unit and drive processive plus-end directed motion using a mechanism similar to the kinesin-3 family kinesin KIF1A (Okada and Hirokawa, 1999).’

(18) Line 422-423, "plus-end directed motion using a mechanism similar to kinesin-3 family kinesins (such as KIF1A)." Please cite a reference supporting this statement.

See above. We cited a paper by (Okada and Hirokawa, 1999).

Reviewer #2 (Recommendations For The Authors):

Please provide a quantification of data shown in Figure 2F-H and described in lines 151-166.

We decided not to provide a quantification for these data due to low sample sizes for some of the constructs (e.g. expression not observed in all cells).

It appears as if the paper more or less follows a chronological order of the experiments that were performed before AF multimer enabled the insightful and compelling structural analysis. That is a matter of style, but in some cases, the writing could be updated, shortened, or re-arranged into a more logical order. Concrete examples:

(i) Line 144: "we did not include CPC2 for further analysis in this study" Although CPC2 features at a prominent and interesting position in the predicted structures of the kinetoplastid CPC, shown in later main figures.

We attempted RNAi-mediated depletion of CPC2 using two different shRNA constructs. However, we cannot exclude the possibility that the knockdown of CPC2 was less efficient compared with the other CPC subunits. For this reason, we decided to remove all the data on CPC2 from Fig. S2.

(ii) The work with the KIN-A motor domain only and KIN-A Δ motor domain (Fig 2) begs the question about a more subtle mutation to interfere with the motor domain. Which is ultimately presented in Fig 6. I think that the final paragraph and Figure 6 follow naturally after Figure 2.

We appreciate the suggestion. However, we would like to keep Figure 6 there.

(iii) The high-confidence structural predictions in Fig 3 and Fig 4 are insightful. The XL-MS descriptions that precede them are not so helpful (Fig 3A and 4G and in the text). To emphasize their status as experimental support for the predicted structures, which is very important, it would be good to discuss the XL-MS after presenting the models.

As suggested, we have re-arranged the text and/or figures such that the AF2 predictions are discussed first and the CLMS data are brought in afterwards.

Figure 1A prominently features an arbitrary color code and a lot of protein IDs without a legend. That is not a very convincing start. Figure S1 is more informative, containing annotated protein names and results of the KIN-A and KIN-B IPs. Please improve Figure 1A, for example by presenting a modified version of Figure S1. In all these types of figures, please list both protein names and gene IDs.

We agree with the reviewer that the IP-MS data in Fig. S1 is more informative and hence decided to swap the heatmaps in Fig. 1A and Fig. S1A. We further annotated the heatmap corresponding to the Aurora BAUK1 IP-MS (now presented in Fig. S1) as suggested by the reviewer.

The visualization of the structural predictions is not consistent among figures:

(i) The structure in Fig 4I is important and could be displayed larger. The pLDDT scores, and especially those of the non-displayed models, do not add much information and should not be a main panel. If the authors want to display the pLDDT scores, I recommend a panel (main or supplement) of the structure colored for local prediction confidences, as in Fig 5A.

(ii) In Figure 5A itself, it is hard to follow the chains in general, and KIN-A in particular, since the structure is pLDDT-coloured. Please present an additional panel colored by chain (consistent with Fig 4I, as mentioned above).

(iii) The summarizing diagram, currently displayed as Fig 4J, should be placed after Fig 5A and take the discovered KIN-A - KKT9-11 connection into account. Ideally, it also covers the suspected importance of the motor domain and serves as a summarising diagram.

We thank the reviewer for the constructive comments. For each structure prediction, we now present two images side by side; one coloured by chain and one colored by pLDDT. We recently re-ran AF2 for the full CPC and also for the KKT7N-KKT8 complex, and got improved predictions. Hence some of the models in Fig. 3/S3 and Fig. 4/S4 have been updated accordingly. For the CLMS plots, we also decided to colour the cross-links according to whether the 30 angstrom distance constraints were fulfilled or not in the AF2 prediction. We also increased the size of the structures shown in Fig. 4. Furthermore, we decided to remove the summarizing diagram from Fig. 4 and instead made a new main Fig. 7, which shows a more detailed schematic, which also takes into account the proposed function of the KIN-A motor domain, as suggested by the reviewer, and other points addressed in the Discussion.

The methods section for the structural predictions lacks essential information. Predictions can only be reproduced if the version of AF2 multimer v2.x is specified and key parameters are mentioned.

As suggested, we have added the details in the Materials and Methods section as follows.

‘Structural predictions of KIN-A/KIN-B, KIN-A310-862/KIN-B317-624, CPC1/CPC2/KIN-A300-599/KIN-B 317-624, and KIN-A700-800/KKT9/KKT11 were performed using ColabFold version 1.3.0 (AlphaFold-Multimer version 2), while those of AUK1/CPC1/CPC2/KIN-A1-599/KIN-B, KKT71-261/KKT9/KKT11/KKT8/KKT12, KKT9/KKT11/KKT8/KKT12, and KKT71-261/KKT9/KKT11 were performed using ColabFold version 1.5.3 (AlphaFold-Multimer version 2.3.1) using default settings, accessed via <https://colab.research.google.com/github/sokrypton/ColabFold>

[/blob/v1.3.0/AlphaFold2.ipynb](#) and <https://colab.research.google.com/github/sokrypton/ColabFold/blob/v1.5.3/AlphaFold2.ipynb>.’

Line 121, please explain the "Unexpectedly" by including a reference to the work from Li and colleagues. A statement with some details would be useful, as the difference between both studies appears to be crucial for the novelty of this paper. Alternatively, refer to this being covered in the discussion.

To clarify this point, we modified this paragraph in the results section:

‘To our surprise, KIN-A-YFP and GFP-KIN-B exhibited a CPC-like localization pattern identical to that of Aurora BAUK1: Both kinesins localized to kinetochores from S phase to metaphase, and then translocated to the central spindle in anaphase (Figs. 1, C-E). Moreover, like Aurora BAUK1, a population of KIN-A and KIN-B localized at the new FAZ tip from late anaphase onwards (Figs. S1, B and C). This was unexpected, because KIN-A and KIN-B were previously reported to localize to the spindle but not to kinetochores or the new FAZ tip (Li et al., 2008). These data suggest that KIN-A and KIN-B are bona fide CPC proteins in trypanosomes, associating with AuroraAUK1, INCENPCPC1 and CPC2 throughout the cell cycle.’

Line 285 refers to "conserved" regions in the C-terminal part of KIN-A, referring to Figure 5. Please expand the MSA in Figure 5B to get an idea about the conservation/variation outside CD1 and CD2.

We now present the full MSA for KIN-A proteins in kinetoplastids in Fig. S5A.

Please specify what is meant by Line 367-369 for someone who is not familiar with the work by Komaki et al. 2022. Either clarify in the text or clarify in the text with data to support it.

We updated the corresponding section in the discussion as follows:

‘Komaki et al. recently identified two functionally redundant CPC proteins in Arabidopsis, Borealin Related Interactor 1 and 2 (BORI1 and 2), which engage in a triple helix bundle with INCENP and Borealin using a conserved helical domain but employ an FHA domain instead of a BIR domain to read H3T3ph (Komaki et al., 2022).’

Data presented in Figure S6A, the microtubule co-sedimentation assay, is not convincing since a substantial amount of KIN-A/B is pelleted in the absence of microtubules. Did the authors spin the proteins in BRB80 before the assay to continue with soluble material and reduce sedimentation in the absence of microtubules? If the authors want to keep the wording in lines 331-332, the MT-binding properties of KIN-A and KIN-B need to be investigated in more detail, for example with a titration and a quantification thereof. Otherwise, they should change the text and replace "confirms" with "is consistent with". In any case, the legend needs to be expanded to include more information.

To address the point above, we have added the following text in the legend corresponding to Fig. S6:

‘Microtubule co-sedimentation assay with 6HIS-KIN-A2-309 (left) and 6HIS-KIN-B2-316 (right). S and P correspond to supernatant and pellet fractions, respectively. Note that both constructs to some extent sedimented even in the absence of microtubules. Hence, lack of microtubule binding for KIN-B may be due to the unstable non-functional protein used in this study.’

We have also updated the main text in the results section:

‘We therefore speculated that anaphase translocation of the kinetoplastid CPC to the central spindle may involve the kinesin motor domain of KIN-A. KIN-B is unlikely to be a functional kinesin based on the absence of several well-conserved residues and motifs within the motor domain, which are fully present in KIN-A (Li et al., 2008). These include the P-loop, switch I and switch II motifs, which form the nucleotide binding cleft, and many conserved residues within the α 4-L12 elements, which interact with tubulin (Fig. S6A) (Endow et al., 2010). Consistent with this, the motor domain of KIN-B, contrary to KIN-A, failed to localize to the mitotic spindle when expressed ectopically (Fig. S2E) and did not co-sediment with microtubules in our in vitro assay (Fig. S6B).’

Details:

The readability of the pAE plots could be improved by arranging sequences according to their position in the structure. For example in Fig4I, KKT8 could precede KKT12. If it is easy to update this, the authors might want to do so.

We re-ran the AF2 predictions for the KKT7N – KKT8 complex in Fig. 4/S4 and changed the order according to the reviewer’s suggestion (KKT9:KKT11:KKT8:KKT12).

The same paper is referred to as Je Van Hooff et al. 2017 and as Van Hooff et al. 2017

Thank you for pointing this out. We have corrected the citation.

Reviewer #3 (Recommendations For The Authors):

(1) Please state at the end of the introduction/start of the results section that this work was performed in procyclic trypanosomes. Given that the cell cycles of procyclic and bloodstream forms differ, this is important.

We added this information at the end of the introduction:

‘Here, by combining biochemical, structural and cell biological approaches in procyclic form *T. brucei*, we show that the trypanosome CPC is a pentameric complex comprising Aurora BAUK1, INCENPCPC1, CPC2 and the two orphan kinesins KIN-A and KIN-B.’

(2) Please define NLS at first use (line 118), and for clarity, explain the rationale for using GFP with an NLS.

NLS refers to a short ‘nuclear localization signal’ (TGRGHKRSREQ) (Marchetti et al., 2000), which ensures that the ectopically expressed construct is imported into the nucleus. When we previously expressed truncations of KKT2 and KKT3 kinetochore proteins, many fragments did not go into the nucleus presumably due to the lack of an NLS, which prevented us from determining which domains are responsible for their kinetochore localization. We have since then consistently used this short NLS sequence in our inducible GFP fusions in the past without any complications. We added a sentence in the Materials & Methods section under Trypanosome culture: ‘All constructs for ectopic expression of GFP fusion proteins include a short nuclear localization signal (NLS) (Marchetti et al., 2000).’ To avoid unnecessary confusion, we removed ‘NLS’ from the main text and figures.

(3) Lines 148-150 - it would strengthen this claim if KIN-A/B protein levels were assessed by Western blot.

We now present a Western blot in Fig. S2C, showing that bulk KIN-B levels are clearly reduced upon KIN-A RNAi. The same is true also to some extent for KIN-A levels upon KIN-B

RNAi, although this is less obvious, possibly due to the lower efficiency of KIN-B compared to KIN-A RNAi as judged by fluorescence microscopy (quantified in Fig. 2D and 2E).

(4) Line 253 - the text mentions the removal of both KKT9 and KKT11, which is not consistent with the figure (Fig 4H) - do you mean the removal of either KKT9 or KKT11?

Yes, we thank the reviewer for pointing out this mistake in the text, which has now been corrected.

(5) Line 337 - please include a reference for the G209A ATPase-defective rigor mutant - has this been shown to result in KIN-A being inactive previously?

Please see above our answer in public review.

(6) It is not always obvious when fluorescent fusion proteins are being expressed endogenously or ectopically, or when they are being expressed in an RNAi background or not without tracing the cell lines in Table S1 - please ensure this is clearly stated throughout the manuscript.

We now made sure that this is clearly stated in the main text as well as in the figure legends.

(7) Line 410 - 'KIN-A C-terminal tail is stuffed full of conserved CDK1CRK3 sites' - what does 'stuffed full' really mean (this is rather imprecise) and what are the consensus sites - are these CDK1 consensus sites that are assumed to be conserved for CRK3? I'm not aware of consensus sites for CRK3 having been determined, but if they have, this should be referenced.

We have modified the corresponding section in the discussion as follows:

'In support of this, the KIN-A C-terminal tail harbours many putative CRK3 sites (10 sites matching the minimal S/T-P consensus motif for CDKs) and is also heavily phosphorylated by Aurora BAUK1 in vitro (Ballmer et al. 2024). Finally, we speculate that the interaction of KIN-A motor domain with microtubules, coupled to the force generating ATP hydrolysis and possibly plus-end directed motion, eventually outcompetes the weakened interactions of the CPC with the kinetochore and facilitates the extraction of the CPC from chromosomes onto spindle microtubules during anaphase. Indeed, deletion of the KIN-A motor domain or impairment of its motor function through N-terminal GFP tagging causes the CPC to be trapped at kinetochores in anaphase. Central spindle localization is additionally dependent on the ATPase activity of the KIN-A motor domain as illustrated by the KIN-A rigor mutant.'

(8) Lines 412-416: this proposal is written rather definitively - given no motor activity has been demonstrated for KIN-A, please make clear that this is still just a theory.

See above.

(9) Fig 1: KKT2 is not highlighted in Fig 1A - given this has been used for colocalization in Fig 1C-E, was it recovered, and if not, why not? Fig 1B-E: the S phase/1K1N terminology is somewhat misleading. Not all S phase cells will have elongated kinetoplasts - usually an asterisk is used to signify replicated DNA, not kinetoplast shape. If it is to be used here for elongation, then for consistency, N should be used for G2/mitotic cells.

Fig. 1A (now Fig. S1A) only shows the top 30 hits. KKT2 was indeed recovered with Aurora BAUK1 (see Table S2) and is often used as a kinetochore marker in trypanosomes by our lab

and others since the signal of fluorescently tagged KKT2 is relatively bright and KKT2 localizes to centromeres throughout the cell cycle.

(10) A general comment for all image figures is that these do not have accompanying brightfield images and it is therefore difficult to know where the cell body is, or sometimes which nuclei and kinetoplasts belong to which cell where DNA from more than one cell is within the image. It would be beneficial if brightfield images could be added, or alternatively, the cell outlines were traced onto DAPI or merged images. Also, brightfield images would allow the stage of cytokinesis (pre-furrowing/furrowing/abscission) in anaphase cells to be determined.

Since this study primarily addresses the recruitment mechanism of the CPC to kinetochores and to the central spindle from S phase to metaphase and in anaphase, respectively, and CPC proteins are not observed outside of the nucleus during these cell cycle stages, we did not present brightfield images in the figures. However, this point is particularly valid for discerning the localization of KIN-A and KIN-B to the new FAZ tip from late anaphase onwards. Hence, we acquired new microscopy data for Fig. S1B and S1C, which now includes phase contrast images, and have chosen representative cells in late anaphase and telophase. We hope that the signal of Aurora BAUK1, KIN-A and KIN-B at the anterior end of the new FAZ can be now distinguished more clearly.

(11) Fig 2A: legend should state that the micrographs show the localisation of the proteins within the nucleus as whole cells are not shown. 2C: can INCENP not be split into 2 lines - the 'IN' looks like 1N at first glance, which is confusing.

We have applied the suggested change in Fig. 2.

(12) Fig 3 (and other AF2 figures): Could the lines for satisfied & not satisfied in the key be thicker so they more closely resemble the lines in the figure and are less likely to be confused with the disordered regions of the CPC components?

We have now made those lines thicker.

(13) Why were different E value thresholds used in Fig 3 and Fig 4?

The CLMS data in Fig. 3 and Fig. 4 now both use the same E value threshold of E-3 (previously E-4 was used in Fig. 4). To determine a sensible significance threshold, we included some yeast protein sequences ('false positives') in the database used in pLink2 for identification of crosslinked peptides. Note that we recently also re-ran AF2 for the full CPC and for the KKT7N-KKT8 complex and got improved predictions. Hence some of the models in Fig. 3/S3 and Fig. 4/S4 have been updated accordingly. For the CLMS plots, we also decided to colour the cross-links according to whether the 30 angstrom distance constraints were fulfilled or not in the AF2 prediction.

(14) Fig 4H legend - please give the expected sizes of these recombinant proteins & check the 3rd elution panel (see public review comments).

See above response in public review.

(15) Fig 4I - please explain what the colours of the PAE plot and the values in the key signify, as well as how the Scored Residue values are arrived at. Please also define the pIDDT in the legend.

We have cited DeepMind's 2021 methods paper, in which the outputs of AlphaFold are explained in detail. We also added a short description of the pLDDT and PAE scores and the corresponding colour coding in the legends of Fig. 3 and Fig. 4, respectively.

From figure 3 legend:

‘(B) Cartoon representation showing two orientations of the trypanosome CPC, coloured by protein on the left (Aurora BAUK1: crimson, INCENPCPC1: green, CPC2: cyan, KIN-A: magenta, and KIN-B: yellow) or according to their pLDDT values on the right, assembled from AlphaFold2 predictions shown in Figure S3. The pLDDT score is a per-residue estimate of the confidence in the AlphaFold prediction on a scale from 0 – 100. pLDDT > 70 (blue, cyan) indicates a reasonable accuracy of the model, while pLDDT < 50 (red) indicates a low accuracy and often reflects disordered regions of the protein (Jumper et al., 2021). BS3 crosslinks in (B) were mapped onto the model using PyXlinkViewer (blue = distance constraints satisfied, red = distance constraints violated, Ca-Ca Euclidean distance threshold = 30 Å) (Schiffrin et al., 2020).’

From Figure 4 legend:

‘(G) AlphaFold2 model of the KKT7 – KKT8 complex, coloured by protein (KKT71-261: green, KKT8: blue, KKT12: pink, KKT9: cyan and KKT11: orange) (left) and by pLDDT (center). BS3 crosslinks in (H) were mapped onto the model using PyXlinkViewer (Schiffrin et al., 2020) (blue = distance constraints satisfied, red = distance constraints violated, Ca-Ca Euclidean distance threshold = 30 Å). Right: Predicted Aligned Error (PAE) plot of model shown on the left (rank_2). The colour indicates AlphaFold's expected position error (blue = low, red = high) at the residue on the x axis if the predicted and true structures were aligned on the residue on the y axis (Jumper et al., 2021).’

| (16) Fig 6 legend - Line 730 should say (F) not (C).

Thank you for pointing out this typo.

| (17) Fig S1A - a key is missing for the colours. Fig S1B/C - cell outlines or a brightfield image are really needed here - see earlier comment. Fig S1D - there doesn't seem to be a method for how this tree was generated.

See above response in public review regarding Fig. S1A and S1B/C. The tree in Fig. S1D is based on (Butenko et al., 2020).

| (18) Fig S2: A: how was protein knockdown validated (especially for CPC2 where there was little obvious phenotype)? Fig S2B: the y-axis should read proportion of cells, not percentage. Fig S2E - NLS should be labelled.

Thank you for pointing out the mistake in the labelling.

| (19) Fig S3: PAE plots should be labelled with protein names, not A-E. Similarly, the pLDDT plots should be labelled as in Fig 4I.

We have corrected the labelling in Fig. S3.

| (20) Fig S5A-D - cell cycle stage labels are missing from images.

Thank you for pointing out the missing cell cycle stage labels.

| Addition by editor:

In line 126 the statement that KIN-A and KIN-B "associate with Aurora-AUK1, INCENP-CPC1 and CPC2 throughout the cell cycle" seems too strong. There is no direct evidence for this. Please re-phrase as "likely associate" or "suggest... that ... may..."

We have modified that sentence according to the editor's suggestion.

References:

- Akiyoshi, B., and K. Gull. 2014. Discovery of Unconventional Kinetochore in Kinetoplastids. *Cell*. 156. doi:10.1016/j.cell.2014.01.049.
- Butenko, A., F.R. Opperdoes, O. Flegontova, A. Horák, V. Hampl, P. Keeling, R.M.R. Gawryluk, D. Tikhonenkov, P. Flegontov, and J. Lukeš. 2020. Evolution of metabolic capabilities and molecular features of diplomids, kinetoplastids, and euglenids. *BMC Biology* 2020 18:1. 18:1–28. doi:10.1186/S12915-020-0754-1.
- Cormier, A., D.G. Drubin, and G. Barnes. 2013. Phosphorylation regulates kinase and microtubule binding activities of the budding yeast chromosomal passenger complex in vitro. *J Biol Chem*. 288:23203–23211. doi:10.1074/JBC.M113.491480. Endow, S.A., F.J. Kull, and H. Liu. 2010. Kinesins at a glance. *J Cell Sci*. 123:3420. doi:10.1242/JCS.064113.
- Fink, S., K. Turnbull, A. Desai, and C.S. Campbell. 2017. An engineered minimal chromosomal passenger complex reveals a role for INCENP/Sli15 spindle association in chromosome biorientation. *J Cell Biol*. 216:911–923. doi:10.1083/JCB.201609123.
- van der Horst, A., M.J.M. Vromans, K. Bouwman, M.S. van der Waal, M.A. Hadders, and S.M.A. Lens. 2015. Inter-domain Cooperation in INCENP Promotes Aurora B Relocation from Centromeres to Microtubules. *Cell Rep*. 12:380–387. doi:10.1016/J.CELREP.2015.06.038.
- Ishii, M., and B. Akiyoshi. 2020. Characterization of unconventional kinetochore kinases KKT10/19 in *Trypanosoma brucei*. *J Cell Sci*. doi:10.1242/jcs.240978.
- Jeyaprakash, A.A., C. Basquin, U. Jayachandran, and E. Conti. 2011. Structural Basis for the Recognition of Phosphorylated Histone H3 by the Survivin Subunit of the Chromosomal Passenger Complex. *Structure*. 19:1625–1634. doi:10.1016/J.STR.2011.09.002.
- Jeyaprakash, A.A., U.R. Klein, D. Lindner, J. Ebert, E.A. Nigg, and E. Conti. 2007. Structure of a Survivin–Borealin–INCENP Core Complex Reveals How Chromosomal Passengers Travel Together. *Cell*. 131. doi:10.1016/j.cell.2007.07.045.
- Jumper, J., R. Evans, A. Pritzel, T. Green, M. Figurnov, O. Ronneberger, K. Tunyasuvunakool, R. Bates, A. Žídek, A. Potapenko, A. Bridgland, C. Meyer, S.A.A. Kohl, A.J. Ballard, A. Cowie, B. Romera-Paredes, S. Nikolov, R. Jain, J. Adler, T. Back, S. Petersen, D. Reiman, E. Clancy, M. Zielinski, M. Steinegger, M. Pacholska, T. Berghammer, S. Bodenstein, D. Silver, O. Vinyals, A.W. Senior, K. Kavukcuoglu, P. Kohli, and D. Hassabis. 2021. Highly accurate protein structure prediction with AlphaFold. *Nature* 2021 596:7873. 596:583–589. doi:10.1038/s41586-021-03819-2.
- Kang, J.S., I.M. Cheeseman, G. Kallstrom, S. Velmurugan, G. Barnes, and C.S.M. Chan. 2001. Functional cooperation of Dam1, Ipl1, and the inner centromere protein (INCENP)-related protein Sli15 during chromosome segregation. *J Cell Biol*. 155:763–774. doi:10.1083/JCB.200105029.
- Klein, U.R., E.A. Nigg, and U. Gruneberg. 2006. Centromere targeting of the chromosomal passenger complex requires a ternary subcomplex of Borealin, Survivin, and the N-terminal domain of INCENP. *Mol Biol Cell*. 17:2547–2558. doi:10.1091/MBC.E05-12-1133.

- Komaki, S., E.C. Tromer, G. De Jaeger, N. De Winne, M. Heese, and A. Schnittger. 2022. Molecular convergence by differential domain acquisition is a hallmark of chromosomal passenger complex evolution. *Proc Natl Acad Sci U S A*. 119. doi:10.1073/PNAS.2200108119/-/DCSUPPLEMENTAL.
- Li, Z. 2012. Regulation of the Cell Division Cycle in *Trypanosoma brucei*. *Eukaryot Cell*. 11:1180. doi:10.1128/EC.00145-12.
- Li, Z., J.H. Lee, F. Chu, A.L. Burlingame, A. Günzl, and C.C. Wang. 2008. Identification of a Novel Chromosomal Passenger Complex and Its Unique Localization during Cytokinesis in *Trypanosoma brucei*. *PLoS One*. 3. doi:10.1371/journal.pone.0002354.
- Mackay, A.M., D.M. Eckley, C. Chue, and W.C. Earnshaw. 1993. Molecular analysis of the INCENPs (inner centromere proteins): separate domains are required for association with microtubules during interphase and with the central spindle during anaphase. *J Cell Biol*. 123:373–385. doi:10.1083/JCB.123.2.373.
- Marchetti, M.A., C. Tschudi, H. Kwon, S.L. Wolin, and E. Ullu. 2000. Import of proteins into the trypanosome nucleus and their distribution at karyokinesis. *J Cell Sci*. 113 (Pt 5):899–906. doi:10.1242/JCS.113.5.899.
- Nakajima, Y., A. Cormier, R.G. Tyers, A. Pigula, Y. Peng, D.G. Drubin, and G. Barnes. 2011. Ipl1/Aurora-dependent phosphorylation of Slh1/INCENP regulates CPC-spindle interaction to ensure proper microtubule dynamics. *J Cell Biol*. 194:137–153. doi:10.1083/JCB.201009137.
- Noujaim, M., S. Bechstedt, M. Wiczkorek, and G.J. Brouhard. 2014. Microtubules accelerate the kinase activity of Aurora-B by a reduction in dimensionality. *PLoS One*. 9. doi:10.1371/JOURNAL.PONE.0086786.
- Okada, Y., and N. Hirokawa. 1999. A processive single-headed motor: Kinesin superfamily protein KIF1A. *Science* (1979). 283:1152–1157. doi:10.1126/SCIENCE.283.5405.1152.
- Rice, S., A.W. Lin, D. Safer, C.L. Hart, N. Naber, B.O. Carragher, S.M. Cain, E. Pechatnikova, E.M. Wilson-Kubalek, M. Whittaker, E. Pate, R. Cooke, E.W. Taylor, R.A. Milligan, and R.D. Vale. 1999. A structural change in the kinesin motor protein that drives motility. *Nature* 1999 402:6763. 402:778–784. doi:10.1038/45483.
- Sablin, E.P., F.J. Kull, R. Cooke, R.D. Vale, and R.J. Fletterick. 1996. Crystal structure of the motor domain of the kinesin-related motor ncd. *Nature* 1996 380:6574. 380:555–559. doi:10.1038/380555a0.
- Samejima, K., M. Platani, M. Wolny, H. Ogawa, G. Vargiu, P.J. Knight, M. Peckham, and W.C. Earnshaw. 2015. The Inner Centromere Protein (INCENP) Coil Is a Single α -Helix (SAH) Domain That Binds Directly to Microtubules and Is Important for Chromosome Passenger Complex (CPC) Localization and Function in Mitosis. *J Biol Chem*. 290:21460–21472. doi:10.1074/JBC.M115.645317.
- Schiffrin, B., S.E. Radford, D.J. Brockwell, and A.N. Calabrese. 2020. PyXlinkViewer: A flexible tool for visualization of protein chemical crosslinking data within the PyMOL molecular graphics system. *Protein Sci*. 29:1851–1857. doi:10.1002/PRO.3902.